Naval Surface Warfare Center
Carderock Division
West Bethesda, MD 20817-5700

NSWCCD-TR-65–97/36 September 1997

Survivability, Structures, and Materials Directorate

Technical Report

Fatigue Behavior and Damage Accumulation of Fiber-Reinforced Plastic Laminates and Joints

by

G. Michaelov, M. Kharrazi, K. Momenkhani, S. Sarkani

The George Washington University
School of Engineering and Applied Science
Department of Civil, Mechanical, and Environmental Engineering
Center for Structural Dynamics Research, Ashburn, Virginia Campus

and

D. P. Kihl

Naval Surface Warfare Center, Carderock Division

NSWCCD-TR–65-97/36 Fatigue Behavior and Damage Accumulation of Fiber-Reinforced Plastic Laminates and Joints

DEPARTMENT OF THE NAVY

NAVAL SURFACE WARFARE CENTER, CARDEROCK DIVISION
9500 MACARTHUR BOULEVARD
WEST BETHESDA MD 20817-5700

9078
Ser 65-93
22 Sep 97

From: Commander, Naval Surface Warfare Center, Carderock Division
To: Commander, Naval Sea Systems Command (SEA 03R1)
Chief of Naval Research (Code 334)

Subj: FATIGUE DAMAGE IN VARIOUS FIBER-REINFORCED PLASTIC (FRP) LAMINATES

Ref: (a) Advance Composites for Surface Ship Applications (ACFS) Program, Naval Sea Systems Command Work Request N00024-95-WR11036

(b) Hull Structures Task of the FY97 BA2 Surface Ship Hull, Mechanical and Electrical Technology Program, Program Element 0602121N.

Encl: (1) NSWCCD-TR-65–97/36, *Fatigue Behavior and Damage Accumulation of Fiber-Reinforced Plastic Laminates and Joints*

1. References (a) and (b) directed the Department of Civil, Mechanical, and Environmental Engineering at the Center for Structural Dynamics Research of The George Washington University (GWU) and the Naval Surface Warfare Center, Carderock Division (NSWCCD) to characterize fatigue mechanisms of various FRP laminates. Enclosure (1) documents a collaborative effort between NSWCCD and GWU to investigate the fatigue behavior and cumulative damage of joint details made of fiber-reinforced composite laminates. Use of different S/N curves (stress level versus number of cycles to failure) for composite fatigue modeling and cumulative fatigue damage theories are discussed. Test results from different details are also discussed. One set of joints consisted of bolted, bonded, and bolted and bonded double lapped connections made of 0/90 degree woven roving glass fabric and vinyl ester resin. Another set consisted of load bearing and non-load bearing bolt configurations using the same material in first a 0/90-degree lay-up, and then a ±45-degree lay-up. The test specimens were subjected to axially-applied, constant-amplitude and random-amplitude loads.

2. Comments or questions may be referred to Dr. David P. Kihl, Code 653; telephone (301) 227-1956; e-mail, kihl@oasys.dt.navy.mil.

J. E. BEACH
By direction

Subj: FATIGUE DAMAGE IN VARIOUS FIBER-REINFORCED PLASTIC (FRP) LAMINATES

Copy to:

COMNAVSEASYSCOM WASHINGTON DC
[PEO SUB-RB (Spero), PMS 400D,
SEA 03DB (Comstock), SEA 03H, SEA 03H3,
SEA 03M, SEA 03M3 (Ingle), SEA 03P,
SEA 03P1, SEA 03P1 (Kadala),
SEA 03P4 (Kurzweil), SEA 03R,
SEA 03R11 (Camponeschi), SEA 91T]

CNR ARLINGTON VA [ONR 332 (Kelly),
ONR 334 (Barsoum), ONR 334 (Gagorik),
ONR 334 (Rajapakse), ONR 334 (Vasudevan)]

Center for Structural Dynamics Research
The George Washington University
Virginia Campus
Ashburn, Virginia 20147
[G. Michaelov, M. Kharrazi, K. Momenkhani,
S. Sarkani]

DTIC FORT BELVOIR VA

NAVSURFWARCEN CARDEROCKDIV
BETHESDA MD [Codes 011, 3442 (TIC),
60 (w/o encl), 601 (w/o encl), 604, 614, 65, 65R (2),
65 (files, w/o encl), 651, 652, 653 (10), 653 (Kihl),
654, 655, 6551, 6551 (Bartlett), 6551 (Nguyen),
6551 (Potter), 6552, 6552 (Gipple), 6552 (Cross),
6553 (Williams)]

Naval Surface Warfare Center
Carderock Division
West Bethesda, MD 20817-5700

NSWCCD-TR-65–97/36 September 1997

Survivability, Structures, and Materials Directorate

Technical Report

Fatigue Behavior and Damage Accumulation of Fiber-Reinforced Plastic Laminates and Joints

by

G. Michaelov, M. Kharrazi, K. Momenkhani, S. Sarkani

The George Washington University
School of Engineering and Applied Science
Department of Civil, Mechanical, and Environmental Engineering
Center for Structural Dynamics Research, Ashburn, Virginia Campus

and

D. P. Kihl

Naval Surface Warfare Center, Carderock Division

Enclosure (1)

REPORT DOCUMENTATION PAGE

Form Approved OMB No. 0704-0188

1. AGENCY USE ONLY *(Leave blank)*	2. REPORT DATE	3. REPORT TYPE AND DATES COVERED
	September 1997	Final

4. TITLE AND SUBTITLE
Fatigue Behavior and Damage Accumulation of Fiber-Reinforced Plastic Laminates and Joints

5. FUNDING NUMBERS
N00024-95-WR11036 (NAVSEA)
PE0602121N (ONR)

6. AUTHOR(S)
G. Michaelov, M. Kharrazi, K. Momenkhani, S. Sarkani (GWU) and D.P. Kihl (NSWC)

7. PERFORMING ORGANIZATION NAME(S) AND ADDRESS(ES)
Naval Surface Warfare Center
Carderock Division
9500 MacArthur Boulevard
West Bethesda, MD 20817-5700

The George Washington Univ.
School of Eng. & App. Science
Dept. of Civil, Mechanical and Environmental Engineering
Ashburn, VA 20147

8. PERFORMING ORGANIZATION REPORT NUMBER
NSWCCD-TR-65-97/36

9. SPONSORING/MONITORING AGENCY NAME(S) AND ADDRESS(ES)
Naval Sea Systems Command
(SEA 03R1)
2531 Jefferson Davis Hwy.
Arlington, VA 22242-5160

Chief of Naval Research
(ONR 334)
Ballston Centre Tower One
800 North Quincy St.
Arlington, VA 22217-5660

10. SPONSORING/MONITORING AGENCY REPORT NUMBER

11. SUPPLEMENTARY NOTES

12a. DISTRIBUTION/AVAILABILITY STATEMENT
Approved for public release; distribution is unlimited.

12b. DISTRIBUTION CODE

13. ABSTRACT *(Maximum 200 words)*

Aspects of fatigue damage in various fiber-reinforced plastic (FRP) laminates are discussed. Different S-N curves (stress level versus number of cycles to failure) for composite fatigue modeling are presented. Cumulative damage theories applicable to composite materials are investigated. Results of an experimental program in constant- and random-amplitude fatigue of FRP laminates and joints are presented. Constant-amplitude fatigue test results of the FRP laminates indicate a fairly good fit to the traditional power law S-N curve model for cross-ply laminates. In contrast, constant amplitude fatigue tests of angle-ply laminates and bonded, bolted, and bonded-bolted joints exhibit significantly less favorable fit to the power-law model. Random-amplitude fatigue tests show an inconsistent trend as compared to predictions made using Rayleigh approximation. Fatigue life prediction of the laminate specimens tend to be non-conservative for low RMS levels and conservative for high RMS values. The opposite behavior is observed for the joint specimens, where conservative fatigue life estimates are obtained for low RMS levels and non-conservative estimates for high RMS levels.

14. SUBJECT TERMS
ship structures; materials fatigue; fiber-reinforced plastic
FRP; composite materials; composite joints

15. NUMBER OF PAGES
159

16. PRICE CODE

17. SECURITY CLASSIFICATION OF REPORT	18. SECURITY CLASSIFICATION OF THIS PAGE	19. SECURITY CLASSIFICATION OF ABSTRACT	20. LIMITATION OF ABSTRACT
UNCLASSIFIED	UNCLASSIFIED	UNCLASSIFIED	SAR

NSN 7540-01-280-5500

Standard Form 298 (Rev. 2-89)
Prescribed by ANSI Std. Z39-18
298-102

Table of Contents

FIGURES

FIGURES (con't)

FIGURES (con't)

FIGURES (con't)

FIGURES (con't)

FIGURES (CON'T)

Page

TABLES

ADMINISTRATIVE INFORMATION

This work was performed by the department of Civil, Mechanical, and Environmental Engineering at the Center for Structural Dynamics Research of The George Washington University and by the Structures and Composite Department, Code 65, of the Survivability, Structures, and Materials Directorate at the Naval Surface Warfare Center, Carderock Division (NSWCCD). This work was sponsored by the Naval Sea Systems Command (SEA 03R1) under the 6.4 Advanced Composites for Surface Ship Applications (ACFS) program, PE06030513 S1712, authorized under Work Request N0002495WR11036, and completes the milestone requirements for the fatigue task. Additional funding was provided by the Office of Naval Research (ONR 334), under the hull structures task of the FY97 BA2 Surface Ship Hull, Mechanical, and Electrical Technology Program (PE0602121N).

ACKNOWLEDGMENTS

The authors would like to thank the following individuals at the Naval Surface Warfare Center for their support and interest in this project : Gene Camponeschi, Loc Nguyen, Karin Gipple, and Scott Bartlett of the Structures and Composites Department of NSWCCD for their guidance and support. The authors would also like to express their appreciation to those at the University of Delaware and Hardcore Du Pont Composites, L.L.C. for panel fabrication, ARTECH Testing, L.L.C. and Thomas Lange of the Engineering and Facilities Group of NSWCCD for fabricating and preparing specimens for testing.

INTRODUCTION

The use of fiber-reinforced plastics (FRP) is increasing in marine structural applications ranging from naval ships (e.g., hulls of minehunters, deckhouses, appendages) to high-performance yachts to offshore structures (e.g., piers, risers, topside structures). This trend is expected to continue for two reasons. First, the price of FRP material is steadily decreasing, approaching a level comparable to that of metals. Second, low-cost and high-quality manufacturing techniques, such as autoclave and resin transfer molding processes, have been developed, making production of FRP more attractive.

FRP applications in marine environment often prompt questions about fatigue of the material because ship structures are constantly subjected to cyclic wave-induced loading. In addition to wave action, submersible vehicles can experience a sufficient number of diving and re-surfacing cycles to cause low-cycle compressive fatigue damage [Smith (1990)]. Fatigue issues in FRP marine structures, have received little attention because the design of most FRP ships has been constrained by the material stiffness rather than by strength limitations. Such designs have resulted in low operational stress levels at which fatigue failures were not expected during the specified service life. This situation is changing, however, due to two main factors. First, when some FRP ships complete the operational period initially intended, a question may arise about whether this period can be extended. Second, FRPs are increasingly preferred for replacement weight-saving solutions, in which case, many critical parts can experience fatigue-stimulating stress levels. In addition to these two factors, there is always the issue of fatigue in the structural joints, which are usually zones of stress concentration, complex multi-axial loading, and low-quality workmanship. Therefore, fatigue is becoming an important issue for FRP marine structures.

Design against fatigue failure is sometimes difficult, even for structures made of metals such as steel and aluminum, because of the interrelated influence of a number of factors. These include microstructure and material properties, dimensions and geometry, production techniques, loading history, and environmental effects. Nevertheless, design against fatigue in metal structures has been relatively successful; because, regardless of the effects of these factors, metals, as well as welded joints, tend to follow power law stress-fatigue life relations and the linear fatigue damage accumulation [Palmgren (1924), Miner (1945)]. By contrast, design against fatigue in FRP structures encounters two major difficulties. First, the number of factors affecting their fatigue life inevitably increases given the complex structure of the FRP laminate, which is a combination of two components, matrix and fibers, with quite different properties. The second difficulty, and probably more important, is that the limited number of studies for marine applications suggest that the damage accumulation processes in FRP may not obey the simple linear relations encountered in metals. Such a difficulty suggests that current fatigue guidelines for steel ship structures may be totally inadequate for FRP ship structures. A simple example is the fact that FRP damage accumulation may be affected by the loading frequency, which is not usually the case with metals; this means that a frequency parameter must be included in the damage accumulation model for an FRP structure.

In order to address the aforementioned difficulties, an experimental and analytical investigation was undertaken at the Center for Structural Dynamics Research of The George Washington University. The investigation concentrated on two major tasks. The first task was an extensive literature search for publications that concern fatigue-related issues for FRP composite laminates and joints. Specific attention was paid to all pertinent fatigue damage accumulation theories proposed in the literature. The second task encompassed an extensive testing program to

enhance the understanding of fatigue processes in FRP laminates, provide enough experimental data for assessment and improvement of the methodologies identified under the first task, and to serve as a basis for development of new such methodologies.

This report summarizes the most important findings under both tasks. It contains two major sections, each dealing with one of the tasks. The first section describes the physical aspects of fatigue damage in FRP laminates, the analytical means of characterizing constant amplitude fatigue data, and the more significant damage accumulation studies reported. The issues related to the effect of parameters such as loading frequency, void and fiber content, temperature, and environment, (seawater and humidity) are not considered here. These efforts are recommended for future studies. The second section discusses the testing program and the preliminary results obtained.

FATIGUE DAMAGE OF FRP LAMINATES

PHENOMENOLOGICAL ASPECTS

In FRP laminates, fatigue damage may manifest itself as either fiber breakage or matrix cracking, but, in most cases, it is a combination of both. The particular form of damage depends on the laminate reinforcement type (uni-, bi- or multi-directional), the loading mode (tensile or compressive), and the orientation of the loading with respect to the fibers.

When a unidirectional composite is loaded by longitudinal tensile stress parallel to the fibers, the surrounding matrix may undergo a fatigue process of cracking in the direction transverse to the fiber direction before any local fiber breaks [Talreya (1987)]. These cracks are initially randomly distributed and, if the local strains are low, remain arrested by the surrounding fibers.

When the local strains become higher than a certain threshold, a fiber may break; the event being assisted by the previously created matrix cracks. A broken fiber causes shear stress concentration and debonding of the fiber-matrix interface near the two broken tips. The debonded zone acts as a stress concentrator leading to additional matrix cracking in a direction perpendicular to that of the loading and the fiber. Such progressive crack growth eventually leads to a visible macro-crack extending to the free interface of the laminate. Unidirectional composites are known to be quite sensitive to loading inclined to the direction of the fibers: only a few degrees of misalignment can cause the strain at failure to reduce by half [Reifsnider (1990)]. In such a case, the predominant damage mode is matrix cracking along the fiber-matrix interface; this is the process that controls the fatigue strength.

Unidirectional composites are rarely used in practice. More common are the angle-ply laminates in which unidirectional laminas are stacked in alternating directions. Angle-ply laminates are usually composed by 0/90° stacking (cross-ply laminates), although plies at other angles, usually $\pm 45°$, are also included in the stack to obtain more uniform (isotropic) material properties in all directions. The primary fatigue damage of angle-ply laminates consists of matrix cracking along the fiber direction in those plies whose fibers are not aligned with the loading direction [Reifsnider (1980)]. The cracking process continues until each off-axis ply attains a stationary crack saturation state. After that, no new cracks develop because adjacent cracks reduce the local stress to such an extent that the material between them cannot develop new cracks. Such a saturation state is characteristic for the matrix and fiber materials and the laminate stacking sequence but seems to be independent of the loading. Therefore, it is commonly referred to as the "characteristic damage state" (CDS) [Talreya (1987)].

Fatigue damage is also assisted by interlaminar shear stresses and normal stresses in the

thickness direction. Such stresses naturally exist around free edges of undamaged laminates but also develop in areas damaged to the point of CDS. Therefore, the damage state following CDS is characterized by ply delamination. Delamination further promotes fatigue damage by allowing cracks in adjacent plies to connect with one another in the through-thickness direction. Once the matrix is weakened enough by cracking, fibers start to break and ultimate failure occurs at the maximum load of a cycle.

In addition to angle-ply laminates, two other types of FRP have found a wide application in marine structures. These are the chopped strand mat (CSM) and woven roving (WR) laminates. CSM composites, which are common in commercial marine craft, do not have a continuous, oriented fiber system: the fibers are relatively short and are randomly dispersed in the matrix during manufacturing. It has been found that the fatigue damage they develop is similar to those of laminates with continuous fibers [Owen and Howe (1968)]. The matrix-fiber interface first debonds along those fibers that happen to be oriented perpendicular to the loading direction. As the load cycling continues, damage spreads to fibers aligned at smaller angles to the loading direction. Damage accumulation seems to be accelerated by matrix cracking in the zones where the fiber density is lower as a result of the manufacturing process. This type of damage usually governs the fatigue behavior of CSM laminates at low stress cycles, which suggests that fatigue properties of these laminates in marine environment may be predominately matrix-controlled.

WR[1] laminates are common on larger naval ships such as minehunters. Three stages of fatigue damage are usually observed when a WR laminate is loaded in the warp direction

[1] A woven fabric consists of two sets of interlaced yarns in two (usually perpendicular) directions; one of the directions (usually in the direction of the loading) is referred to as 'warp' and the other is termed as 'weft'. The crossovers are known as 'undulations'.

[Tanimoto and Amijima (1975)]. First, transverse cracks initiate in the matrix at the undulations and gradually reach a stationary value. Second, these cracks propagate in a transverse direction along the weft fibers and tend to cause longitudinal cracks in the warp direction. The third and final stage is that of longitudinal crack saturation and laminate failure. Apparently, the undulations are the "weak links" of the WR laminates: they serve as local stress concentrators due to fiber bending. In general, WR laminates show fatigue resistance superior to that of CSM laminates but inferior to the non-woven uni-directional and cross-ply laminates [Davis, etal (1964)]. Their primary advantage over the cross-ply laminates is in reducing manufacturing costs, especially when the woven fabric is used in combination with a highly efficient fabrication method (e.g., the resin transfer molding process).

Obviously, there is significant difference between fatigue failures in metals and in FRP materials. Fatigue damage in metals tends to localize in the form of a single fatigue macro-crack. As it extends, a crack carries a severe stress concentration at its tip and therefore propagates until it reaches a region of low stress or some natural obstacle (e.g., a bolt hole). Fatigue damage in FRP laminates, as is evident from the previous discussion, is much more diffuse. Such a diffuse damage property inevitably exhibits local reduction of elastic moduli which attenuates any stress concentration and prohibits damage propagation. (Experiments with specimens containing a large rectangular hole with saw-cut corners, [Smith (1990)], showed that following one million load cycles, the only evidence of fatigue damage were whitened patches extending approximately 1.25" from the hole corners.) In general, catastrophic fatigue failure of an FRP structure by through-thickness crack propagation in the laminate is highly unlikely to occur.

Such a conclusion, however, does not suggest that structural design should disregard fatigue damage accumulation in FRP structures; it only points out that the concern for fatigue

failure should concentrate primarily on the structural joints. Three common types of joints used in FRP structures are bonded, bolted, and bonded-bolted. Fatigue damage in any of these joints may manifest in different ways than it does in the composite laminate itself. A bonded joint may fail due to a crack in the adhesive, while a bolted joint may exhibit bearing failure of the bolt hole. In any joint configuration, these failures may be supplemented by fatigue damage of the adherent laminate plates. Therefore, fatigue damage processes in FRP laminates should be studied in the context of structural joints. This conclusion to a large extent motivates the selection of geometry and configuration of the test specimens described later in the experimental section.

MODELING OF FATIGUE DAMAGE IN FRP LAMINATES

Modeling of fatigue damage has two major aspects: establishing a fatigue failure criterion and a damage accumulation rule. In the traditional approach to fatigue, the failure criterion relates fatigue failure (i.e. fatigue life) to the number of applied loading cycles to cause that failure (usually having fixed or constant amplitude). An analytical expression of the fatigue failure criterion is the S-N curve, which plots the stress level, S, of the constant-amplitude cycles against the characteristic[2] number of cycles to failure, N, at this stress level. In modeling fatigue damage with an S-N curve, the shape of the curve is usually fixed by an empirical parametric expression; these parameters are used to match the shape to a particular set of experimental data. Because of the large scatter of experimental fatigue lives, particularly at lower stress levels, practical measurement

[2] 'Characteristic' here is used to emphasize that fatigue is a highly stochastic phenomenon, thereby different cycles to failure may be associated with a particular stress level. In a most general sense, *N* should be treated as random number and assigned probability distribution. Accordingly, *N* is usually taken as the 'expected' cycles to failure but can be the cycles to failure corresponding to a certain probability of failure.

of these shape parameters requires statistical methods, such as linear and nonlinear regression analysis. The S-N curve alone cannot be used to predict fatigue failures under variable-amplitude loadings. A damage accumulation rule is thus postulated, usually by prescribing the damage done by n ($n<N$) cycles of magnitude S. This rule is often formulated independently from the S-N curve choice.

Probably a more sound approach, from a physical point of view, is to treat damage accumulation as the process of evolution of a damage parameter under the loading history. This evolution is most naturally specified in terms of a differential equation with respect to the loading cycles, although other mathematical expressions may also prove appropriate. Examples for the damage parameter are the residual stiffness and the residual strength reviewed later in the report. In association with such an approach, the failure criterion is postulated in terms of a critical (failure) value for the chosen damage parameter. Integration of the evolutionary damage equation can be done for both constant or variable-amplitude loadings. For the constant amplitude case, analytical integration is often possible, which also allows a relationship between the critical damage parameter and the fatigue life, N, to be established. From this relationship, an S-N curve model can also be derived, which puts the S-N curve approach on a more sound basis.

It is evident from the previous discussion, that, for theoretical as well as practical purposes, fatigue damage modeling should consider both constant and variable-amplitude loading situations. However, we prefer to discuss S-N curves, damage parameters, evolutionary and failure equations, and all other issues with constant-amplitude damage accumulation in FRP laminates in this section of the report. The next section of this report is devoted to the specific issues associated with fatigue damage modeling under variable-amplitude loadings.

Among all structural materials, fatigue of metals has been studied most extensively, and it

has been found that, almost exclusively, a metal's S-N curve is best expressed in the form of a power law as

$$N S^m = K \tag{1}$$

where m and K are known as the fatigue exponent and the fatigue coefficient. These are material parameters, determined usually from a linear regression fit of log (S) versus log (N) from experimental data. Another power-law relationship established in metal fatigue is the Manson-Coffin relationship, usually expressed as

$$\varepsilon_{ap} = \varepsilon_f (N)^c \tag{2}$$

in which ε_{ap} is the applied plastic strain amplitude, and ε_f and c are fatigue coefficients. The Manson-Coffin equation is usually employed in the context of local approaches to fatigue damage accumulation; only in such a situation can plastic strain magnitude be quantified from local material response due to stress concentration and/or residual stresses.

Because it is difficult to define plastic strain for composite materials, the Manson-Coffin relation has not found any application. However, due to its universality, the power law S-N curve is often used to characterize fatigue failures, especially when little information on the fatigue behavior of a particular material exists. In composite fatigue, this relationship is usually associated with the names of Hahn and Kim [1976] who preferred to express it as

$$s N^d = c \tag{3}$$

In this equation, d and c are model (material) parameters, and s is the ratio of the applied stress, S, and the material's ultimate strength, S_{ult}, i.e.,

$$s = \frac{S}{S_{ult}} \tag{4}$$

This ratio has found a considerable application as a measure of the loading severity in fatigue studies. Hahn and Kim also consider the semi-logarithmic S-N curve model in which the applied stress level is related to log(N). This is expressed as

$$s = k \log(N) + b \tag{5}$$

where k and b are material parameters and s is given by Equation (4).

These two models are compared in [Hahn and Kim (1976)] for experimental data obtained from $[0/\pm 45/90]$ glass/epoxy laminates for up to 10^6 cycles. It was concluded that, overall, Equation (3) gives a better fit than Equation (5) when the two models are compared over the entire range of fatigue lives obtained, although in the low-cycle fatigue range Equation (5) can provide superior results.

Another simple analytical S-N curve model is that proposed by Hwang and Han [1986a, 1986b]. The main difference between this model and those previously specified is that it represents in inverse power law, i.e.,

$$N = [B(1-s)]^{1/C} \tag{6}$$

in which B and C are model parameters. Equation (6) is derived as a particular case of the fatigue modulus concept combined with a strain failure criterion; both are discussed below in more detail.

Based on the fatigue data reported by Hwang and Han [1986b] for aerospace types of FRP laminates, and on that reported by Howson, etal. [1992], and Owen [1968] for marine types of composites, Read and Shenoi [1995] performed a comparison of the models specified by Equations (3), (5), and (6). They plotted all test data on a semi-logarithmic scale. (On such a scale Equation (5) plots as a straight line, Equation (3) plots as a bottom convex, and Equation (6) plots as a bottom concave.) The data from Hwang and Han [1986b], obtained from glass/epoxy laminates, is of typical low-cycle fatigue type (less than 10^5 cycles). For these data, the best fit was provided by Equation (6), but it was only marginally better than Equation (5). Howson, etal, [1992] reports results from two types of composites: one made of glass fibers in polyester, and another made of hybrid glass-aramid fibers. The longest fatigue lives obtained are above 10^5 but less than 10^6 cycles. For both composites it was concluded that Equation (5) provides the best overall fit. However, it could be easily observed that the fit was particularly poor for low- and high-cycle fatigue. For the low-cycle fatigue data alone (less than 20 cycles) Equation (3) gave the best fit. Owen and Howe [1968] report high-cycle fatigue results from glass/polyester CSM composites. The best fit was again obtained with Equation (6).

Although fatigue data for typical marine FRP laminates are relatively limited compared to aerospace laminates, it is evident from the quoted investigations that the fatigue behavior of the variety of FRP types encountered in marine applications may not be characterized by a single analytical form of the S-N curve. Moreover, which S-N curve model is to be used may have to be decided for each particular material. Therefore, it is highly desirable to have a more general fatigue damage model, based on the micro mechanisms of composite damage, from which particular

damage models can be formulated to fit particular applications. In FRP fatigue, theoretical background for such a model is provided by three somewhat related concepts: stiffness degradation, fatigue modulus degradation, and strength degradation.

The concept of stiffness degradation stems directly from the diffuse character of the fatigue damage in composite laminates, as discussed previously. On the macroscopic scale, the effects of the numerous matrix cracks, fiber-matrix debonds, fiber breaks, and ply delaminations result in reduction of stiffness. The reduction of stiffness can therefore be used as a measure of the damage developed. The residual stiffness approach was proposed by Yang, et al. [1989, 1990]. The basic assumption of the approach is that the rate of degradation of residual stiffness is a power function of the number of cycles. This can be expressed as

$$\frac{d E_n}{dn} = -E_0 Q v n^{v-1} \tag{7}$$

in which E_0 and E_n are the initial stiffness and the stiffness after n applied cycles, respectively. Q and v are model parameters which account for the influence of applied stress level, loading frequency, and environment. Integration of Equation (7) renders:

$$E_n = E_0(1 - Q n^v) \tag{8}$$

Based on the experimental data, it was suggested that Q depends on v linearly, i.e.

$$Q = a_1 + a_2 v \tag{9}$$

and that, ν, on its part depends linearly on the applied stress level, S, i.e.

$$\nu = a_3 + B\,S \tag{10}$$

By using Equations (9) and (10), Equation (8) can be expressed as

$$E_n = E_0[1-(a_1 + a_2 a_3 + a_2 BS)n^{a_3+BS}] \tag{11}$$

Thus four parameters, a_1, a_2 ,a_3, and B, independent of the applied stress level S, completely define the above residual stiffness model.

If a failure criterion is postulated, an S-N curve expression based on Equation (11) can be developed. In a later study, Lee, et al., [1996] postulated that failure takes place when critical strain is reached. This study actually deals with variable-amplitude damage accumulation but, as explained in the next section, the specifics of the approach allows it to be applied to constant-amplitude situations as well. Accordingly, the strain at the failure cycle N is defined somewhat empirically as

$$\varepsilon_N = \frac{S}{E_0} + a_0 \frac{S_{ult}}{E_0} \tag{12}$$

From Equation (11), the fatigue life, N, can be expressed as a function of the stiffness at failure, E_N, as

$$N = \left[\frac{1 - E_N / E_0}{a_1 + a_2 a_3 + a_2 B\,S}\right]^{1/(a_3+B\,S)} \tag{13}$$

Considering that $E_N = S / \varepsilon_N$ and taking into account Equation (12), the fatigue life can be expressed as

$$N = \left[\frac{1 - \dfrac{S}{S + a_0 S_{ult}}}{a_1 + a_1 a_2 + a_2 B S} \right]^{1/(a_3 + B S)} \tag{14}$$

which is the sought after S-N curve formula. Evidently, it provides for five independent model parameters, a_0, a_1, a_2 ,a_3, and B, which are to be determined from experimental data. Obviously, this is a much more involved task than determining the two coefficients of the power law S-N curve (3). To this end, according to the procedure suggested by Yang, etal, [1990], residual stiffness is measured during a constant amplitude test at a particular stress level: E_1, E_2, ..., E_k. at cycles n_1, n_2, ..., n_k. respectively. By linear regression of the residual stiffnesses, E_k, with respect to the loading cycles, n_k, the model parameters Q and v can be determined as evident from Equation (8). By subsequent regressions with respect to different loading levels, S, the parameters a_1, a_2 ,a_3, and B can also be found as suggested by Equations(9) and (10).

It is worth noting that in the approach described by Yang, et al., [1989, 1990], the residual stiffness approach is applied in a probabilistic form. In particular, the initial stiffness, E_0, and the two model parameters, Q, v, and B are considered to be random variables. At the same time, a_0, a_1, a_2, and a_3 are still treated as deterministic. The experiments indicated that the distributions of both E_0 and B are reasonably well modeled as log-normal. Thus, the probability distribution of E_0 is fully characterized by the mean and the standard deviation of $\ln(E_0)$, μ_0 and σ_0; and that of B, by the mean and the standard deviation of $\ln(B)$, μ_B and σ_B. Accordingly, the probability distribution of the residual stiffness at the nth cycle, E_n, depends on three deterministic parameters,

a_1, a_2, and a_3, and on the probability distributions of two random variables, E_0 and B. This brings to seven the total number of independent parameters of the model (a_1, a_2, a_3, μ_0, σ_0, μ_B, and σ_B) if the interest is on the probability distribution of the residual stiffness only.

With this objective Yang, et al [1990], applied the residual stiffness to analyze experimental data from constant-amplitude fatigue tests of graphite/epoxy [0°, ±45°, 90°] laminates. They compared the experimentally obtained distribution of the residual stiffness with the theoretical obtained through Equation (11). Fairly good correlation between the experimental results and the theoretical predictions was reported.

If the objective is to compute the parameters of the S-N curve (14), the initial stiffness E_0 does not have to be estimated, but the static ultimate strength, S_{ult}, must be considered. In [Halpin, etal (1973)], S_{ult} was modeled as a random variable whose probability distribution is a two-parameter Weibull, i.e.

$$p_{S_{ult}}(S) = \frac{\alpha}{\beta}\left(\frac{S}{\beta}\right)^{\alpha-1} \exp\left[-\left(\frac{S}{\beta}\right)^{\alpha}\right] \tag{15}$$

If the theorem of total probability is applied to Equation (14) along with the expressions for the probability distributions of B and S_{ult},, the probability distribution of N and any other statistical parameter (e.g., its expected value) can be found. The total number of material parameters that need to be estimated from testing is eight (a_0, a_1, a_2, a_3, μ_B, σ_B, α and β). Note that only the first six of them are computed from the fatigue tests, while the distribution parameters of the ultimate static strength, α and β, are obtained from the static tests. In general, Yang's residual stiffness approach is quite complex and experimentally expensive, and therefore should be considered only if

other more simple approaches fail to provide satisfactory modeling of fatigue damage.

Based on the notion of degrading stiffness, Hwang and Han [1986a and 1986b] proposed the concept of fatigue modulus that is different from the stiffness (elastic modulus). Accordingly, fatigue modulus at the nth cycle, F_n, is defined as

$$F_n = \frac{S}{\varepsilon_n} \tag{16}$$

where ε_n is the resultant strain at the maximum load of the cycle. The basic assumption is again that the modulus degradation rate is a function of the number of fatigue cycles, which can be expressed in a form similar to Equation (7) with stiffness replaced by fatigue modulus [Hwang, etal, (1986b)]. More recently, it was suggested that this degradation rate is a function of both the number of fatigue cycles and the current value of the fatigue modulus [Hwang, etal, (1995)]. By following this more general assumption, the fatigue modulus degradation rate can be expressed as

$$\frac{dF_n}{dn} = -A\frac{C n^{C-1}}{B F^{B-1}} \tag{17}$$

in which A, B, and C are model parameters to be obtained from experimental data. Integration of this general equation renders

$$F_n^B - F_0^B = -A n^C \tag{18}$$

Thus, the number of cycles to failure, N, can be expressed as

$$N = [(F_0^B - F_f^B)/A]^{1/C} \tag{19}$$

in which F_f is the fatigue modulus at failure. Note that the above equation simply associates the number of cycles with the fatigue modulus at failure, but does not relate either of them to the magnitude of the stress cycle. A way out of this difficulty is offered again by the failure criterion. Similarly to Equation (12), it is possible to associate failure with the advent of failure strain. In a more simple form, the failure criterion can postulate that fatigue failure occurs at the same strain as the static failure of undamaged material, i.e.,

$$\frac{S}{F_f} = \frac{S_{ult}}{F_0} \tag{20}$$

Another approach, chosen by Hwang, et al., [1986b], is to model failure indirectly, by addition of another model parameter. To this end, they introduce a reference fatigue modulus, F_R, such that

$$\frac{F_f}{F_R} = \frac{S}{S_{ult}} = s \quad , \quad \frac{F_0}{F_R} = p \tag{21}$$

It can be shown that the p-parameter in the above equation has a simple physical meaning: it is the ratio of the strain at fatigue failure, ε_f, to the strain at static failure of undamaged material, ε_{ult}. Accordingly, the case p=1 corresponds to the strain failure criterion, Equation (20). The experimental data presented by Hwang, etal, [1995] demonstrates that, in all cases, "p" is quite close to unity.

The fatigue life, Equation (19), can now be expressed as

$$N = [M\,(p^B - s^B)\,]^{1/C} \tag{22}$$

where $M = F_R^B / A$. Although developed from the fatigue modulus concept, the above equation has no explicit use of fatigue modulus parameters. Instead, it contains four model parameters (p, M, B, C) that should be determined from the constant-amplitude experimental data.

Again, Equation (22) provides a generalized S-N curve model for fatigue life under constant-amplitude loading. Hwang, etal, [1995] refer to it as the modified fatigue life prediction equation (MFLPE). Note that for p=1 (strain failure criterion) and B=1 it results in the inverse power law S-N curve, Equation (6). Other S-N curve models can also be derived from the fatigue modulus concept, although not directly from Equation (17) or Equation (22). Consider the following particular forms of the general fatigue modulus degradation:

$$\frac{dF_n}{dn} = -A\frac{F}{n} \quad \text{(a)} \qquad \frac{\mathrm{dF_n}}{\mathrm{dn}} = -\frac{\mathrm{A}}{\mathrm{n}} \quad \text{(b)} \tag{23}$$

Integrating the above equations (this time taking n to vary from 1 to N) and taking into account Equation (21), renders for the fatigue cycles at failure

$$N = \left(\frac{s}{p}\right)^{-\frac{1}{A}} \quad \text{(a)} \qquad \mathrm{N} = \exp\left[\mathrm{M}(\mathrm{p}^{\mathrm{B}} - \mathrm{s}^{\mathrm{B}})\right] \quad \text{(b)} \tag{24}$$

respectively. The first of these equations is a form of the power law S-N curve, Equation (3), while the second is a form of the semi-logarithmic S-N curve, Equation (5). Thus, Hwang's

formula indeed provides quite a general framework for development of different fatigue damage models.

Fatigue damage within a composite laminate can not only degrade the elastic moduli, but can also lower its static strength. Based on this observation, the residual strength was proposed by Halpin, etal, [1973] as the physical parameter describing damage in composites. Much work on the residual strength approach has been done by Yang, etal, [1980, 1981 and 1983]. In particular they suggested that an equation for the rate of change of the residual strength S_r during the nth loading cycle can be expressed as

$$\frac{dS_r}{dn} = - A \frac{S_r^{1-m}}{m} \tag{25}$$

in which A and m are model parameters. It was also suggested that A depends on the applied stress at the nth cycle, S, and the initial static strength, S_{ult}. By integrating this equation, expressions similar to those developed for the residual stiffness and the fatigue modulus concept can be derived.

Literature reveals that the residual strength concept was proposed earlier than those of residual stiffness and fatigue modulus. It seems, though, that the residual strength concept has lost popularity among fatigue analysts at the expense of the residual stiffness approach (and the related fatigue modulus approach). The reasons are pointed out by Hashin [1985]. Clearly, because the residual stiffness is a non-destructive parameter, it can not only be calculated from specimen response without even interrupting the test but can also be measured on a structure of interest. Moreover, residual stiffness can in principle be determined analytically from a given crack

distribution. It has also been demonstrated that residual stiffness exhibits much less statistical scatter than residual strength. Finally, it may be noted that within Kachanov's concept of 'continuum damage', the residual strength approach would be equivalent to the residual stiffness approach as long as the material does not exhibit significant ductility (which is usually the case with FRP composites). Thus, it is highly unlikely if any practical model for fatigue damage accumulation in FRP laminates can be developed exclusively on the residual strength concept.

MODELING DAMAGE ACCUMULATION IN FRP LAMINATES

Cumulative damage theory is probably the only approach that can predict the fatigue life of a composite laminate under a multi-level stress history because application of fracture mechanics techniques is highly questionable due to the diffuse nature of fatigue damage in composites. In general, the cumulative damage approach postulates that a damage function, D, exist such that

$$D = \begin{cases} 0 & \textit{material never subjected to loading} \\ 1 & \textit{at failure} \end{cases} \tag{26}$$

In addition to the above requirements, damage, D, is postulated to be a monotonically increasing function of the loading.

For modeling damage accumulation due to fatigue, the main objective is to analytically express damage, D, caused by a segment of n constant-amplitude cycles with magnitude S given that, the applied cycles, n, is less than the constant-amplitude fatigue life, N. Following Hwang, etal, [1986a], for a composite material it can be most generally expressed as

$$D = D(D_0,\ n,\ S,\ f,\ T,\ M,...) \tag{27}$$

where D_0 is initial damage existing prior to the application of the considered loading segment, n is the number of fatigue cycles, S is the applied stress level, f is the loading frequency, T is the temperature, and M is the moisture content. The effect of the last three parameters on fatigue damage will not be considered in this section.

Considering the combined influence of the other three parameters, D_0, n, and S, on the fatigue damage accumulation, damage is assumed to be caused by a multi-level stress history. Therefore, not only does the damage contribution from each loading cycle need to be added, but the influence of the loading of each cycle on the damage caused by subsequent cycles needs to be identified, as well. This is quite a complex situation, which is rarely employed in practice. The first simplification is done by neglecting the effect of D_0; that is, by assuming that damage caused by the sequence of n cycles with magnitude S is always the same regardless of where this sequence occurs in the loading history. Such damage accumulation rules have been considered in the context of fatigue of FRP laminates and are discussed below.

The simplest damage accumulation law, which is commonly known as the Palmgren-Miner rule, [Palmgren (1924), Miner (1945)], assumes that damage contribution from each cycle of the loading history is independent from the other cycles. Therefore, the damage inflicted by n stress cycles with magnitude of S is simply

$$D = \frac{n}{N} \tag{28}$$

where N denotes the cycles to failure at S from the constant-amplitude S-N curve. For all stress levels this damage rule yields

$$D = \sum_{i=1}^{m} \frac{n_i}{N_i} \tag{29}$$

where n_i is the number of cycles having amplitude S_i.

In many situations, the rate of fatigue damage accumulation in composites may deviate significantly from that assumed in Equation (28). For example, Owen and Howe [1968] report that

$$D = B\left(\frac{n}{N}\right) - C\left(\frac{n}{N}\right)^2 \quad B, C > 0 \tag{30}$$

fits much better constant-amplitude data they obtained from CSM composites. Such an equation, however, has no particular benefit over the linear damage accumulation rule, Equation (28). Making damage a function of the ratio of n/N only implies that it is always the same regardless of the cycle's position in the loading sequence. Therefore, there is always a measure of damage which accumulates linearly under constant-amplitude loadings.

In connection with Equation (1), the Palmgren-Miner rule, Equation (29), is used almost exclusively in metal fatigue. By treating a multi-level stress time-history as a random process, Equations (1) and (29) allow a simple stochastic approach to be used to estimate cumulative damage. This approach is applicable when the loading can be described as a zero-mean, Gaussian, and narrowband stochastic process. In such a case, the amplitudes of the fatigue cycles possess a Rayleigh probability distribution, which can be expressed as

$$p_S(S) = \frac{S}{S_{rms}^2} \exp\left(-\frac{S^2}{2 S_{rms}^2}\right) \tag{31}$$

In the above formula S_{rms} denotes the root-mean-square value of the stochastic stress history. By using the Palmgren-Miner hypothesis, Equation (28), and the power-law S-N curve, Equation (1), the expected fatigue damage E[D] and the expected cycles to failure E[N] are expressed as

$$E[D] = \frac{1}{E[N]} = \frac{1}{K} E[S^m] = \frac{1}{K} \int_0^\infty \frac{S^{m+1}}{S_{rms}^2} \exp\left(-\frac{S^2}{2 S_{rms}^2} \right) dS \tag{32}$$

The integration of the above equation renders

$$E[D] = \frac{1}{E[N]} = \frac{1}{K} 2^{\frac{m}{2}} S_{rms}^m \Gamma\left(1 + \frac{m}{2} \right) \tag{33}$$

where $\Gamma(\bullet)$ is the gamma function. Equation (33) is known as the "Rayleigh approximation" equation [Miles (1954)].

An expression similar to Equation (33) can be derived if the Palmgren-Miner rule is applied in conjunction with the semi-logarithmic S-N curve model, Equation (5). To this end, assume first that the semi-logarithmic model is expressed as

$$\log(N) = b - a S \tag{34}$$

in which b and a are the parameters of the model obtained from a linear regression of the experimental data. This equation can be further rearranged as

$$N = 10^{b-aS} = e^{\bar{b}-\bar{a}S} \tag{35}$$

where

$$\bar{b} = b\ln(10) \quad \bar{a} = a\ln(10) \tag{36}$$

The expected damage can then be expressed as

$$E[D] = \frac{1}{E[N]} = e^{-\bar{b}} \int_0^{\infty} \frac{S}{S_{rms}^2} \exp\left(-\frac{S^2}{2S_{rms}^2} + \bar{a}S \right) dS \tag{37}$$

Performing the integration in Equation (37) gives

$$E[D] = \frac{1}{E[N]} = e^{-\bar{b}} \left[1 + \bar{a} S_{rms} \exp\left(\frac{\bar{a}^2 S_{rms}^2}{2} \right) \Phi(\bar{a} S_{rms}) \sqrt{2\pi} \right] \tag{38}$$

in which $\Phi(\bullet)$ denotes the Gaussian cumulative distribution function.

Damage accumulation rules in which D cannot be expressed as a function of n/N have also been applied to composite materials. A compilation of such models can be found in Hwang, etal, [1986a]. The damage function in such a case can be expressed as D(n,S), as suggested in Equation (29), or alternatively as D(n,N) because S is always a single-valued function of N. Derivation of such models can be based on pure empirical considerations from particular experimental data or on the grounds of a more physical damage hypothesis such as the residual strength, residual stiffness, or fatigue modulus concepts reviewed in the previous section.

An example of the empirical approach is the damage accumulation rule suggested by Hashin [1985]. Based on observations that fatigue damage varies nearly logarithmically with the

number of cycles, he suggests that damage accumulated after n constant-amplitude cycles with magnitude S is

$$D = \frac{\log(n/N_e)}{\log(N/N_e)} \tag{39}$$

in which N_e is a model parameter.

An example of the physical approach is a damage accumulation model based on the residual strength concept also proposed by Hashin [1985]. The model is expressed as

$$D = \frac{1 - s_r}{1 - s} \tag{40}$$

in which s_r is the ratio of the residual strength, S_r, to the ultimate static strength, S_{ult}. The relationship between s_r and the applied number of cycles, n, is provided by Equation (25).

Another damage model of this type is proposed by Hwang and Han [1986b]. This model is based on Equations (23b) and (24b) and is expressed as

$$D = \left(\frac{s}{1-s}\right)\left(\frac{n^c}{B - n^c}\right) \tag{41}$$

The model parameters B and C in the above equation are found from the inverse power law S-N curve, Equation (6).

Many possibilities for development of nonlinear damage accumulation laws exist when the process is based on the degradation models discussed in the previous section. Hwang, et al.,

[1986b, 1995] demonstrate this in the context of the fatigue modulus concept. In Hwang, etal, [1995], they considered four different types of damage accumulation. According to these laws, the accumulated fatigue damage after n cycles with amplitude S is taken as

$$D=\frac{F_0-F_n}{F_0-F_f}\ (\mathrm{I}) \quad D=\frac{\varepsilon_n}{\varepsilon_f}\ (\mathrm{II}) \quad D=\frac{\varepsilon_n-\varepsilon_0}{\varepsilon_f-\varepsilon_0}\ (\mathrm{III}) \quad D=\frac{F_0^B-F_n^B}{F_0^B-F_f^B}\ (\mathrm{IV}) \tag{42}$$

In the above equation, (F_0, ε_0), (F_n, ε_n), and (F_f, ε_f) are the fatigue modulus and the maximum strain at the beginning, after n cycles, and at failure under constant-amplitude loading, respectively. Application of the above damage accumulation hypotheses to different degradation models derived as particular cases of Equations (19) and (24) allowed these damage models to be expressed in terms of the p, M, A, B, and C parameters defined in Equations (19) and (24). In particular, Equation (19) expresses the damage models of Equations (42) as

$$D=\frac{1}{p-q}\left[p-\left(p^B-\frac{n^C}{M}\right)^{1/B}\right] \quad (\mathrm{I}) \qquad D=q\left(p^B-\frac{n^C}{M}\right)^{-1/B} \quad (\mathrm{II})$$

$$D=\frac{q}{p-q}\left[p\left(p^B-\frac{n^C}{M}\right)^{-1/B}-1\right] \quad (\mathrm{III}) \qquad D=\left(\frac{n}{N}\right)^C \quad (\mathrm{IV}) \tag{43}$$

Use of nonlinear damage models such as Equations (39)-(43) in multi-level stress histories cannot be done by simply adding up damage due to cycles with different stress levels. To perform the summation, a procedure based on the concept of 'equivalent damage' is usually applied. To explain the procedure, assume that damage is specified in the form D(n,S) and that a loading

history consisting of n_1 cycles of magnitude S_1, n_2 cycles of magnitude S_2, n_3 cycles of magnitude S_3, and so on, is applied. After the application of n_1 cycles of magnitude S_1 the accumulated damage is

$$D_1 = D(n_1, S_1) \quad D_1 < 1 \tag{44}$$

The damage-equivalent cycles n_{2e} of magnitude S_2 which cause an amount of damage equal to the accumulated damage, D_1, is found by solving the following equation:

$$D_1 = D(n_{2e}, S_2) \tag{45}$$

The accumulated damage after the application of the second sequence of n_2 cycles of magnitude S_2 is now found as

$$D_2 = D(n_2 + n_{2e}, S_2) \quad D_2 < 1 \tag{46}$$

The procedure is repeated until failure is achieved (D_k=1) or the loading sequence is exhausted.

Such a procedure, although conceptually simple, may actually be quite difficult to apply in practice. First, during each step of obtaining damage-equivalent cycles, Equation (45), a nonlinear equation may have to be solved. This can make the procedure quite expensive computationally, given that maritime loadings of interest may contain millions of cycles before final failure is achieved. A much more serious problem, however, is represented by the broadband loadings. A load cycle identification scheme such as the rainflow algorithm may be used to determine the individual fatigue cycles of a broadband loading history. The lack of order in the fatigue cycles obtained by such a scheme, however, makes the rainflow algorithm practically inapplicable in connection with damage models like those considered above. In other words, the damage

accumulation theory does not possess analytical means to compute accumulated fatigue damage from nonlinear models and broadband loading histories.

A possible way out of this difficulty may be found by systematic application of probabilistic approaches (random vibration methods in particular) to evolutionary damage equations such as the degradation models specified by Equations (7), (17) and (25). However, application of probabilistic approaches to the problem of composite fatigue under variable-amplitude loadings are quite rare. One of the few studies is that of Lee, et al., [1996] who applied Yang's residual stiffness model, Equations (7)-(15), to variable-amplitude fatigue damage accumulation under block-type spectrum loadings. Specifying the fatigue loading in terms of a block-type spectrum is quite common in aerospace applications, however, is rarely used in marine applications. Rather than evaluating the parameters of the model from constant-amplitude loadings, they applied Equations (11) and (14) directly to fatigue data obtained under the block loadings without any modification. In this approach, however, n refers not to the nth loading cycle but to the nth loading block in the spectrum. Accordingly, N designates the block loading number at which failure occurs. The stress variable S in Equation (11) is postulated to be equal to the maximum stress in the block. The other assumptions of the model, particularly those on the probability distributions of E_0, S_{ult}, and B are preserved. To validate this approach, experiments with $[0°/90°/\pm 45°]$ graphite/epoxy laminates were carried out. Four block loading sets with different stress levels were generated. In predicting the statistical distribution of the fatigue life for any one of the data sets, the remaining three data sets were considered as a basic data from which the model parameters were estimated. The theoretical predictions were then correlated with the experimental results of that data set. Fairly good agreement between the predictions and experiments was found. These positive results, however, should be taken as evidence for the

applicability of the residual stiffness model to composite fatigue. At the same time, it seems dubious that the method described above can be applied directly to applications which do not specify the fatigue loading as block-type spectra.

Unfortunately, experimental data on cumulative damage is mostly related to composites in aerospace applications. In fact, the majority of the data is for two-stage loadings and low-cycle fatigue. For such data Read and Shenoi [1995] compare some of the above damage accumulation models. In particular, they considered the Palmgren-Miner rule, Hashin's damage model, Equation (39), (which for two stage-loadings and N_e=1 is the same as a method presented by Hashin and Rotem [1978]), Hashin's residual strength model, Equation (40), and the fatigue modulus model of Hwang and Han , Equation (41). They conclude that, in most cases, the predictions made using Hashin and Rotem's method, are closest to experimental data, while the approach of Hwang and Han tends to give the most inaccurate predictions. In many instances, the predictions of the Palmgren-Miner approach were close to those of Hashin and Rotem's method. Overall, the linear damage accumulation rule made predictions which were on the non-conservative side.

Based on the studies reviewed, the only sure conclusion that can be made is that sufficient experimental data pertinent to fatigue of FRP laminates under multi-level stress histories simply do not exist. Therefore, it is too early at this stage to draw conclusions about which damage accumulation approaches will render the most accurate results in marine/naval applications--all options should be considered in the study.

EXPERIMENTAL EVALUATION OF COMPOSITE LAMINATE AND JOINT DETAILS

The composite test program discussed in this report was set up to provide a realistic insight into the static and fatigue behavior and damage accumulation of FRP laminates and joints. To study the fatigue damage accumulation, several different specimen configurations were designed and fabricated for characterization under constant and variable amplitude fatigue loadings. The objective of the tests on the base specimens was to investigate the fatigue strength of a bi-directional base laminate under four different axial load scenarios. Test scenarios included two loading orientations, 0/90° and $\pm 45°$, with respect to the laminate lay-up, and two different cases of load transfer. One case of load transfer, referred to as 'passive bearing' represented a plate clamped and loaded at its two remote ends. The plate had a hole in the middle which contained a non-load-bearing bolt. The other case of load transfer, referred to as 'active bearing', represented a plate clamped at one remote end and loaded through a pin which passed through a hole close to the non-clamped end.

The base laminate consisted of an alternating 0/90° stacking sequence of thirty plies made of 0.025" thick WR glass fabric and 510-A vinyl ester resin. This lay-up was fabricated by Hardcore DuPont Composites, L.L.C., into several panels measuring 2 feet by 3 feet using the SCRIMP process. The post cure cycle for the panels was 2 hours at 160° F. The panels were then cut into specimens. Figures (1a) and (1b) show the geometry of typical passive-bearing and active-bearing specimens.

To investigate the behavior of composite joints under static, constant amplitude, and variable amplitude cyclic loadings, three different joint configurations were designed and fabricated. These three configurations were: bonded only, bolted only, and both bonded and

bolted. Each configuration represented a single butt-strap joint. Specimens were made of the laminate described above, but with an additional fifteen ply laminate, of the same lay-up, attached to either side of the thicker laminate. Both thicker base laminate and the thinner joint adherends were oriented and loaded along the 0/90° material direction. Figure (2) shows the typical geometries of joint specimens.

STATIC TESTS

The static tests consisted of ultimate tension and compression strength tests which were designed to characterize the static behavior of the specimens and to aid in selecting the appropriate stress levels for the fatigue tests. In all configurations, some test specimens were instrumented with strain gages in order to monitor the structural response at selected points of interest. Strain gage locations are shown in Figures (3) through (5). Static test results for both specimens and joints are presented in Table (1).

The static test results for the passive bearing test of the base laminates are presented in Figures (6) through (14). It can be seen from Figure (6), that the fracture surfaces of tensile specimens pass through the bolt hole forming a 90° and 45° angle with the loading direction, for 0/90° and $\pm 45°$ lay-ups respectively. For the compressive tests, the $\pm 45°$ specimens failed, forming an X- shaped damage zone centered at the hole and swelling in the intersection of the two branches of the X. The 0/90° compressive specimen was loaded up to the capacity of the testing machine and did not fail. During each test, applied load and actuator movement were recorded. Actuator movement was measured using a linearly varying displacement transducer (LVDT). The load-deflection curves of the 0/90° specimens show a significant qualitative difference with those of the $\pm 45°$ lay-up (compare Figure (7) with Figure (11), and Figure (9) with Figure (13)). In the

former figures, the curves remain almost linear up to the failure point, while in the latter figures, there is a considerable increase in the compliance as the load increases. Moreover, the final deflection reading is much higher than that of the cross ply counterpart. This is obvious because of the fundamental difference between the fiber-dominant and matrix-dominant behavior shown by the cross-ply and angle-ply lay-ups, respectively. The same trend can be observed in load-strain curves (compare Figure (8) with Figure (12), and Figure (10) with Figure (14)). As can be seen on the load-strain curves, the constraint provided by the bolts causes the compressive strain at position number 4 of the passive bearing case to almost vanish.

The static test results for the active bearing case are shown in Figures (15) through (25). As shown in Figure (15a), in tension tests, both lay-ups exhibited a shear-out failure; however, the shear-out surfaces in the angle ply case are parallel to the loading direction, while those of the cross-ply lay-up are inclined. This means that both specimens failed in the least fiber-dominant direction. Unlike the passive bearing specimens, the stress-deflection curves for the tensile test of the cross-ply and angle-ply lay-ups have barely any qualitative difference, except for some more ductility in the 0/90° case, as shown in Figure (16). Regarding strains, the somewhat inconsistent final portions of the strain versus nominal stress traces, may be due to local differences intensified by the localized damage. In the compression tests, the stress-deflection curves are totally different. While the angle-ply laminates respond almost monotonically to failure, the cross-ply laminate specimens, besides their higher strength, show a step-like trend, meaning that some kind of secondary resistance forms after each incremental shear-out. This secondary resistance may have been produced by the accumulation of the material removed during the shear-out process in front of the shear-out path, which increases the effective thickness. Both for the cross-ply and angle-ply lay-ups, the compressive tests were terminated due to the limitations dictated by the fixture and

specimen configurations. It is obvious from Figure (15) that the failure is only a partial shear-out, indicating that both specimens may have carried a higher load if the testing equipment were of greater capacity. However, it should also be kept in mind that the active bearing test was intended to characterize the static and fatigue *bearing*, not shear-out, failure; meaning that in both the tensile and compressive strength cases, the tests could be stopped before actual shear out occurred. In fact, in all static active bearing case tests, bearing failure occurred well before shear-out failure. In such cases, a deviation from linearity in the stress-deflection curves was evidenced.

The static test results of the joints are presented in Figures (26) through (37). Although no photograph is available, the adhesive failed in the bonded specimen tests. Figure (26) shows the bolted-bonded joint; after first demonstrating a bond failure, the specimen finally fails in a shear out mode. Figure (27) shows that the bolted joint exhibits a combination of cleavage-tension and shear-out failure. In the compressive regime (Figures (28) and (29)), the bonded joint has delaminated in both laps and one of the adherends failed due to the combined effect of contraction and buckling. Similarly, the bolted joint has shortened and buckled asymmetrically (mode 2) and all joint components have delaminated as a consequence. The bonded-bolted joint showed an early bond failure and a final failure due to a symmetric buckling and a consequent delamination in all components. Comparing the stress-deflection curves of different joints, one can conclude that the bolted-bonded joint is the most advantageous configuration as far as the tensile strength is concerned. The bolted-bonded joint had a higher initial stiffness, a higher failure load and a very good ductility compared with the other two specimens. On the other hand, in the compressive regime, although it had a higher initial stiffness, its strength and ductility were lower than those of the bolted configuration. This may be due to the difference in the buckling mode, since a mode II buckling requires a higher load in order to occur.

FATIGUE TESTS

The fatigue tests typically consisted of two or three specimens tested at each desired constant amplitude or variable amplitude (RMS) stress level. All tests were performed at constant frequency (the frequency and other pertinent test data and results for all specimens are listed in Tables (2) through (7)). The variable amplitude loading represents a segment of a sinusoidal time history composed of 10,000 end points, which, with the assumption of stationarity and ergodicity, can be shown to be a narrowband Gaussian process. This segment is repeated until failure occurs.

The data, presented here for each specimen type, consist of experimental fatigue lives, a brief explanation of the failure modes, peak deflection data, temperature data, S-N curves, and the random fatigue lives predicted by the Rayleigh approximation. A comparison between the geometric mean of the experimental fatigue lives and predicted fatigue lives can be found in Table (8). Before discussing the data, the significance of deflection and temperature data is addressed.

The deflection (actuator displacement) data were used as a measure of the overall specimen compliance. These data were also used as an indicator of fatigue damage. Therefore, when experimentally investigating the damage accumulation, it is useful to collect deflection data. Based on the peak deflection data, the evolution of damage during the fatigue life can be calculated from:

$$D_n = 1 - \delta_i / \delta_n \tag{47}$$

where D_n , δ_i, and δ_n stand for the deflection-based damage at cycle n, initial peak deflection, and the peak deflection at cycle n, respectively. This methodology may be able to predict the variable amplitude damage accumulation as well.

The acquisition of temperature data was prompted both by the early observations in the current fatigue test program and by the survey of existing literature. During the fatigue tests, the temperature of the specimens increased significantly from the ambient temperature in the testing laboratory. The response of the material during the temperature rise was so severe, especially during the low cycle fatigue tests with relatively high frequency (e.g., 3 HZ), that the material appeared to smolder, producing ash and a burnt plastic smell as the test went on. Since such a reaction is clear indication of a change in mechanical properties, one could easily conclude that the material behavior has some level of temperature dependency. This conclusion, when accompanied with the creep observed during the static tests, indicated that the material was visco-thermoelastic. A literature search revealed that the temperature dependence of FRPs is a common concern among researchers. It has been observed that the temperature change during non-isothermal conditions, caused by thermal or mechanical sources, alters the material behavior and thereby controls the mechanical characteristics. The temperature rise may be caused by different damage and/or damping processes occurring in the plastic constituents, especially under cyclic loads. The cyclic energy induced into the system is dissipated by heat convection, different forms of damage in the material, and hysteretic damping. The latter two forms of energy dissipation are associated with temperature increase which, in turn, deteriorates the mechanical properties. Therefore, the mechanical temperature increase and its consequences are expected to worsen when the load frequency is increased. Many authors have investigated the temperature effects in FRPs [Miyano etal (1994) and Nakai and Yamashita (1994)]. Since the temperature dependency of these materials is largely due to the properties of the resin matrix, which typically has a higher volume content in marine type FRPs, the consequences of temperature dependence can be more severe for marine composites. As discussed earlier, the plastic constituents of FRPs are visco-thermoelastic

materials. Therefore, temperature effects are coupled with creep, relaxation, and time-under-load effects. More precisely, while the temperature effects dominate under high frequencies, creep effects dominate at low frequencies. In their 1979 work, Sun and Chan [1979] investigated the interaction of temperature and creep under different stress levels for graphite epoxy composites. They concluded that the fatigue strength of FRPs varies in a two dimensional space formed by stress level and load frequency. The latter axis reflects the effects of creep and temperature in low and high frequency ranges, respectively. While the temperature dependence is discussed by many authors (e.g., Oberbach and Heese [1972], Nakada et al [1991]), many others have considered the other extreme of the frequency axis, investigating the time and creep dependence of the fatigue properties of FRPs. Mandell and Meier [1983] have investigated the effect of loading time on the tensile fatigue of glass-reinforced epoxy. Morinaka, Fujii, and Amijima [1991] have studied the effect of loading and unloading duration on the fatigue damage process of plain woven glass fiber reinforced plastics. They concluded that the fatigue life is affected by both the loading and unloading duration. Based on these and similar observations, which is not our goal to comprehensively cover, it seems necessary to incorporate the temperature, frequency and creep effects in fatigue life and damage accumulation models. In an effort to incorporate the temperature and creep effects in fatigue life models, Sun and Chan in the aforementioned paper, have presented two separate fatigue life models for temperature-dominant and creep-dominant behaviors. Amijima, et al. [1982] have found an experimental frequency dependent S-N curve. Tsai, et al [1987] assumed the strain to beas the governing variable and defined the dynamic modulus (which is affected by test frequency) so as to incorporate the frequency effects in their fatigue life model. Miyano et al [1994] have implemented the invariability of the slope of the S-N curves with temperature and frequency to derive a relationship for predicting the flexural fatigue strength at

arbitrary conditions. While the aforementioned fatigue life models have taken into account the temperature dependence of damage, it is important to note that the material temperature is, in turn, damage dependent. In particular, the damage itself can cause a substantial material temperature increase. Therefore, logically, temperature can be used as a measure of damage. For example, Neubert, Schulte, and Harig [1990] have investigated the damage development in CFRPs by monitoring load-induced material temperature changes. However, in applying the change in temperature as a measure of damage, one should be extremely cautious, since the temperature rise cannot be attributed solely to the damage. Other mechanisms, such as hysteretic damping, may also contribute to the temperature increase. Therefore, the accurate temperature-based damage accumulation model is the one in which other effects are excluded. The following sections describe the data collected for each of the passive, active, and joint specimens.

PASSIVE BEARING CASE

Experimental Fatigue Lives : The fatigue lives obtained from constant and variable amplitude tests of the passive bearing case are presented in Tables (2) and (3), respectively.

Failure Modes : The failure for all fatigue specimens was defined as occurring when the peak deflection reached four times the initial value. For the variable amplitude case, this definition considers the largest of the peaks in each of 10,000 load points. For $0/90^{\circ}$ lay-ups, at failure, a transverse whitened damage band appeared in the specimen passing across the bolt hole, as shown in Figure (38b). For the $\pm 45^{\circ}$ angle-ply lay-up, however, damage was in the form of an X-shaped whitened band passing through the gage section, with each branch of X forming approximately a 45° angle with the loading direction, as shwon in Figure (38a).

Deflection Data : The deflection data are presented in the form of peak deflection versus

number of cycles curves in Figures (39) through (41). All these figures, and subsequent figures, indicate that the tensile deflection governs the failure; and, in most cases, the compressive deflection does not change considerably. The obvious trend of the tensile deflection curves indicates that, no matter what the stress level or lay-up, the peak deflection does not change considerably until the final failure is approached. According to the discussion in the previous paragraphs, a compliance-based experimental damage accumulation curve can be obtained from equation (47). The results for some specimens of the cross-ply and angle-ply lay-ups are shown in Figures (42) and (43), respectively.

Temperature Data : The temperature data are shown in the form of temperature versus normalized number of cycles in Figures (44) through (52) for different stress levels, lay-ups, and loading scenarios. The large number of specimens shows the wide qualitative difference between the curves of different cases, and indicates the temperature rise is a consequence of interaction of many parameters. The specimen temperature can build up in different ways, depending on how those parameters interact. Another noteworthy point is that there is a close resemblance between Figures (42) and (48) and between Figures (43) and (47); which means that the temperature rise has been able to capture the main features of the compliance-based damage accumulation curves very well. This may indicate that temperature is an alternative basis for phenomenological damage accumulation models.

S-N Curves : The experimental fatigue lives from the constant-amplitude tests of the passive-bearing specimens are presented in Figure (53) on a log(S)-log(N) scale and in Figure (54) on a S-log(N) scale. Both logarithmic and semi-logarithmic S-N curve models were fit to these data by linear regression. It can be seen that the experimental data from the 0/90° specimens exhibit very little scatter, and although the data fit both S-N curve models fairly well, a slightly

better fit can be seen using the Log-Log model. The data from $\pm 45^{\circ}$ test setup exhibit much more scatter, and although not fitting either S/N curve model particularly well, appear to fit the logarithmic model better than the semi-logarithmic model.

Random Amplitude Fatigue Lives : Experimental variable amplitude fatigue lives are obtained by applying the aforementioned time history to the specimens at different RMS stress levels; and the analytic fatigue lives are calculated by following the fatigue damage accumulation models (Equations 33 and 38) discussed previously. Comparison between the variable-amplitude fatigue results and the Rayleigh approximation, based on both logarithmic and semi-logarithmic S-N curve models, is provided in Table (8). It can be seen that, for the $\pm 45^{\circ}$ specimens and for both RMS stress levels considered, the classical Rayleigh approximation underestimates the actual fatigue life by about 60%. The same trend is observed for $0/90^{\circ}$ specimens for the higher RMS stress level of 6.0 ksi. At the same time, the fatigue life at the lower RMS stress level of 4.5 ksi is significantly overestimated by Equation (33). For both specimen types, the predictions at the higher RMS stress levels (2.5 and 6.0 ksi, respectively) are somewhat improved by the use of Equation (38), but this improvement is quite marginal. At the same time, Equation (38) leads to further deviation from the experimental mean for the two lower RMS stress levels (1.75 and 4.5 ksi, respectively). These large deviations mainly come from the basic assumptions built in the Rayleigh approximation.

As pointed out in the previous section, the classical Rayleigh approximation formula, Equation (33), is based on both Equation (1) and on the Palmgren-Miner damage accumulation rule Equation (29). Therefore, misrepresentation of the actual stress-life relationship caused by a poor S-N curve function, insufficient S-N data, or disregarding the sequence effects by using the Miner rule, are main reasons for the shortcomings of the Rayleigh approximation in estimating the

variable amplitude fatigue lives.

ACTIVE BEARING CASE

Experimental Fatigue Lives : The constant amplitude and variable amplitude fatigue lives for the active bearing case are presented in Tables (4) and (5), respectively.

Failure Modes : The active bearing specimens were intended to characterize the bearing fatigue behavior and failure of the composite material under constant and variable amplitude loading. The failure was defined as occurring when the peak deflection reached four times the original peak deflection. Figure (55) shows the typical appearance of cross-ply and angle-ply specimens after failure. Obviously, there is no difference between the bearing failure modes of the cross-ply and angle-ply specimens. The elliptic glassy region circumscribing the hole for both lay-ups seems to be a consequence of local delamination which occurs due to bearing stresses.

Peak deflection data : Figures (56) through (58) show the evolution of the peak deflection during the constant amplitude fatigue tests, for the active bearing case. Unlike the passive case, the curves have a shorter low cycle flat portion, and then suddenly the deflection begins to build-up roughly midway through the fatigue life. Also, the downward curvature of the final part of the curves distinguish the active bearing curves from those of the passive case. A common feature of all cases, however, is that the failure is controlled by the tensile deflection.

Temperature data : Figures (59) through (66) present the temperature rise during the fatigue tests of active bearing case. These plots do not exhibit the same behavior as the passive bearing plots nor are they as diverse. Some of the bearing case plots show a short initial increase and some do not. Prior to the final build up, some of the active bearing curves show almost no variation in the temperature, while for some others there is some temperature variation. Also, the

duration of the final temperature rise differs considerably for different specimens.

S-N Curves : The S-N curves for the active bearing specimens are shown in Figures (67) and (68) in log-log and semi-log scales, respectively. From the figures, it can be seen that the scatter of the cross-ply data is less than that of the angle ply data. This agrees with the passive bearing case data.

Random Fatigue Lives : Table (8) summarizes the random fatigue lives obtained from the experiments, as well as the calculated lives. Generally, the difference between the two lives is larger for lower stress levels. Like the passive bearing case, the large difference between the experimental and theoretical results is not consistently conservative, or non-conservative. Effects such as the quality with which the constant amplitude data are represented, load sequence and load frequency may very well be contributing to this lack of consistency.

JOINTS

Experimental Fatigue Lives : Tables (6) and (7) show the constant amplitude and variable amplitude test results for different types of composite joints, respectively.

Failure Modes : Figures (69) and (70) show the typical failures of bonded only, bolted only, and bolted-bonded joints. The failure of the bonded joints is an adhesive failure of the bond, while that of the bolted joints is a bearing followed by a partial shear-out failure. The white powder around the bolt holes is a result of the frictional interaction of the parts. The failure of the bonded-bolted joints occurs in two stages. First, and very early, comes the adhesive failure of the bonds and then, typically after a long time, the bearing and partial shear-out of the bolts occurs.

Deflection Data : Figures (71) through (73) show the peak deflection versus number of cycles curves for the bonded joints. Note that the curves in Figures (72) and (73) are enlarged in

the final failure part to help distinguish the step-like growth of deflection to failure. However, such a trend was not observed in Figure (71). This step-wise failure is not of significance when studying the fatigue damage accumulation and life. However, it may be helpful in failure mechanism investigations. Figures (74) through (77) show the evolution of deflection for bolted joints, and Figures (78) through (80) for bolted-bonded joints. From Figures (74) through (77), the trend resembles that of the passive bearing case, except that in Figure (77), the final build up is more gradual. In the deflection curves of the bolted-bonded joints, the final sudden build up seems to follow a small step-like growth. Figures (81) through (83) exemplify the deflection-based damage accumulation for different types of joints. It is interesting to note the fundamental difference between the three types of joints. For bonded joints, the stress level has a marginal effect on the damage accumulation form. On the other hand, the damage accumulation in bolted joints is governed by the stress level. The bolted-bonded specimens have shown an intermediate trend.

Temperature Data : Figure (84) shows an example of temperature change in a bolted-bonded composite joint. As expected, there is a considerable difference between the temperature of the washer and that of the composite material in the vicinity of the washer.

S-N Curves : The constant-amplitude data for all joint configurations are summarized in the form of S-N curves in Figure (85) and (86). The curves indicate a definite deviation from the logarithmic S-N curve model for all joint configurations. Neither S/N curve model appears to represent the data particularly well.

Random Lives : The experimental and theoretical random lives are summarized in Table (8). Like the previous two cases, it can be seen that the Rayleigh approximation generally has not been able to predict the lives accurately. Predictions tend to be conservative low RMS levels and non-conservative at higher RMS levels. This is most likely due to the poor representation of the

S/N curves to constant amplitude data, or possibly due to sequence effects.

CONCLUSIONS

Fatigue damage in FRP laminates occurs in the form of diffuse zones containing micro-cracks in the matrix, fiber-matrix debonding sites, ply delamination, and broken fibers. This damage leads to degradation of the elastic moduli of the laminate; FRP fatigue damage accumulation is best modeled by stiffness degradation approaches. Various S-N curve models for constant-amplitude fatigue damage characterization can be described in terms of the fatigue modulus concept of Hwang and Han. Very little investigation has been done using fatigue damage accumulation techniques. Most available data deal with two-stage loading cases only. A few cumulative damage hypotheses have been proposed. However, due to limited experimental data, it is not clear which of these hypotheses are most suitable for naval applications. The constant and variable amplitude fatigue studies on WR laminates and joints conducted at The George Washington University indicate a fair fit of the S-N data for the cross-ply laminate of both passive and active bearing cases to the power law S-N curve. The fit is not as good for the angle-ply lay-ups. At the same time, the laminate joints tested show a definite trend toward deviation from the power law S-N curve model. Random-amplitude fatigue tests with narrowband stress histories demonstrate significant deviation of the observed fatigue lives from those predicted with the Rayleigh approximation; tending to overpredict for joints at the high RMS level and underpredict for the low RMS level. Although not as consistent, the active and passive bearing specimens tend to exhibit just the opposite behavior, overpredicting at the low RMS level and underpredicting at the high RMS level. Such agreement may be attributed to an inadequacy of the Palmgren-Miner's damage accumulation

rule to accurately reflect the fatigue damage accumulation behavior in composite materials. Other reasons for the deviation include a poor representation or insufficiency of the constant amplitude data to be represented by an analytical expression, as well as temperature and load frequency effects which have not yet been quantified and incorporated into a fatigue damage accumulation model. In general however, use of the Log-Log S/N curves produced slightly better predictions.

RECOMMENDATIONS

The data generated and presented in this report provide an initial step in understanding fatigue damage accumulation in marine-grade composite laminates and joints subjected to constant and random amplitude loadings. Several problems have been identified in the course of this effort; most notably, the inability to properly represent the constant amplitude fatigue data by traditional power law forms and a general lack of sufficient data. This problem alone may have been the most important factor in the inability to accurately and consistently predict failure lives of test specimens subjected to random loads. Other effects, such as temperature and load frequency, undoubtedly have influenced these results, but it is not known by how much.

Follow-on efforts should include characterizing temperature and load frequency quantities so their effects can be incorporated into a fatigue damage accumulation model. In addition, predictions should be made with the other models described in this report and compared with the experimental results. Further, tests under constant and random amplitude loadings will likely need to be repeated, this time varying load frequency while monitoring the temperature.

Different geometries and methods of attachment/adhesives should also be investigated to improve the fatigue behavior of both laminates and joints.

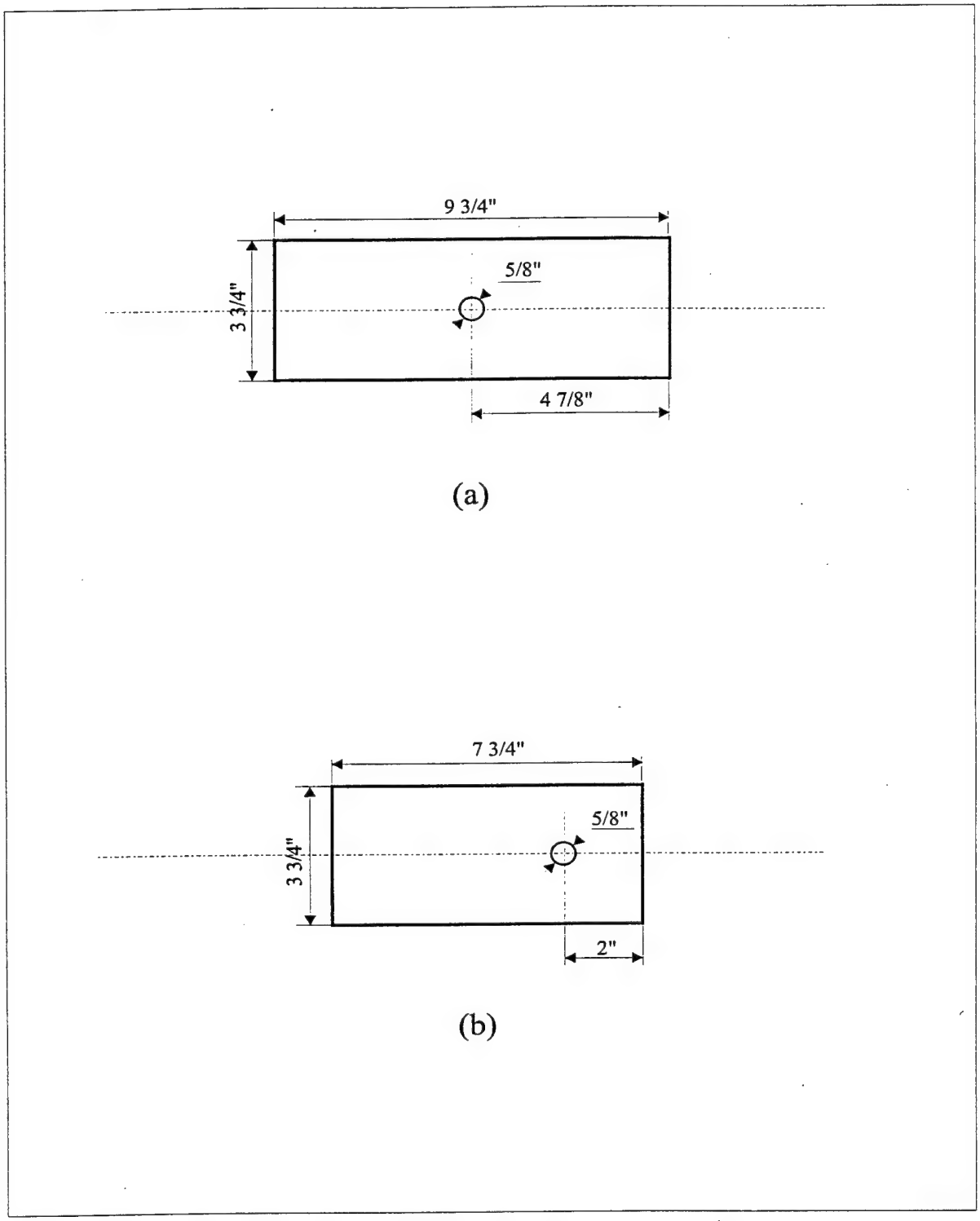

Figure 1 - Geometry of Base Laminates : Passive Bearing Case (a) and Active Bearing Case (b)

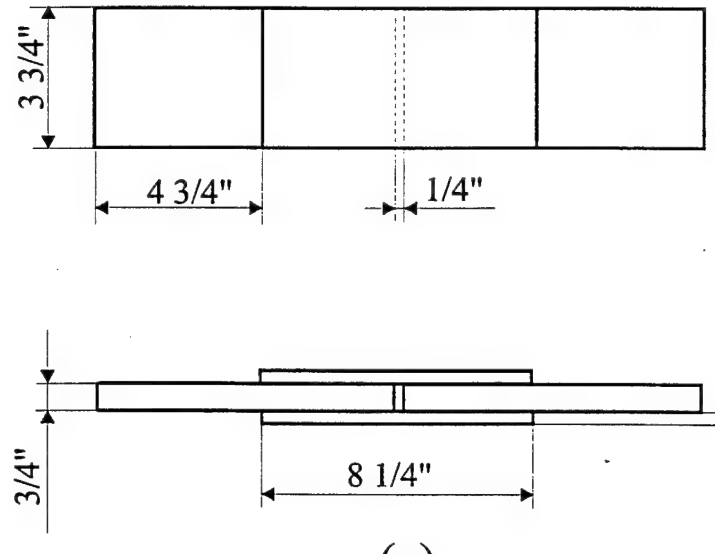

(a)

Typical Bonded only Specimen

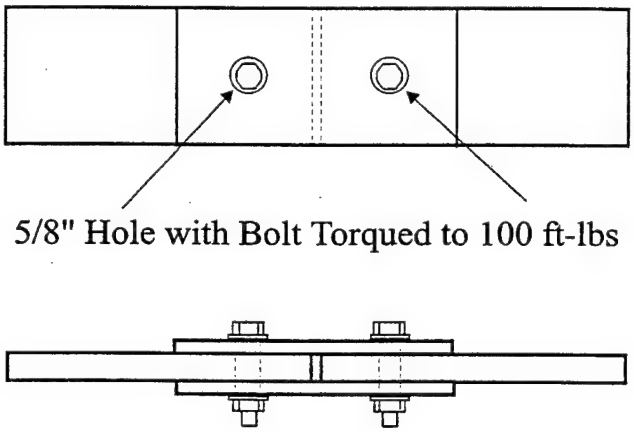

(b)

Typical Bolted only and Bonded & Bolted Specimen

Figure 2 - Geometry of Different Types of Composite Joints

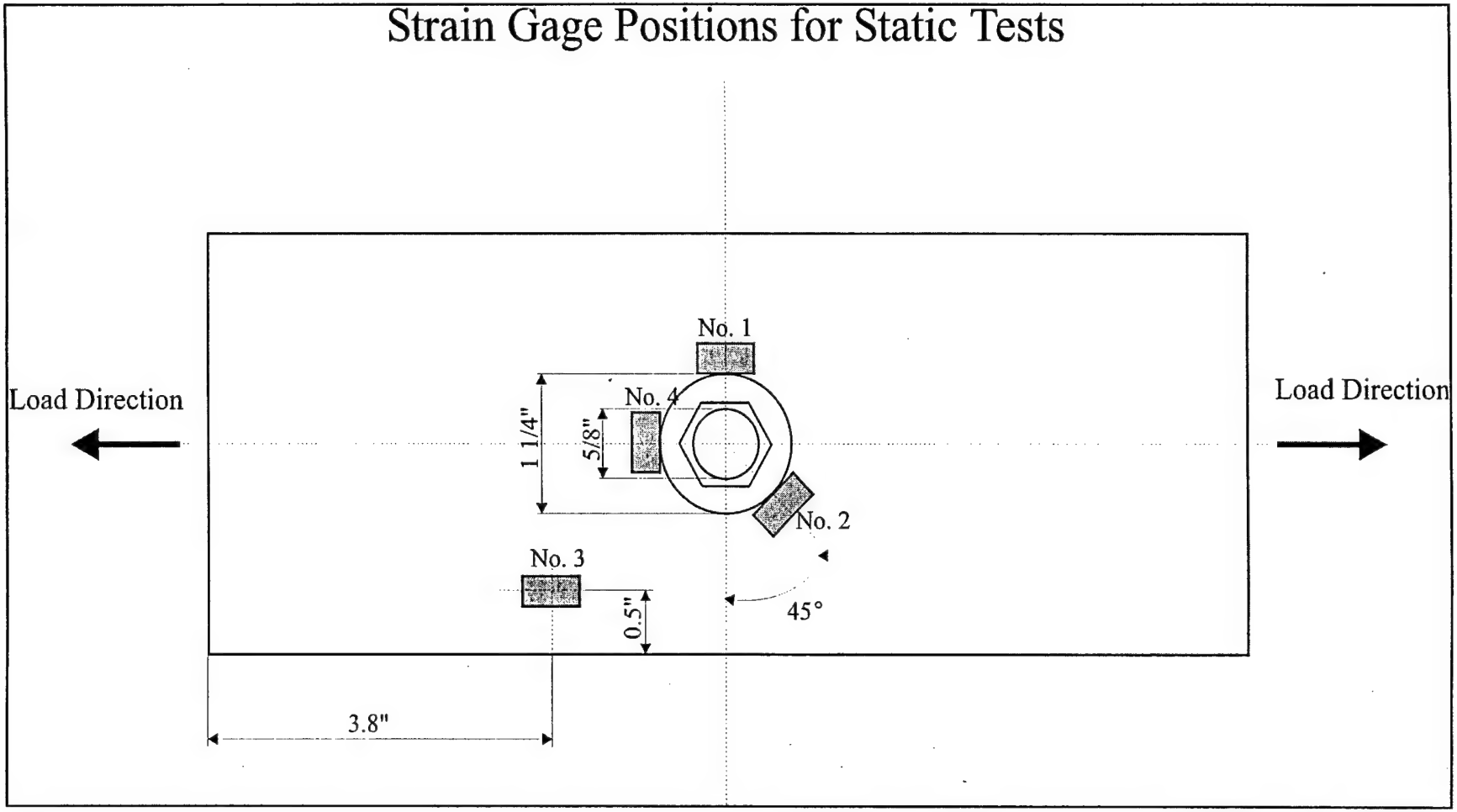

Figure 3 - Strain Gage Locations in Passive Bearing Case; Static Test Specimens

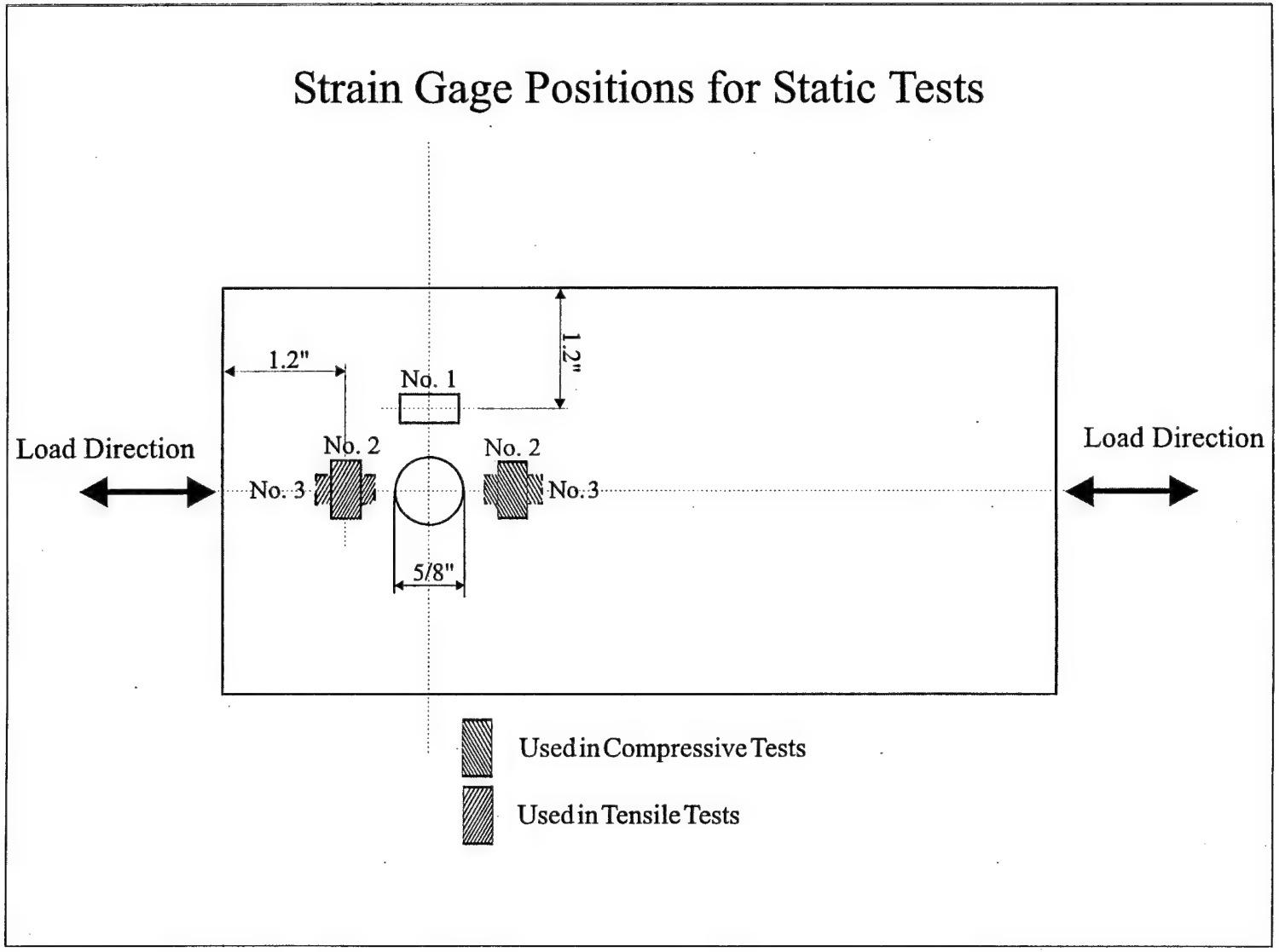

Figure 4 - Strain Gage Locations in Active Bearing Case; Static Test Specimens

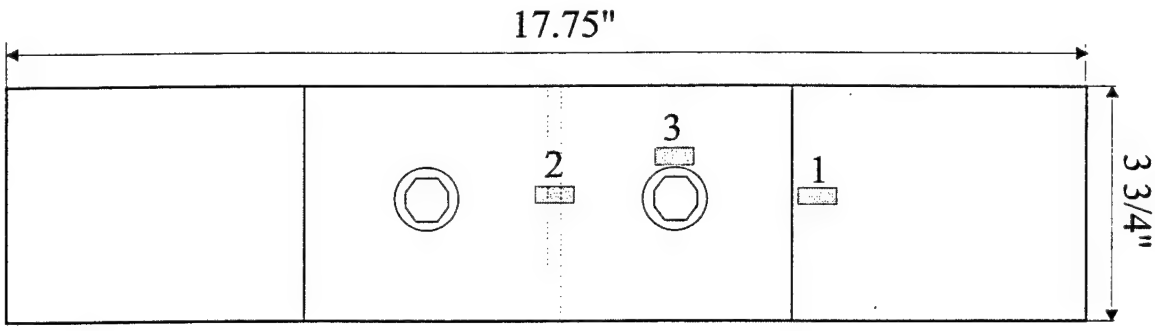

Strain Gage Positions for Bolted only and Bolted & Bonded Specimens

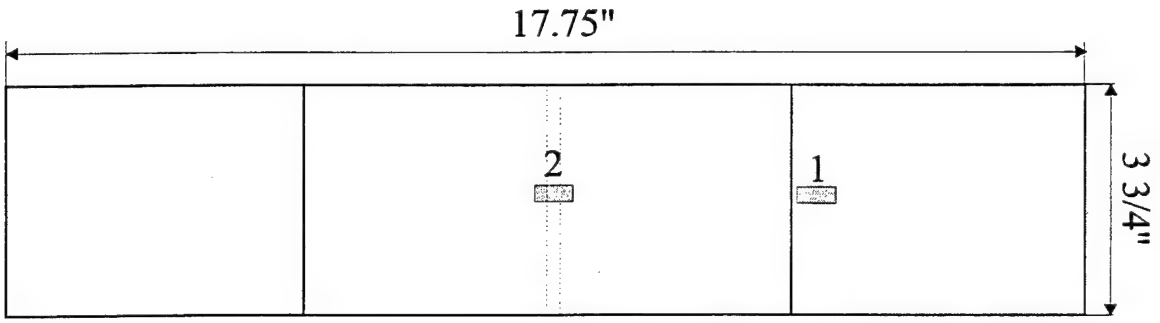

Strain Gage Positions for Bonded only Specimens

Figure 5 - Strain Gage Locations in Static Tests of Joint Specimens

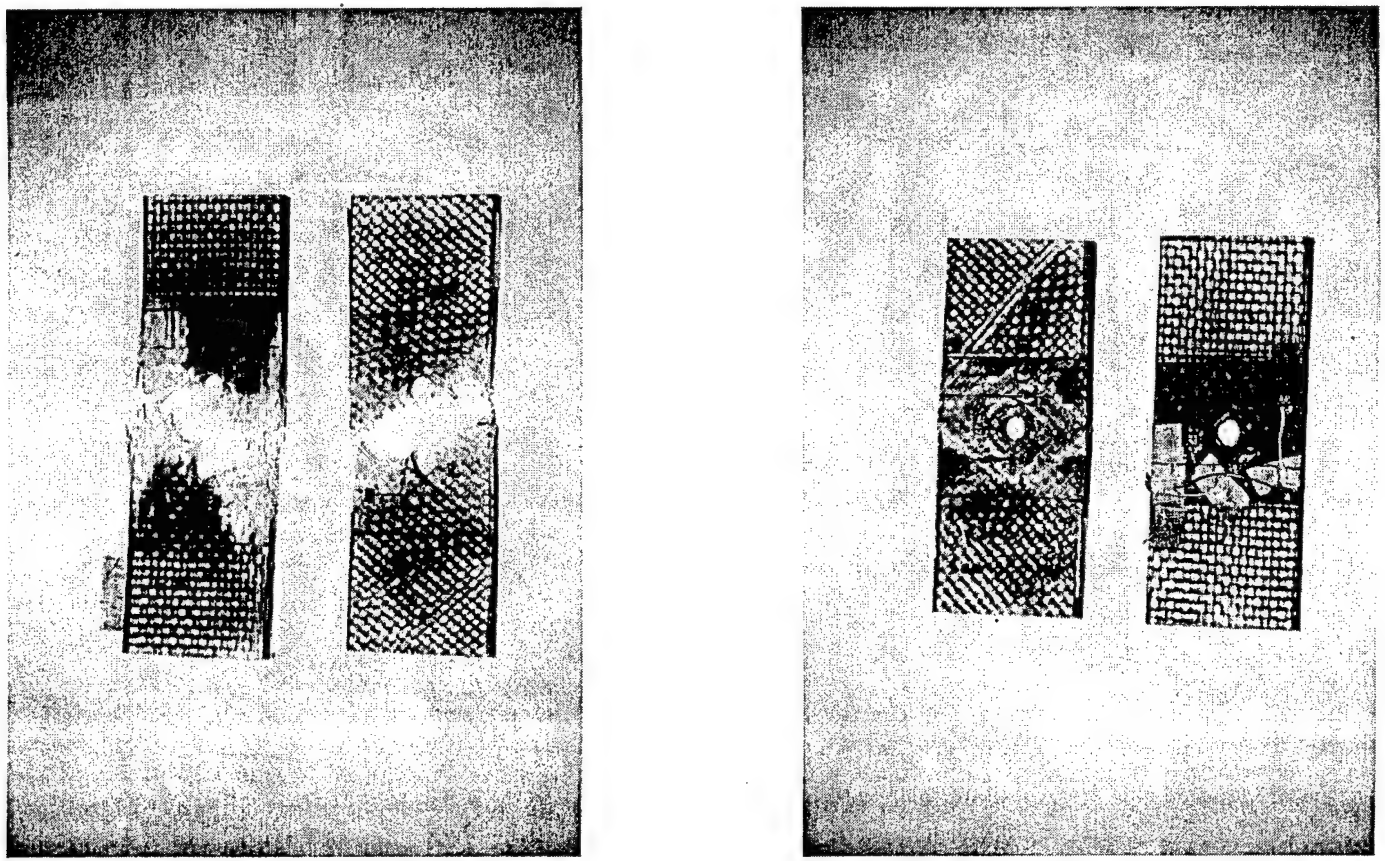

(a) TENSILE SPECIMENS

(b) COMPRESSIVE SPECIMENS

Figure 6 - Failure Modes for Strength Tests of Passive Bearing Case

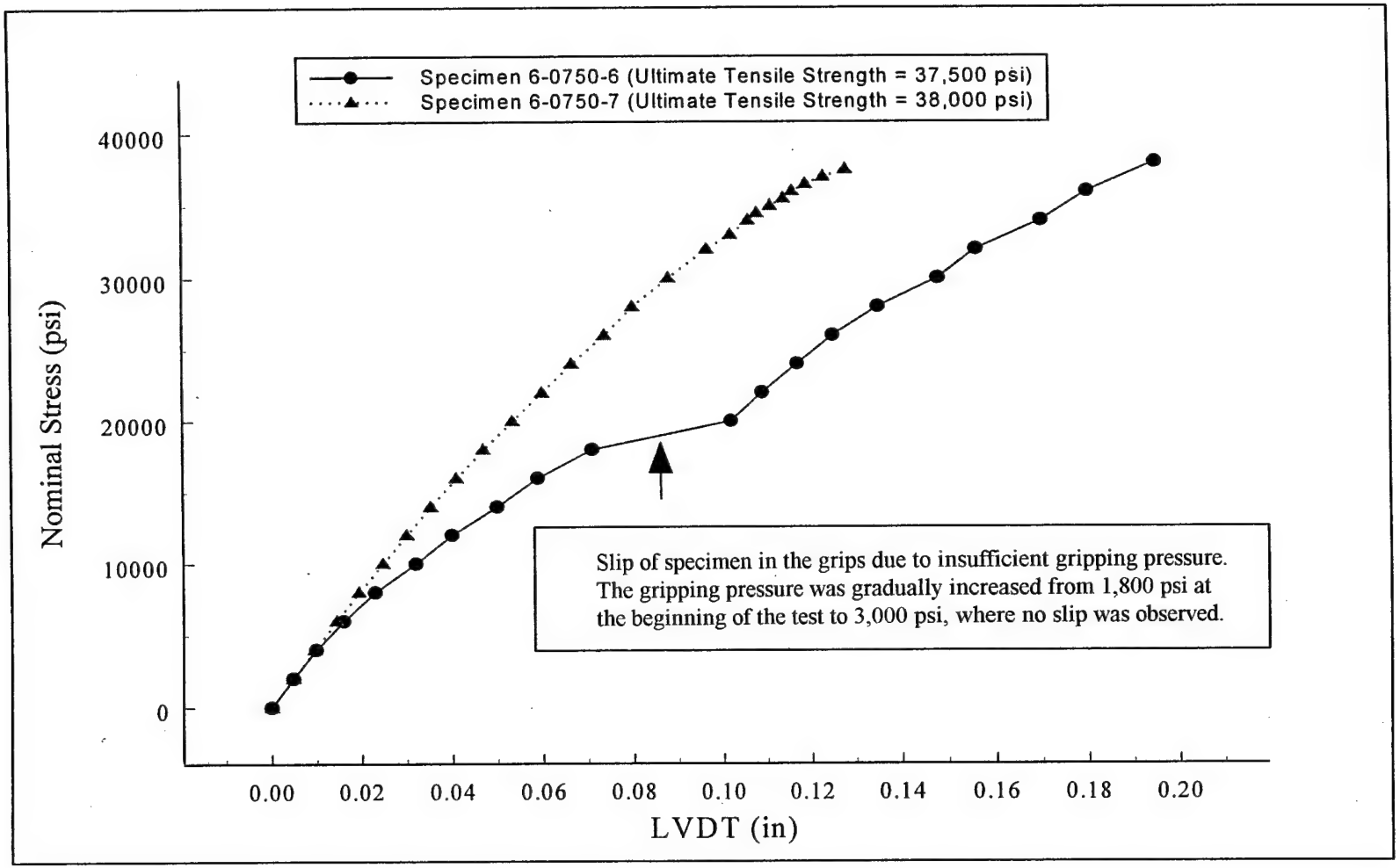

Figure 7 - Stress-Deflection Curves for Ultimate Tensile Strength Tests of 0/90° Passive Specimens

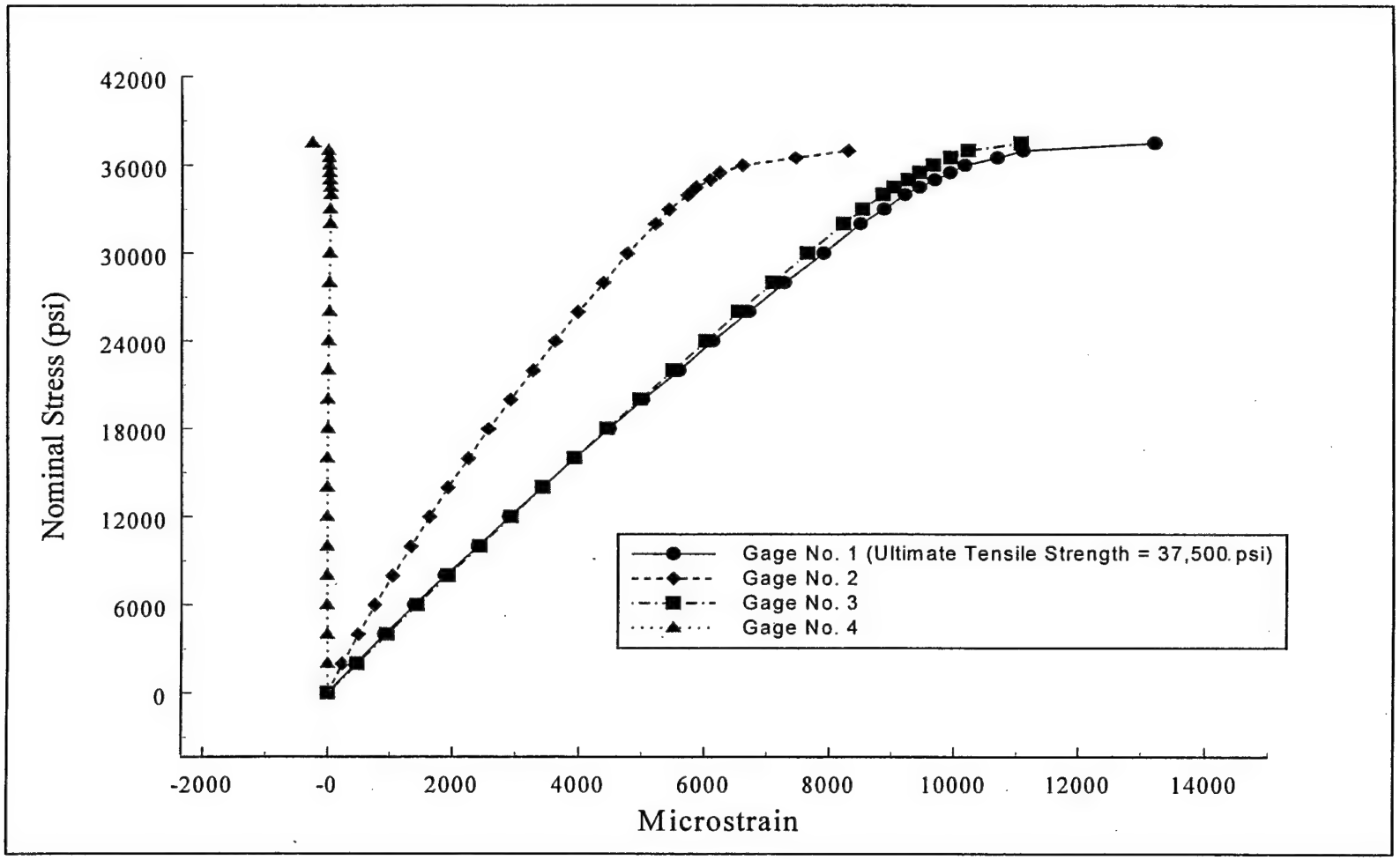

Figure 8 - Strain Gage Readings During Ultimate Tensile Strength Tests of 0/90° Passive Specimens; Specimen 6-0750-6

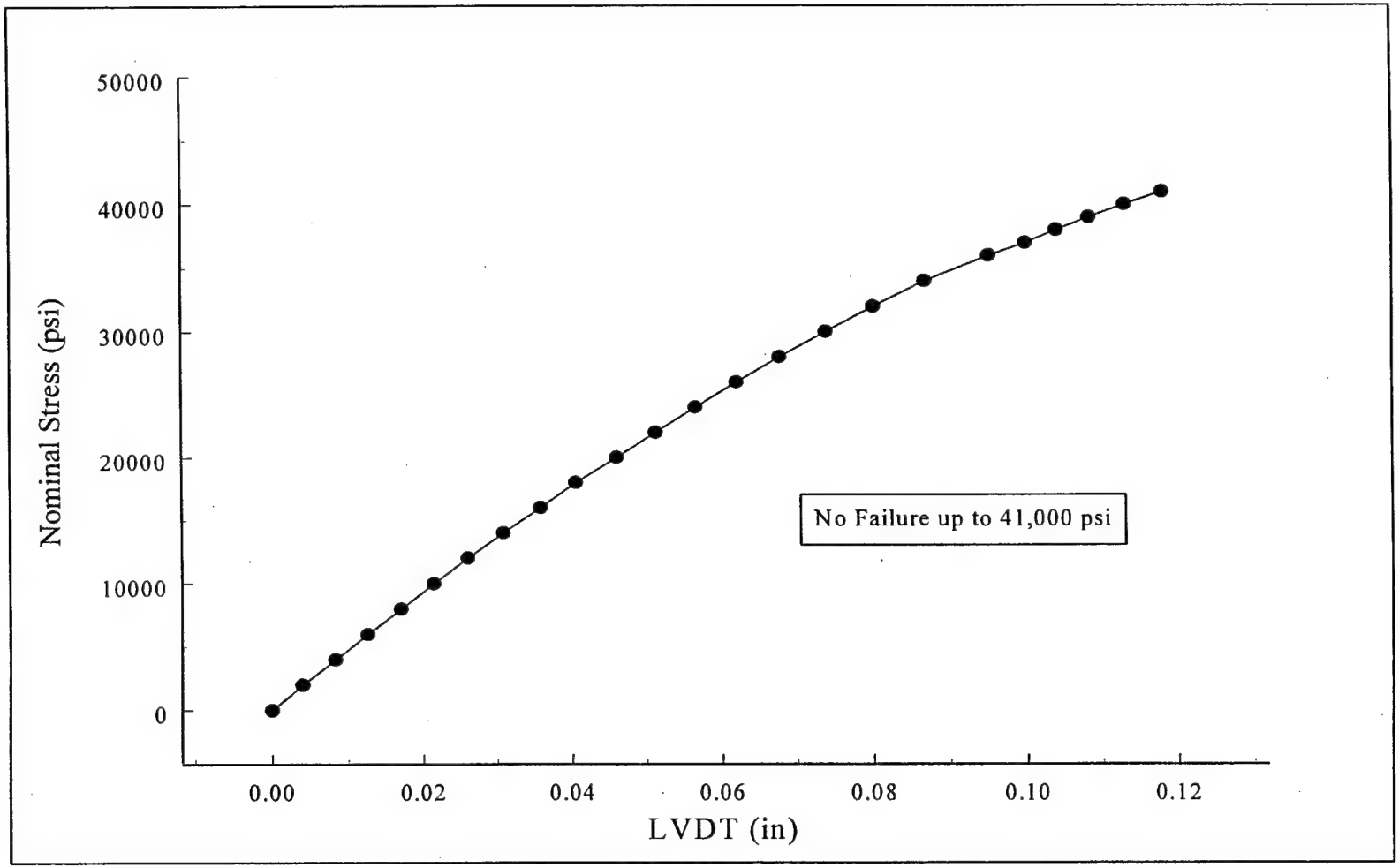

Figure 9 - Stress-Deflection Curve for Ultimate Compressive Strength Tests of 0/90° Passive Specimen

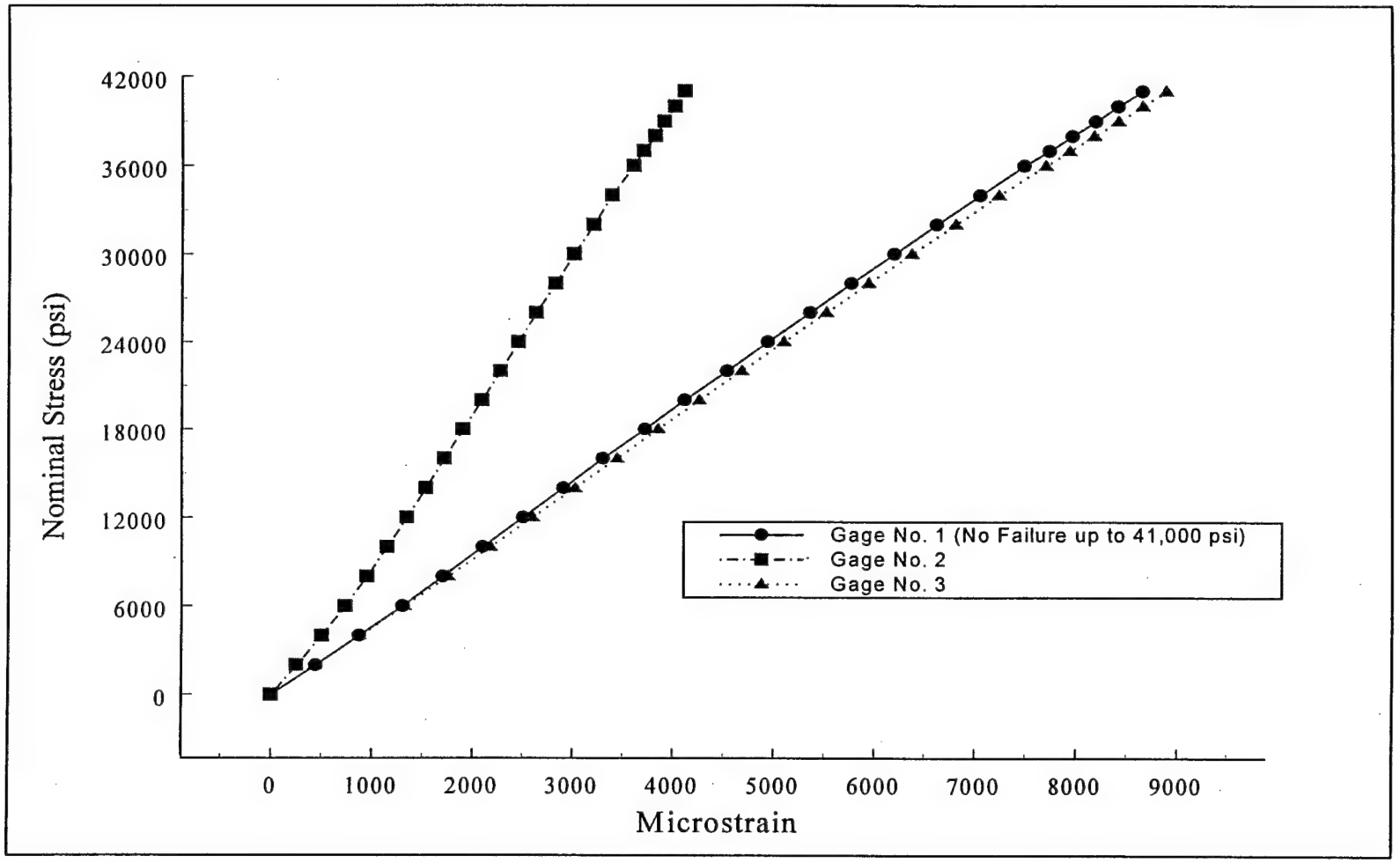

Figure 10 - Strain Gage Readings During Compressive Strength Test of 0/90° Passive Specimens

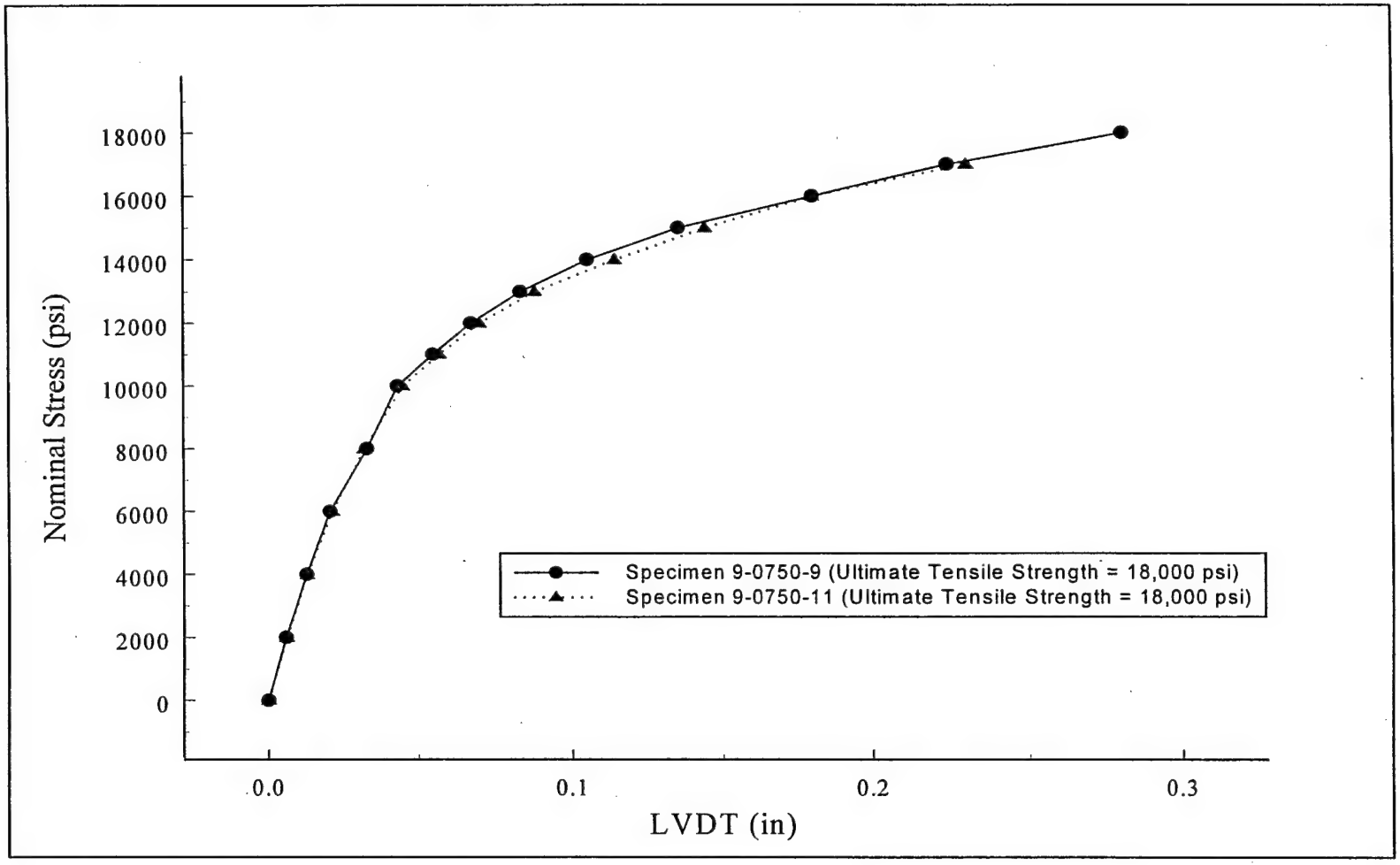

Figure 11 - Stress-Deflection Curves for Ultimate Tensile Strength Tests of $\pm 45^{\circ}$ Passive Specimens

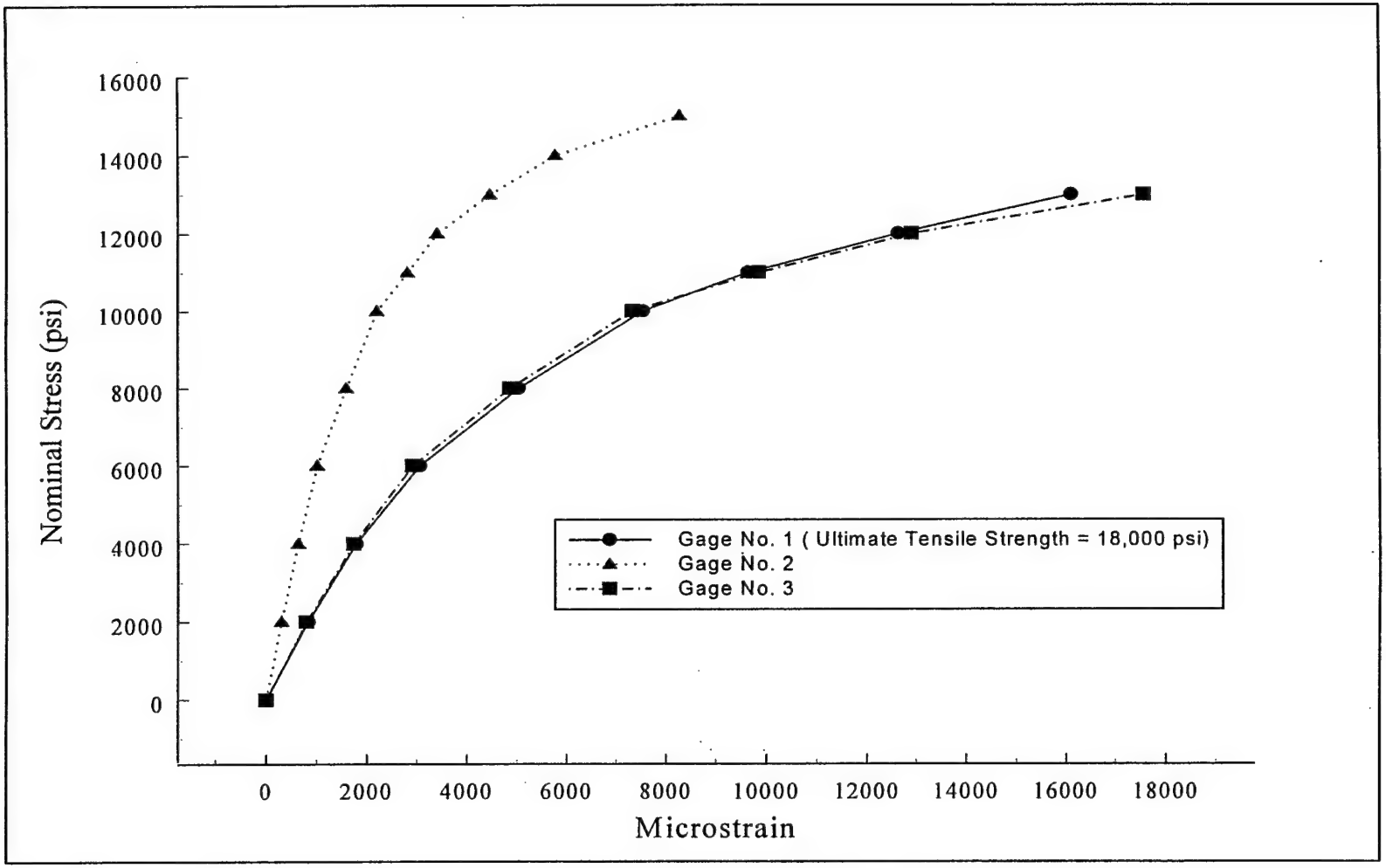

Figure 12 - Strain Gage Readings During Ultimate Tensile Strength Tests of $\pm 45^{\circ}$ Passive Specimens; Specimen 9-0750-9

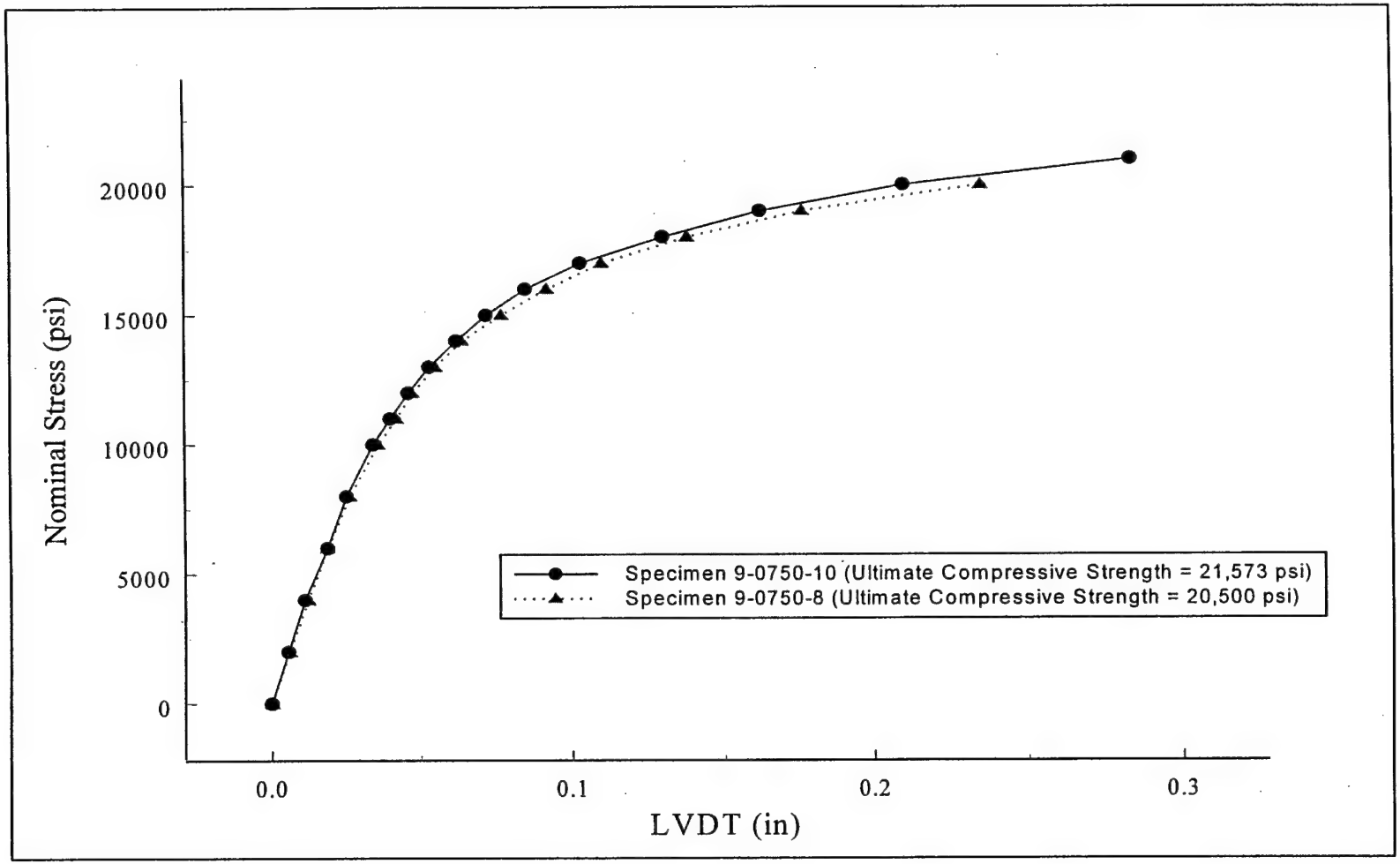

Figure 13 - Stress-Deflection Curves for Ultimate Compressive Strength Tests of $\pm 45^{\circ}$ Passive Specimens

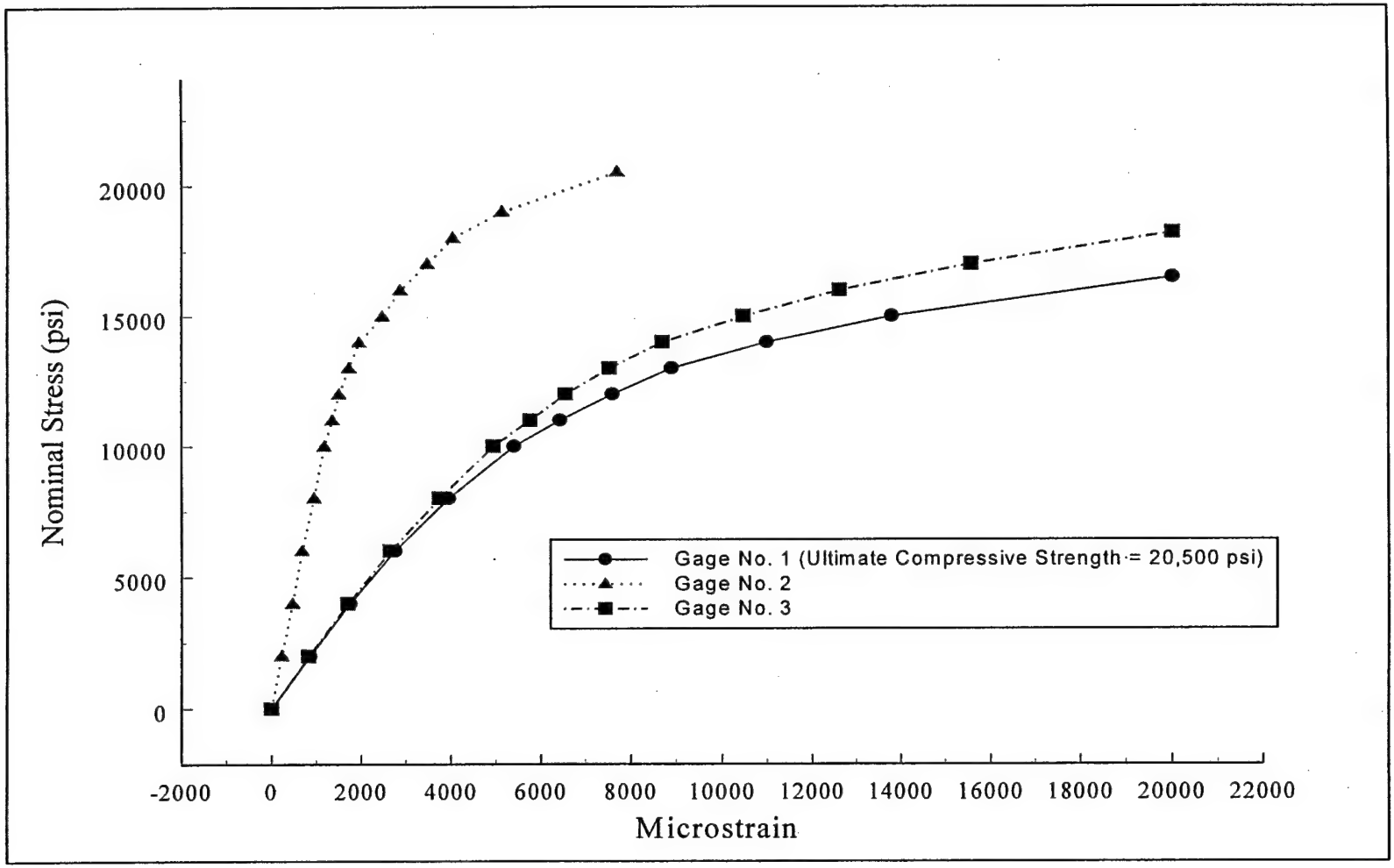

Figure 14 - Strain Gage Readings During Ultimate Compressive Strength Tests of $\pm 45^{\circ}$ Passive Specimens; Specimen 9-0750-8

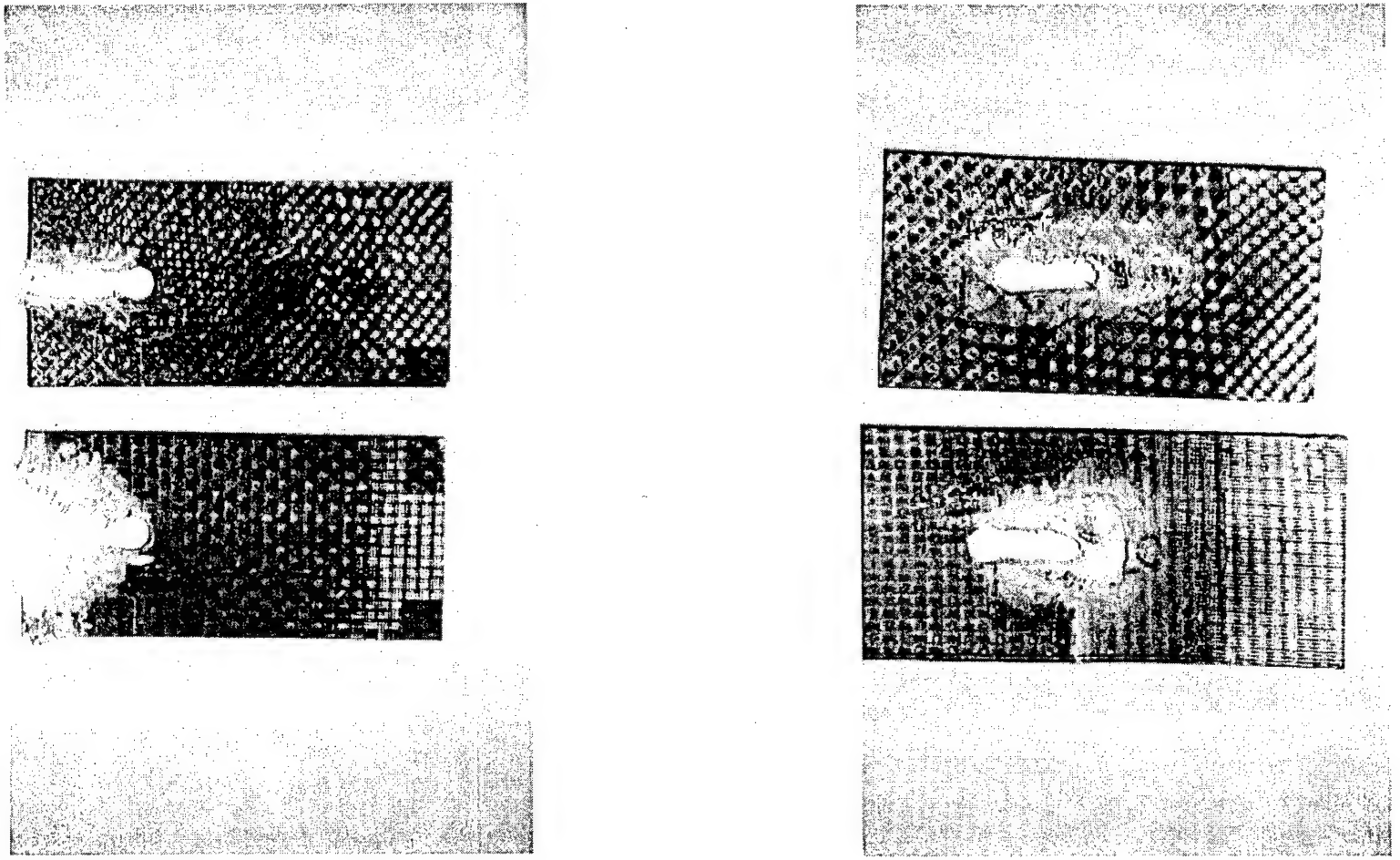

(a) TENSILE TESTS

(b) COMPRESSIVE TESTS

Figure 15 - Failure Modes for Strength Tests of Active Bearing Case

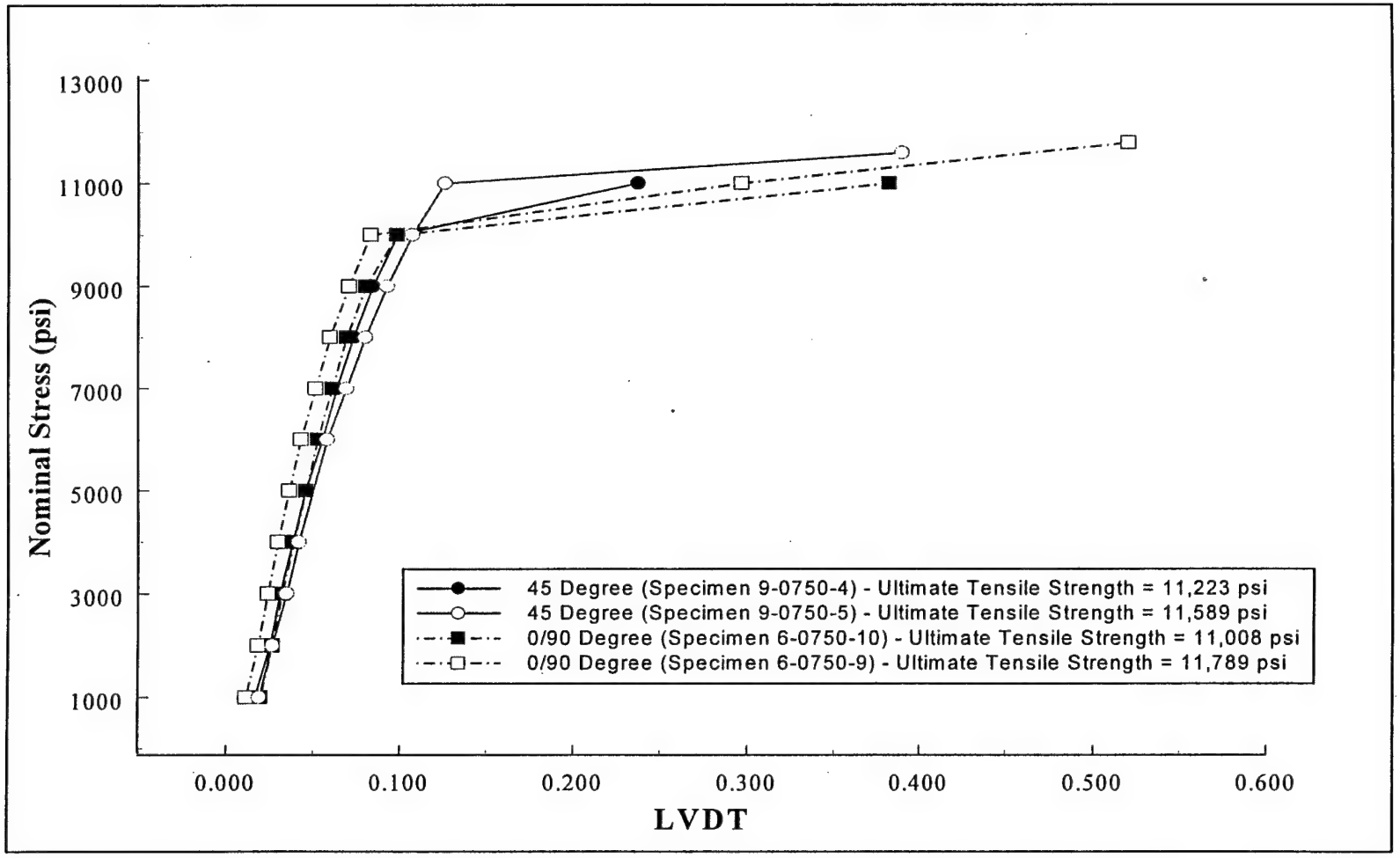

Figure 16 - Stress-Deflection Curves for Active Bearing Case: Tensile Strength Tests

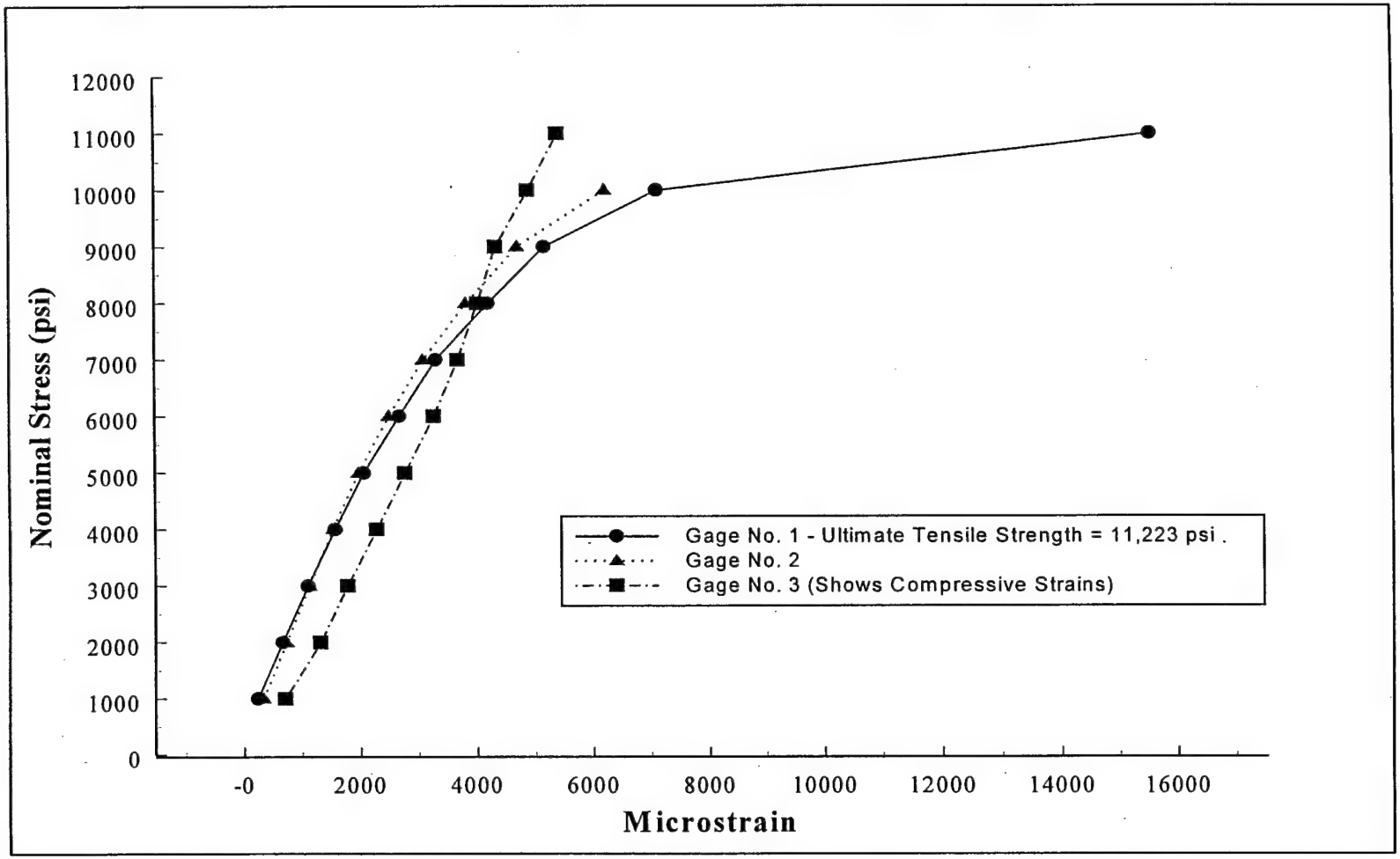

Figure 17 - Strain Gage Readings for Tensile Strength Tests of Active Bearing Specimens; Specimen 9-0750-4 ($\pm 45^{o}$)

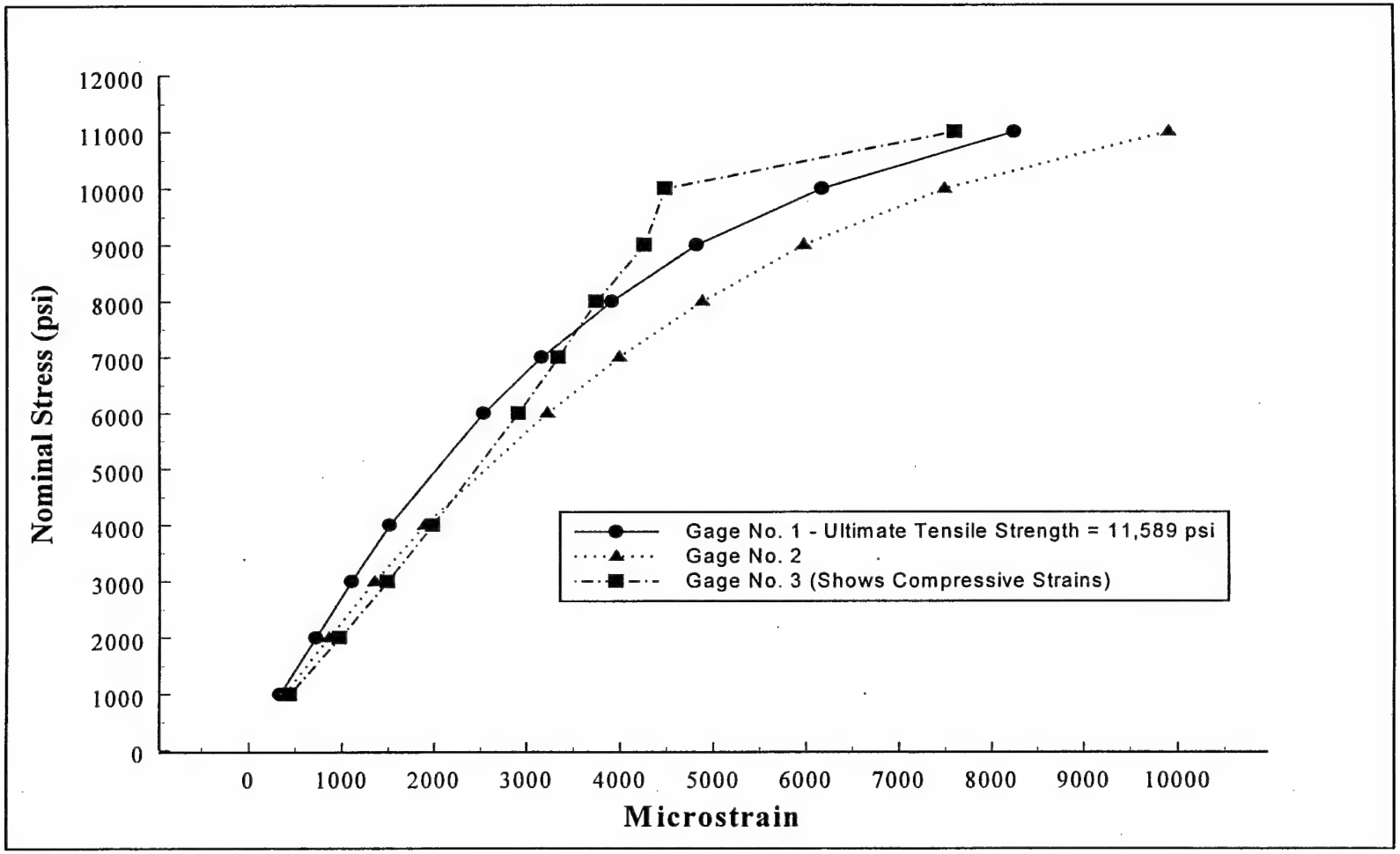

Figure 18 - Strain Gage Readings for Tensile Strength Tests of Active Bearing Specimens; Specimen 9-0750-5 ($\pm 45°$)

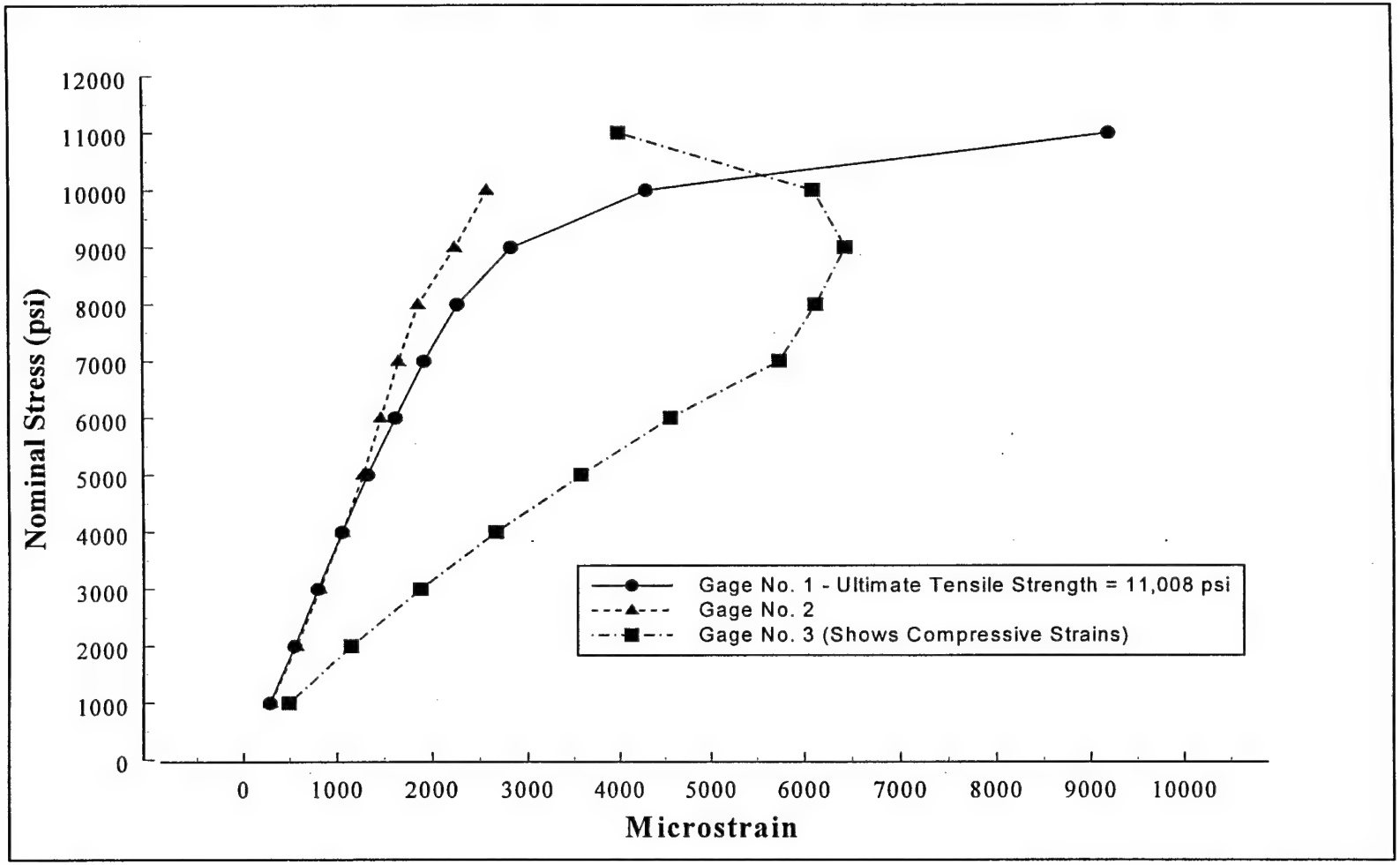

Figure 19 - Strain Gage Readings for Tensile Strength Tests of Active Bearing Specimens; Specimen 6-0750-10 (0/90°)

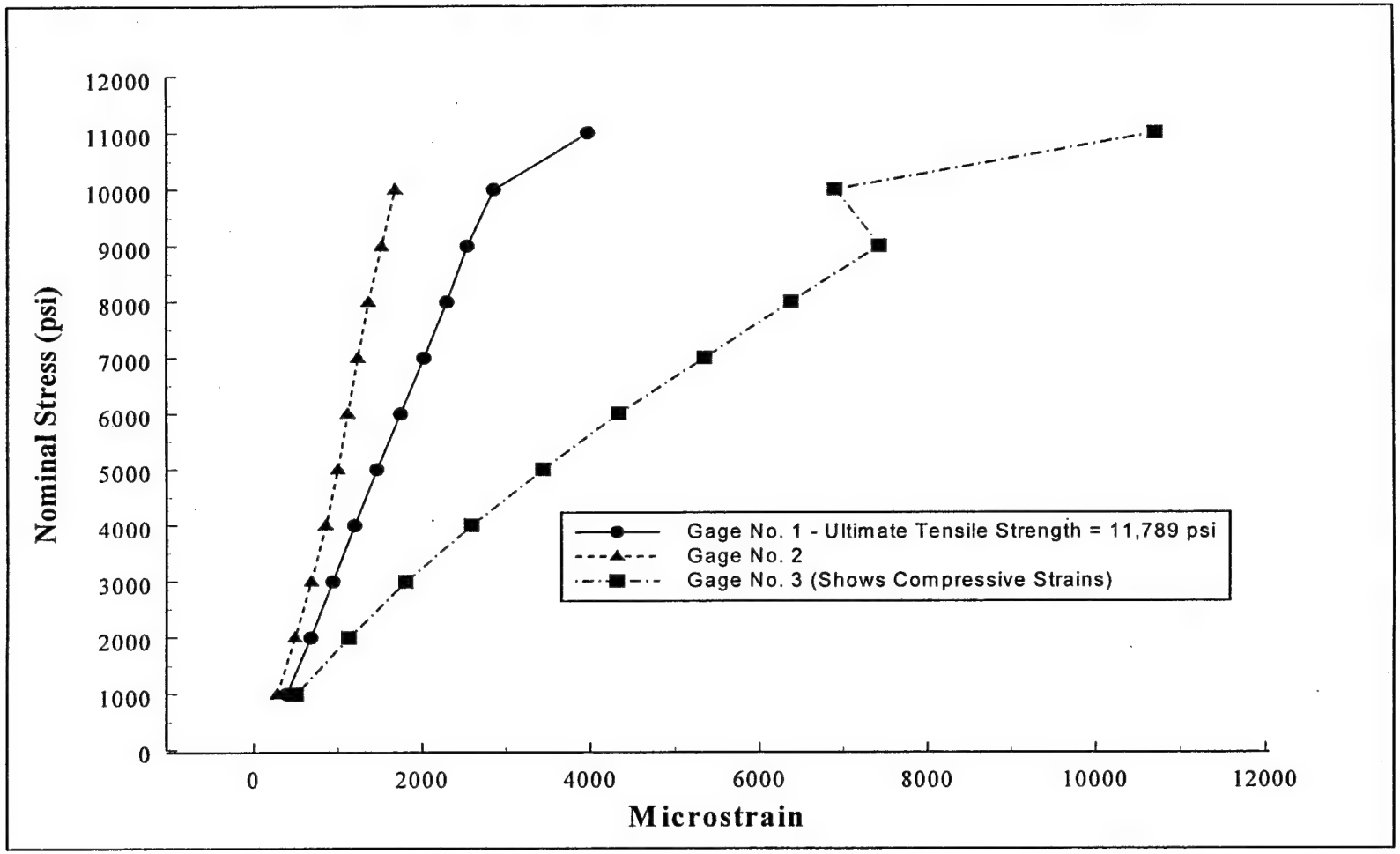

Figure 20 - Strain Gage Readings for Tensile Strength Tests of Active Bearing Specimens; Specimen 6-0750-9 (0/90°)

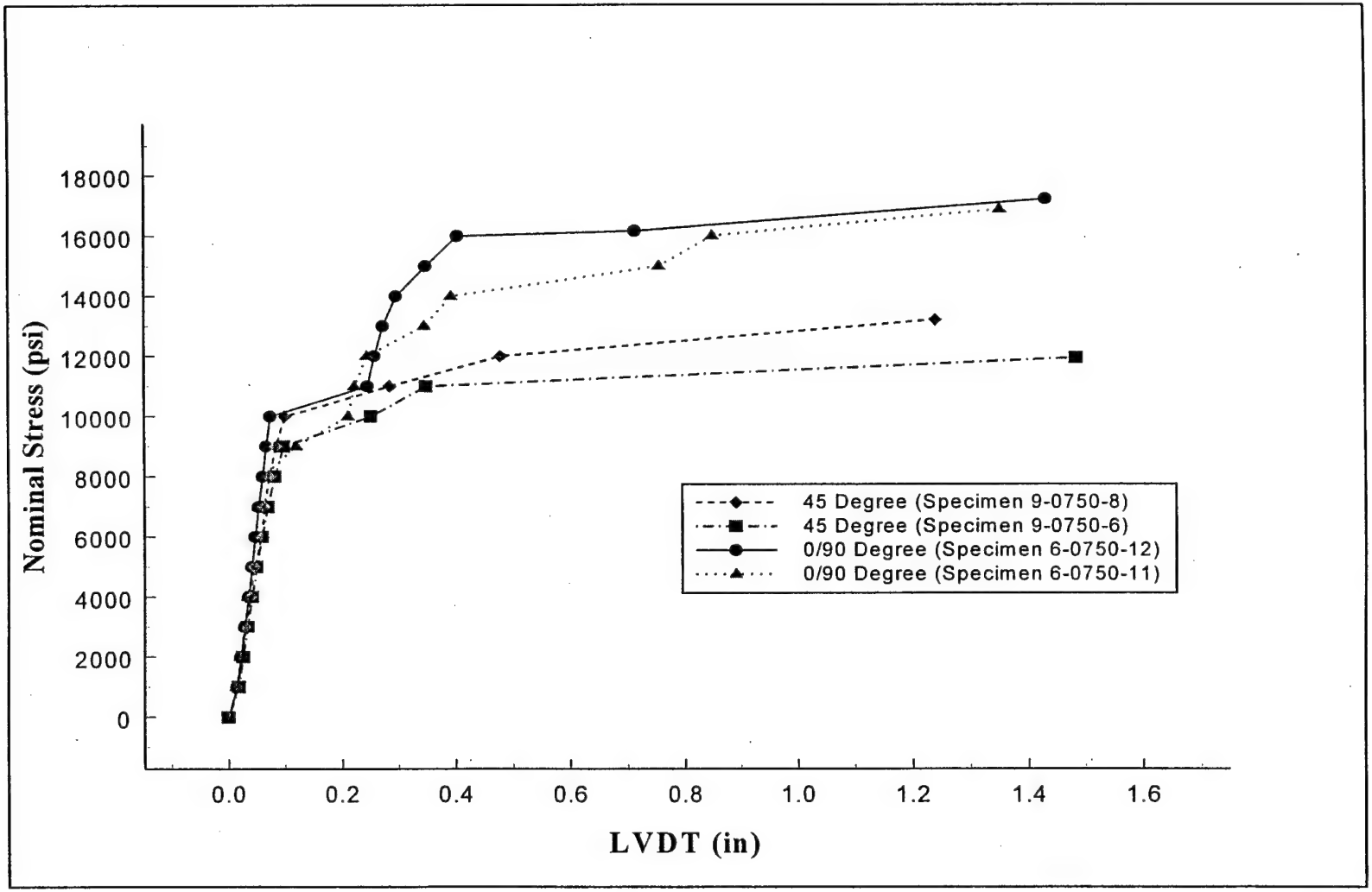

Figure 21 - Stress-Deflection Curves for Compressive Strength Tests of Active Bearing Case

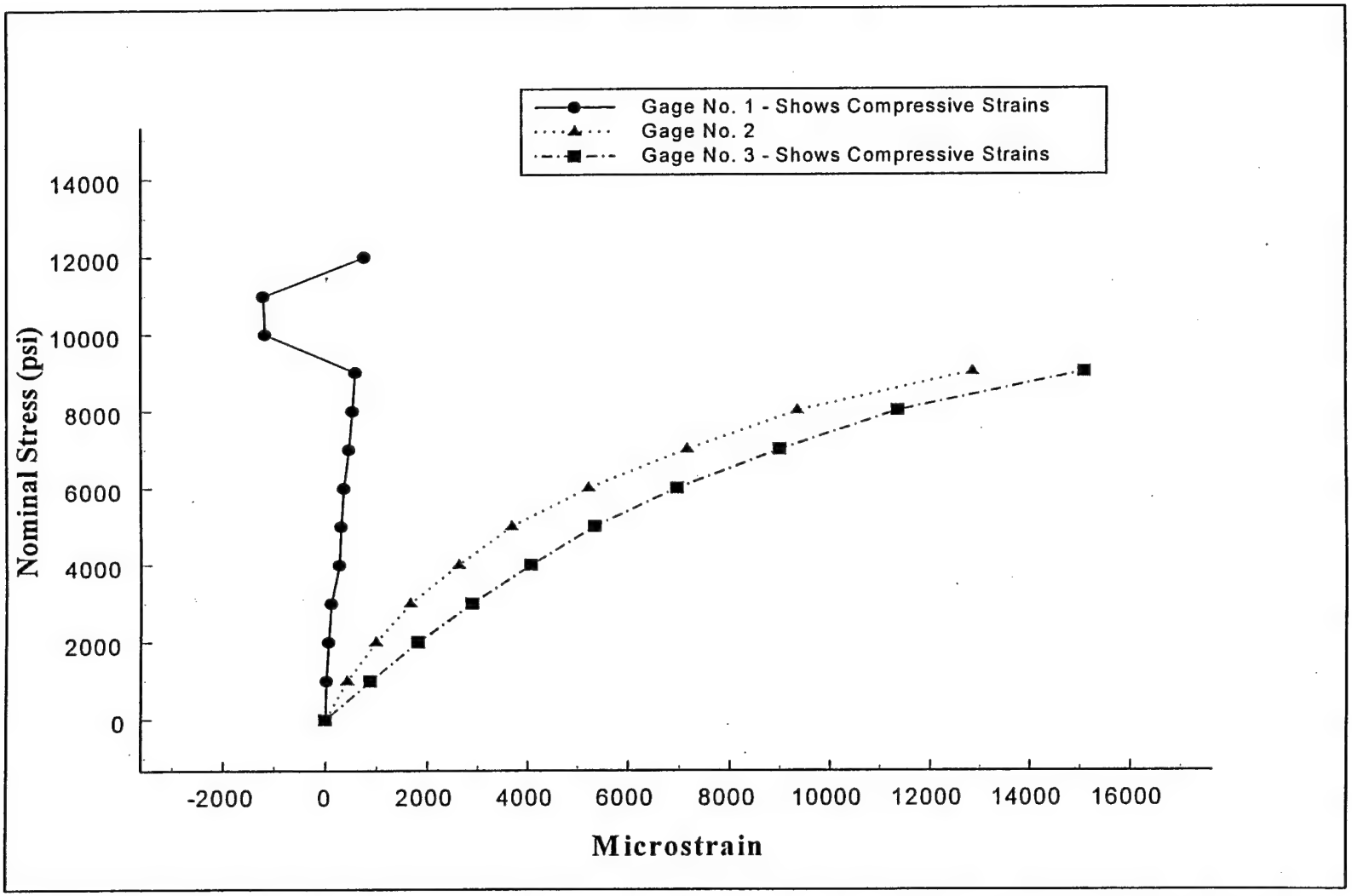

Figure 22 - Strain Gage Readings in Active Bearing Case: Compressive Strength Tests; Specimen 9-0750-8 ($\pm 45^{o}$)

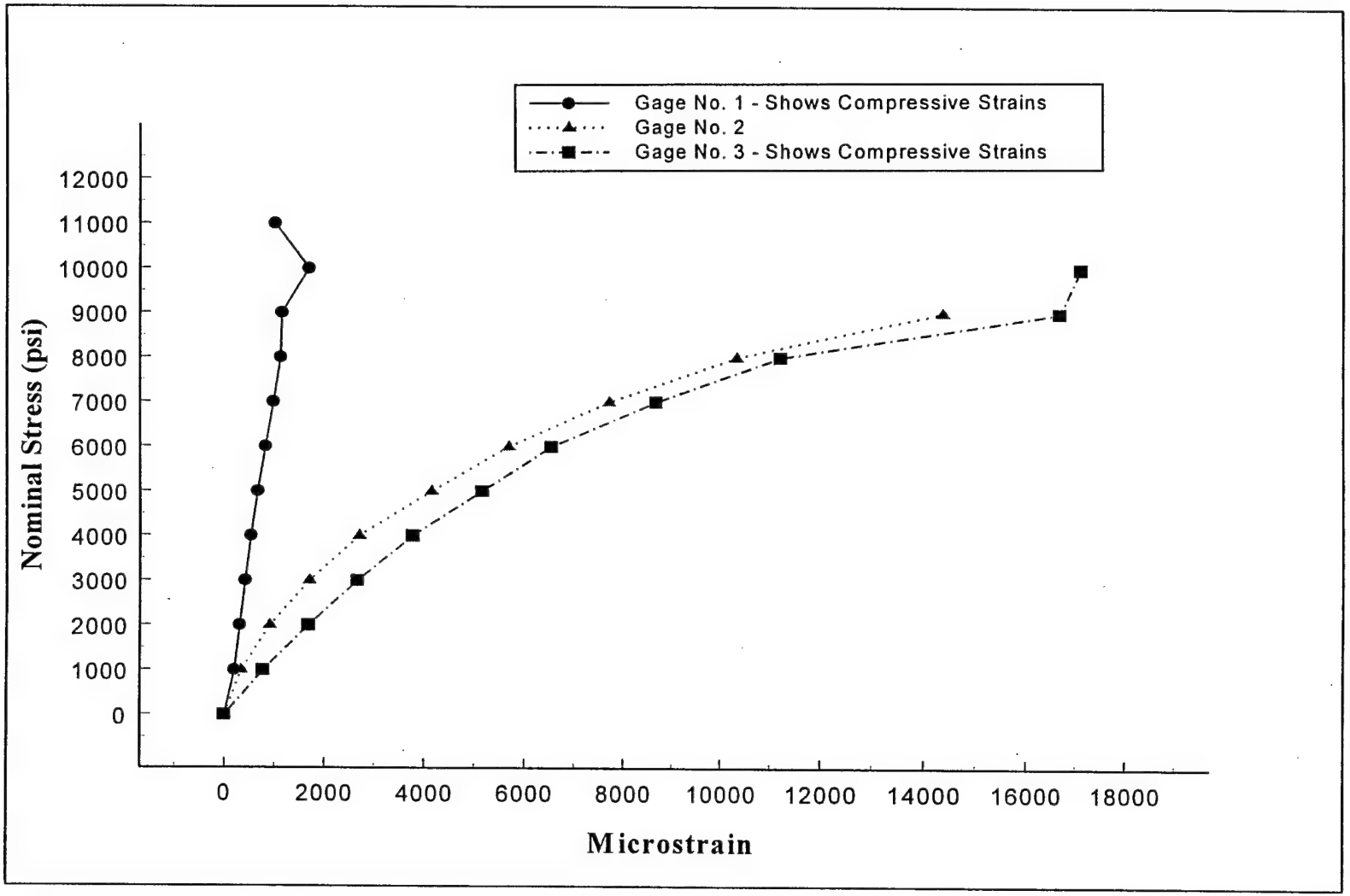

Figure 23 - Strain Gage Readings in Active Bearing Case: Compressive Strength Tests; Specimen 9-0750-6 ($\pm 45^{\circ}$)

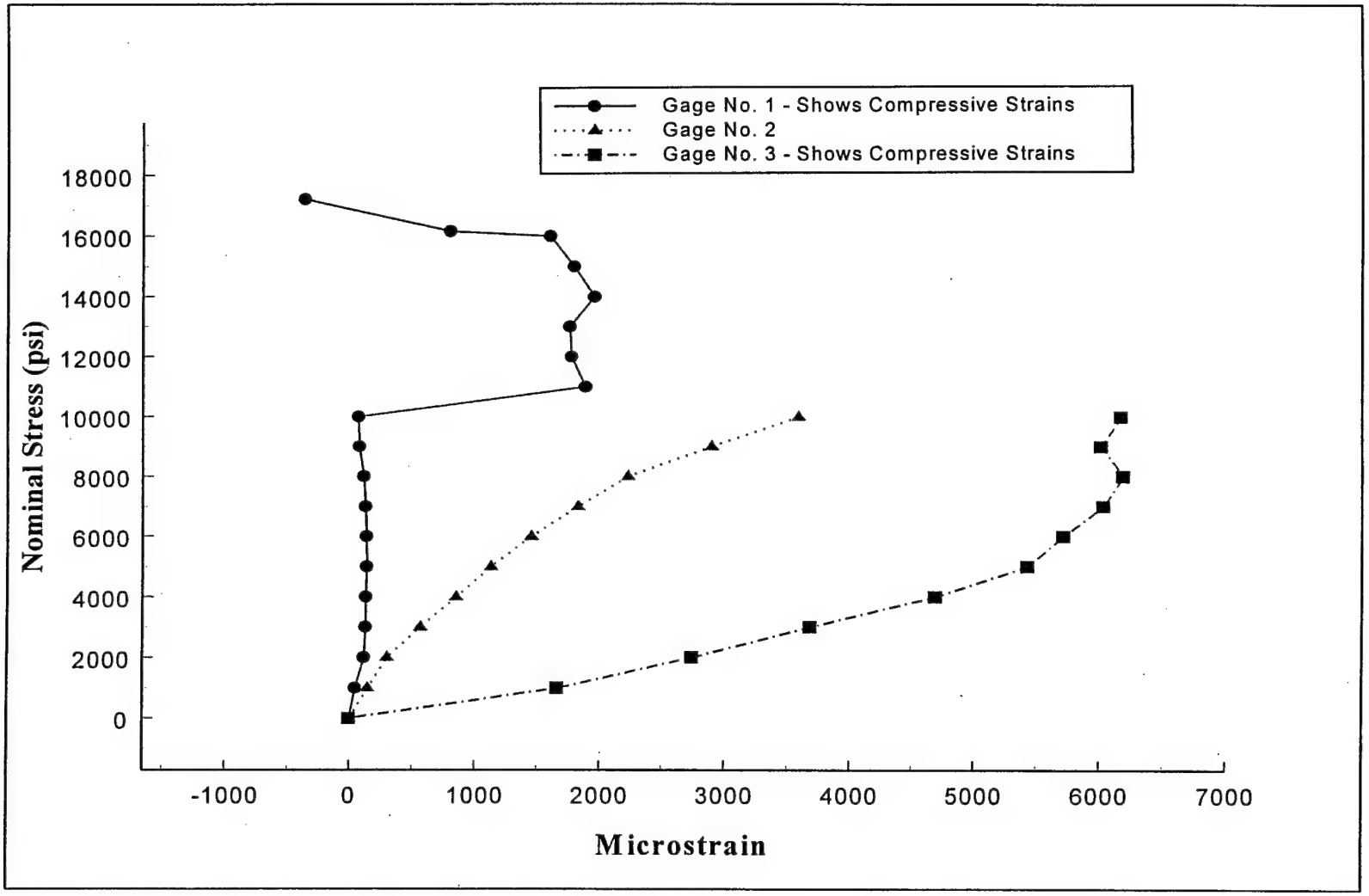

Figure 24 - Strain Gage Readings in Active Bearing Case: Compressive Strength Tests; Specimen 6-0750-12 (0/90°)

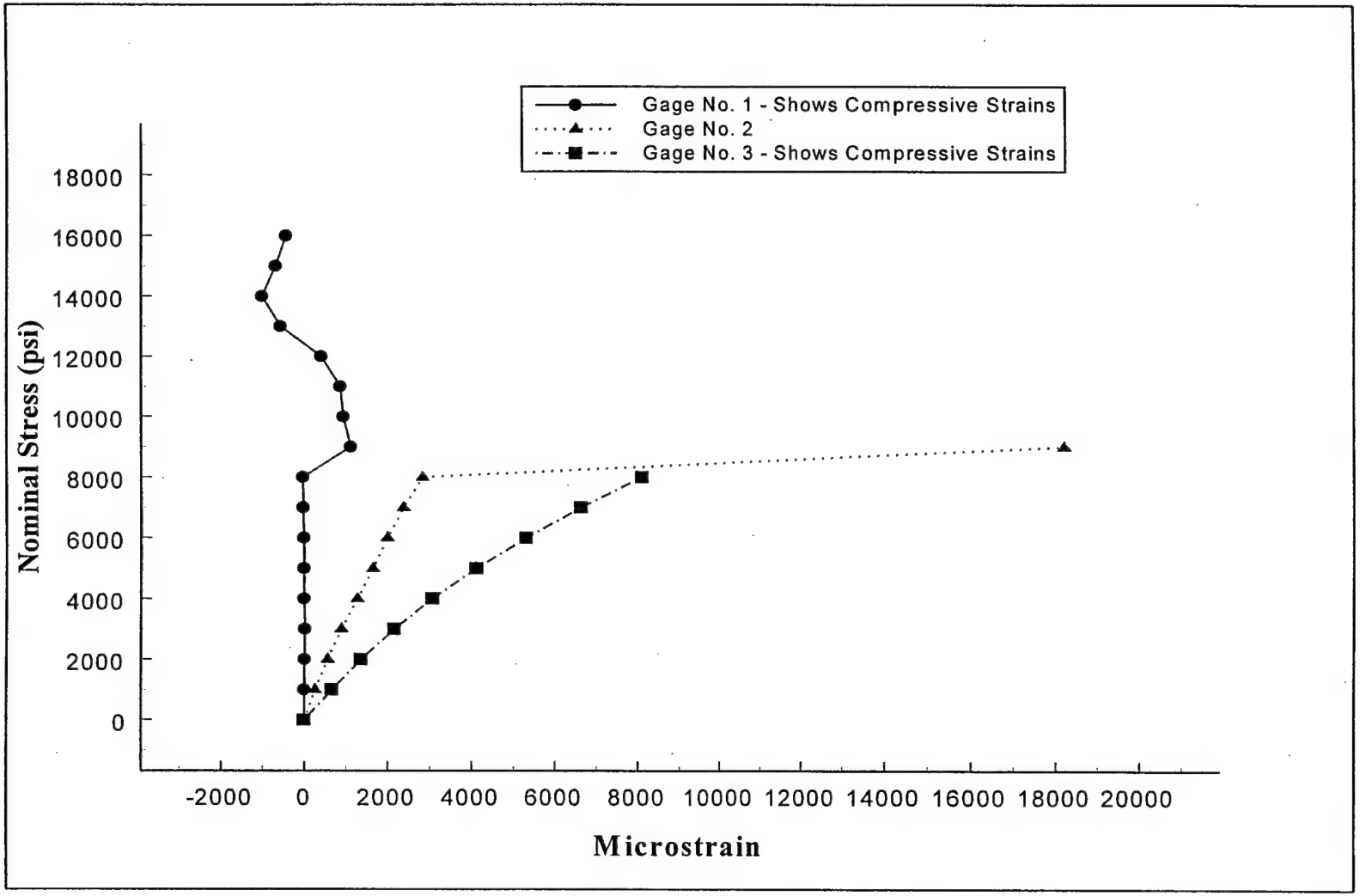

Figure 25 - Strain Gage Readings in Active Bearing Case: Compressive Strength Tests; Specimen 6-0750-11 (0/90°)

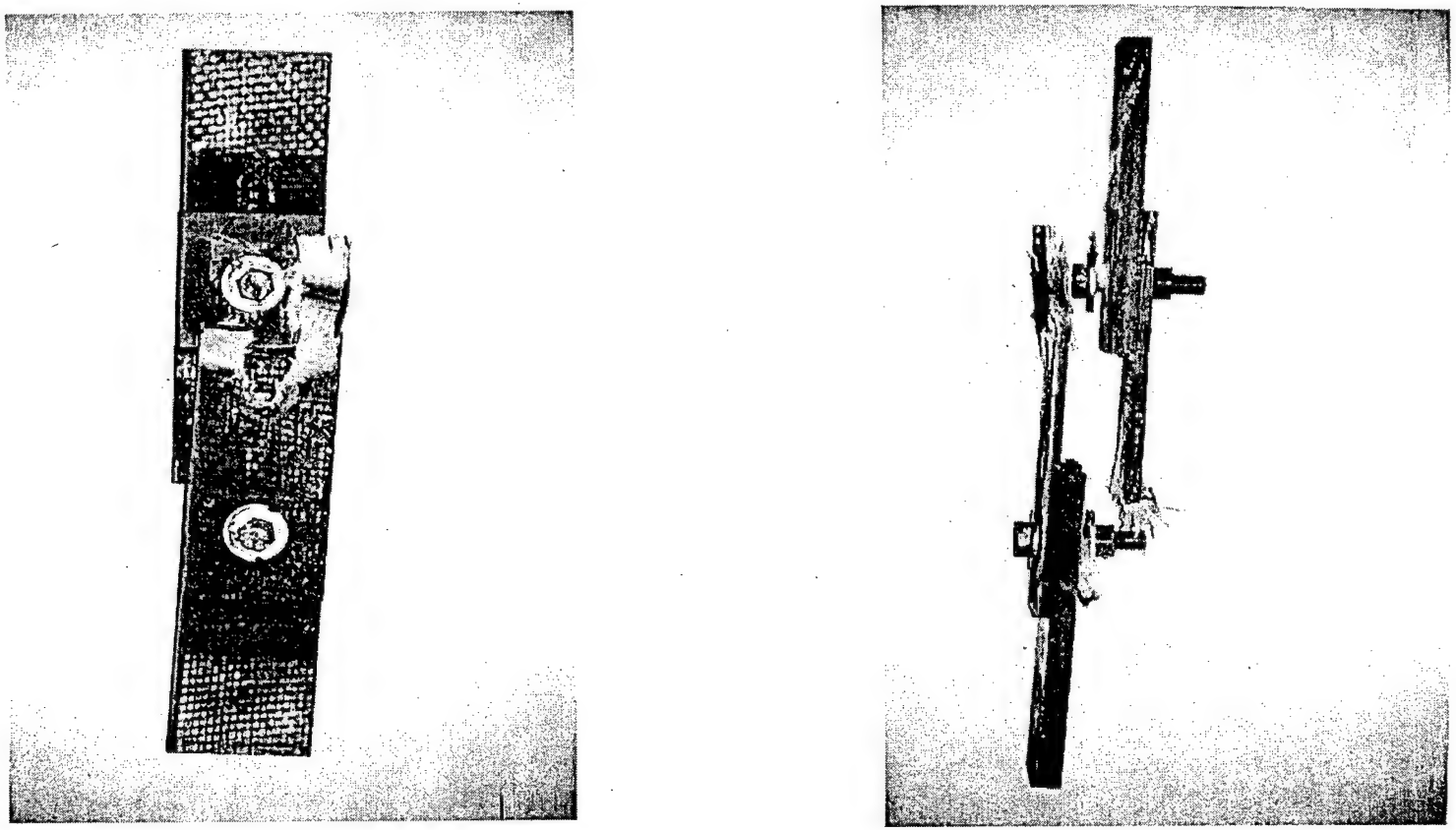

Figure 26 - Two Views of the Tensile Strength Bolted-Bonded Joint after Failure

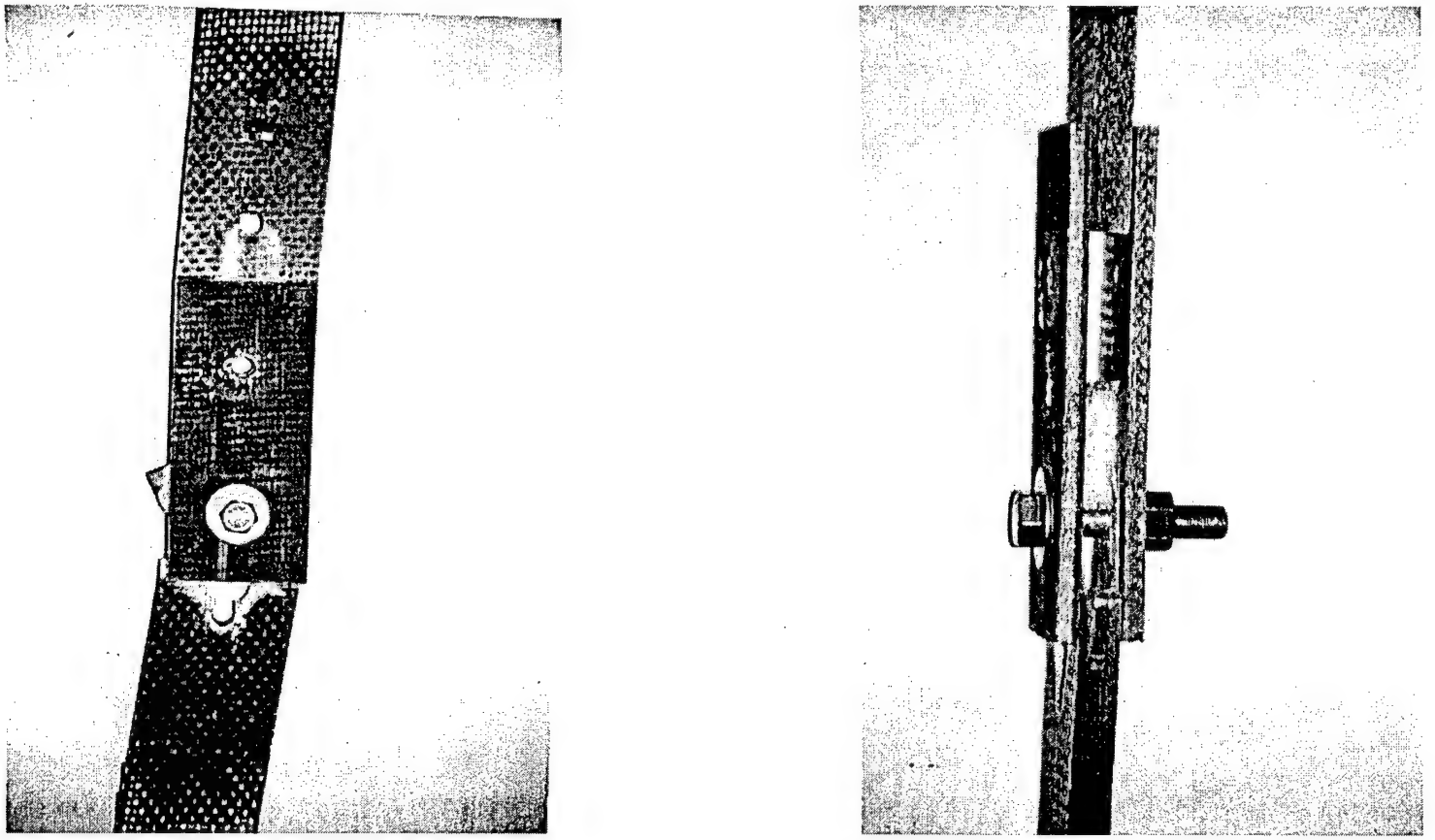

Figure 27 - Two Views of the Tensile Strength Bolted Joint after Failure

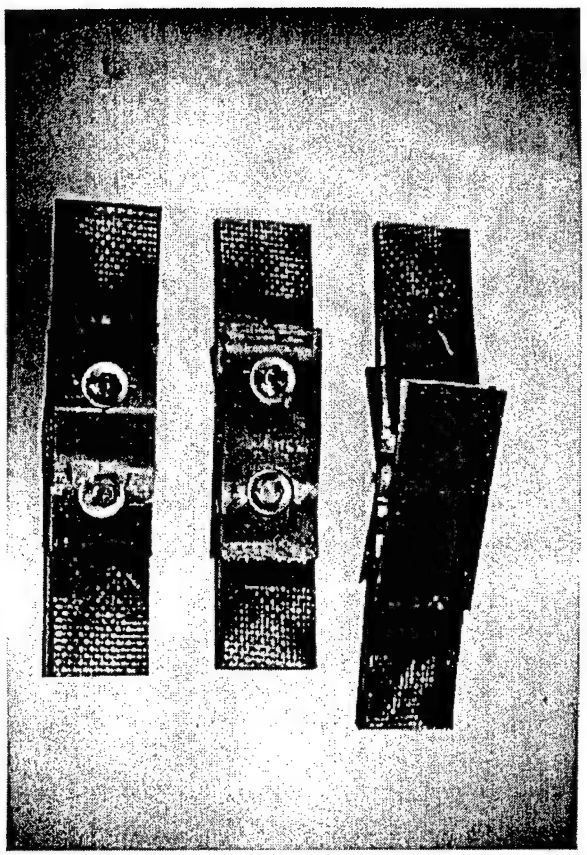

(a) FRONT VIEW

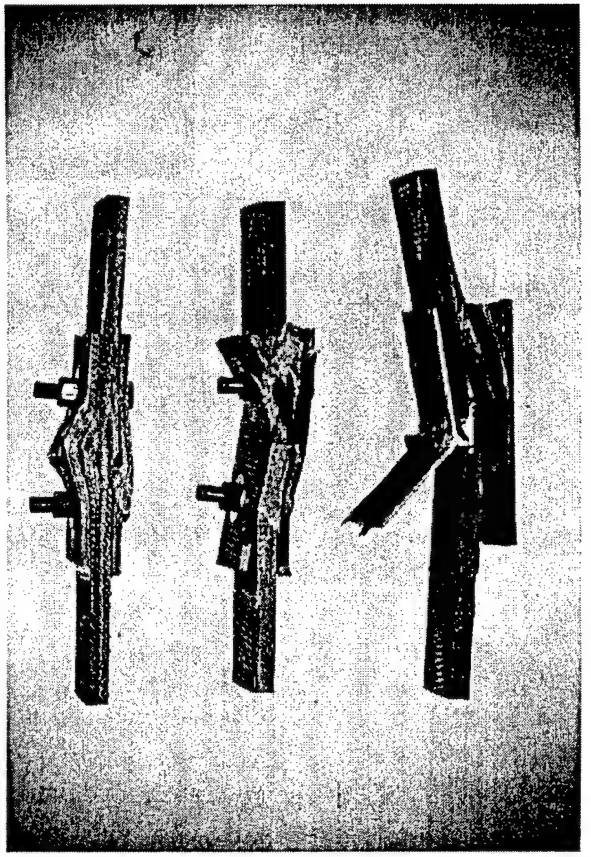

(b) SIDE VIEW

Figure 28 - Appearance of Composite Joints after Compressive Strength Tests

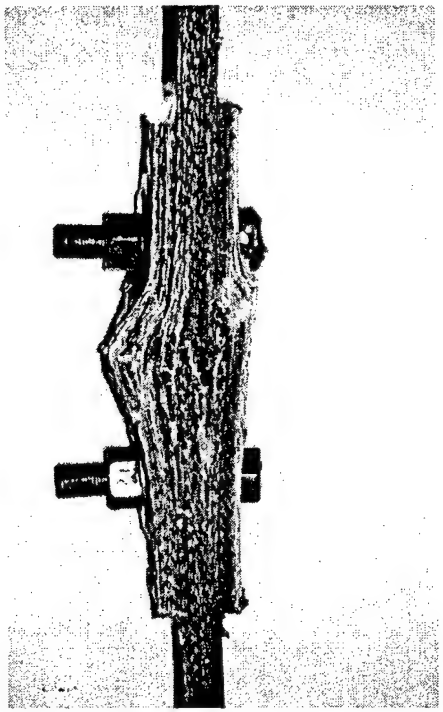

(a) BOLTED-BONDED

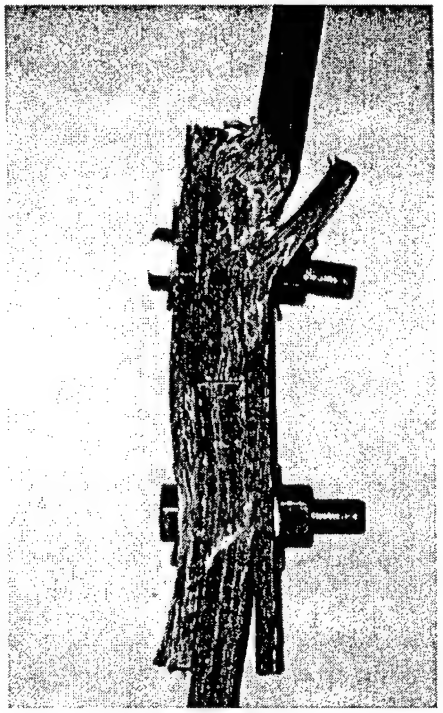

(b) BOLTED

(c) BONDED

Figure 29 - Side View of Buckled Joints after Compressive Strength Tests

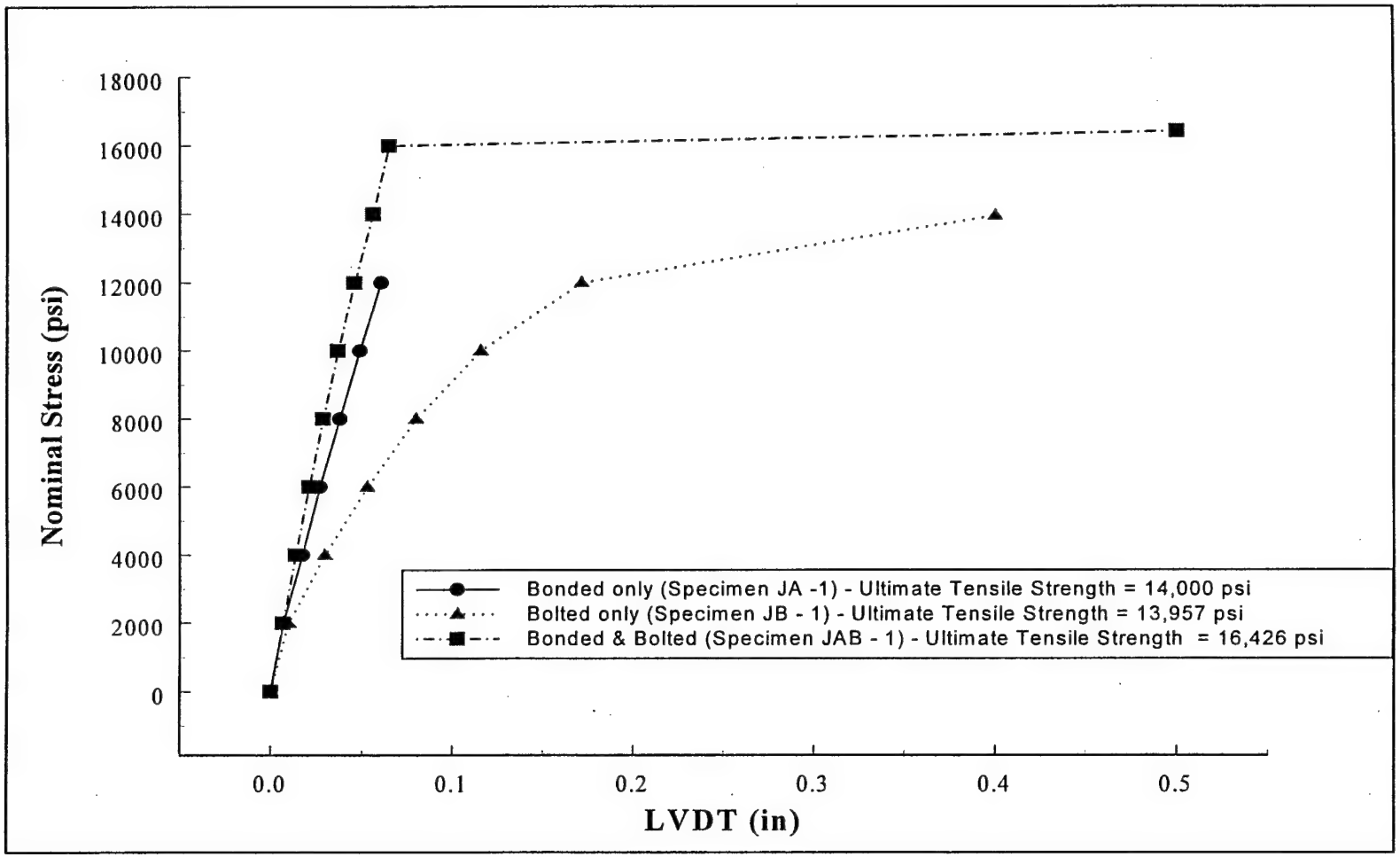

Figure 30 - Stress-Deflection for Tensile Strength Tests of Composite Joints

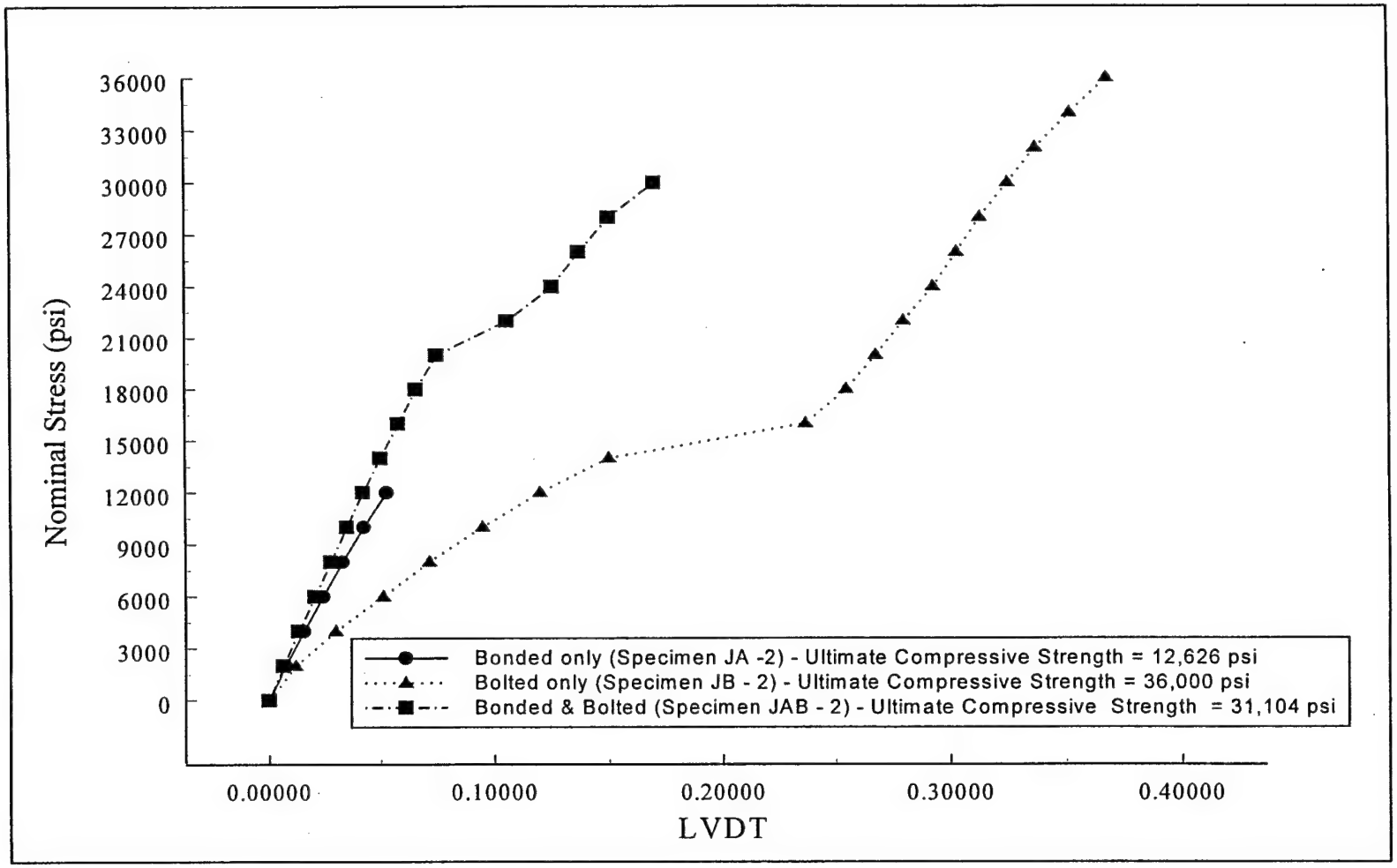

Figure 31 - Stress-Deflection for Compressive Strength Tests of Composite Joints

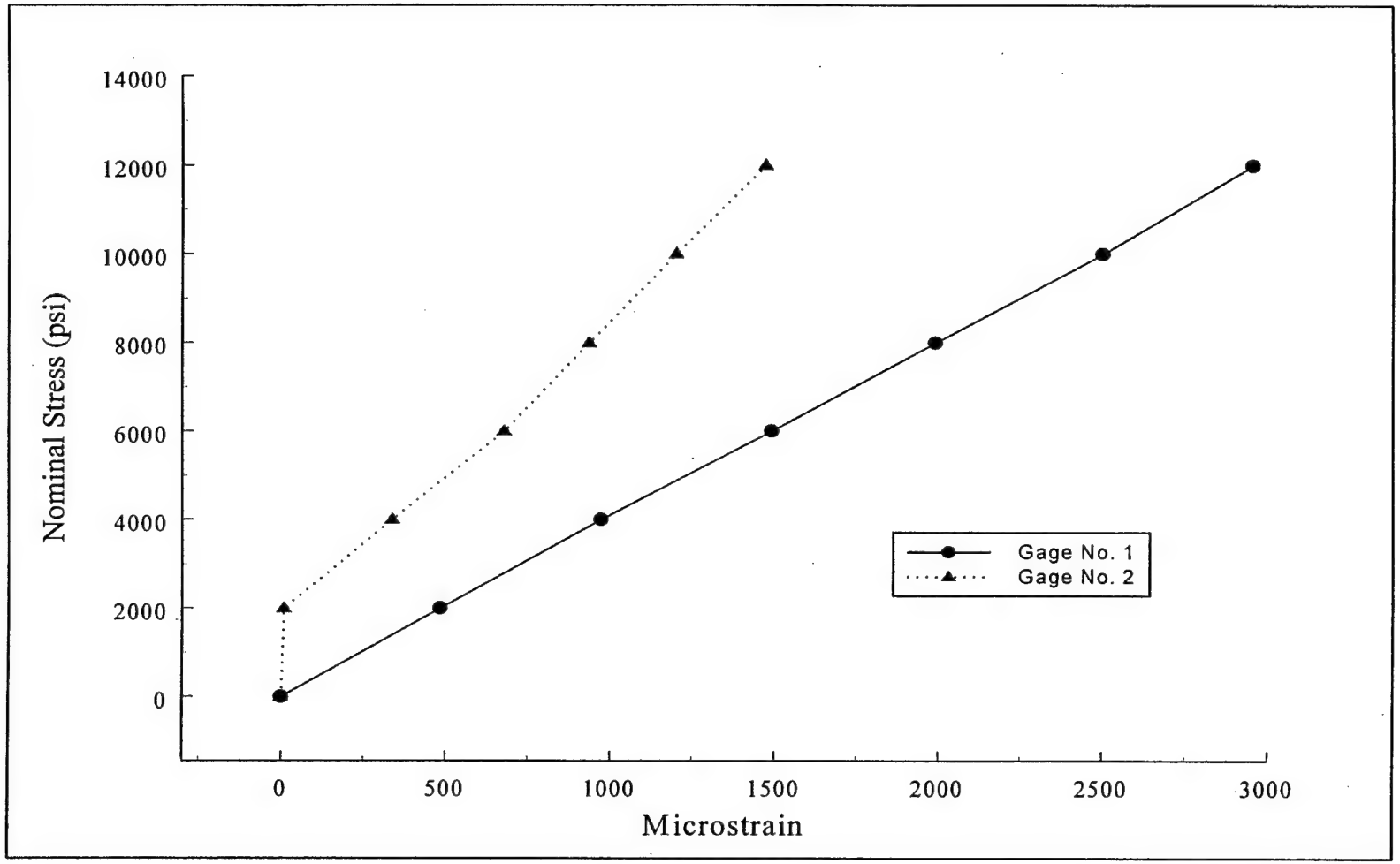

Figure 32 - Strain Gage Readings for Tensile Strength Test of Bonded Joints

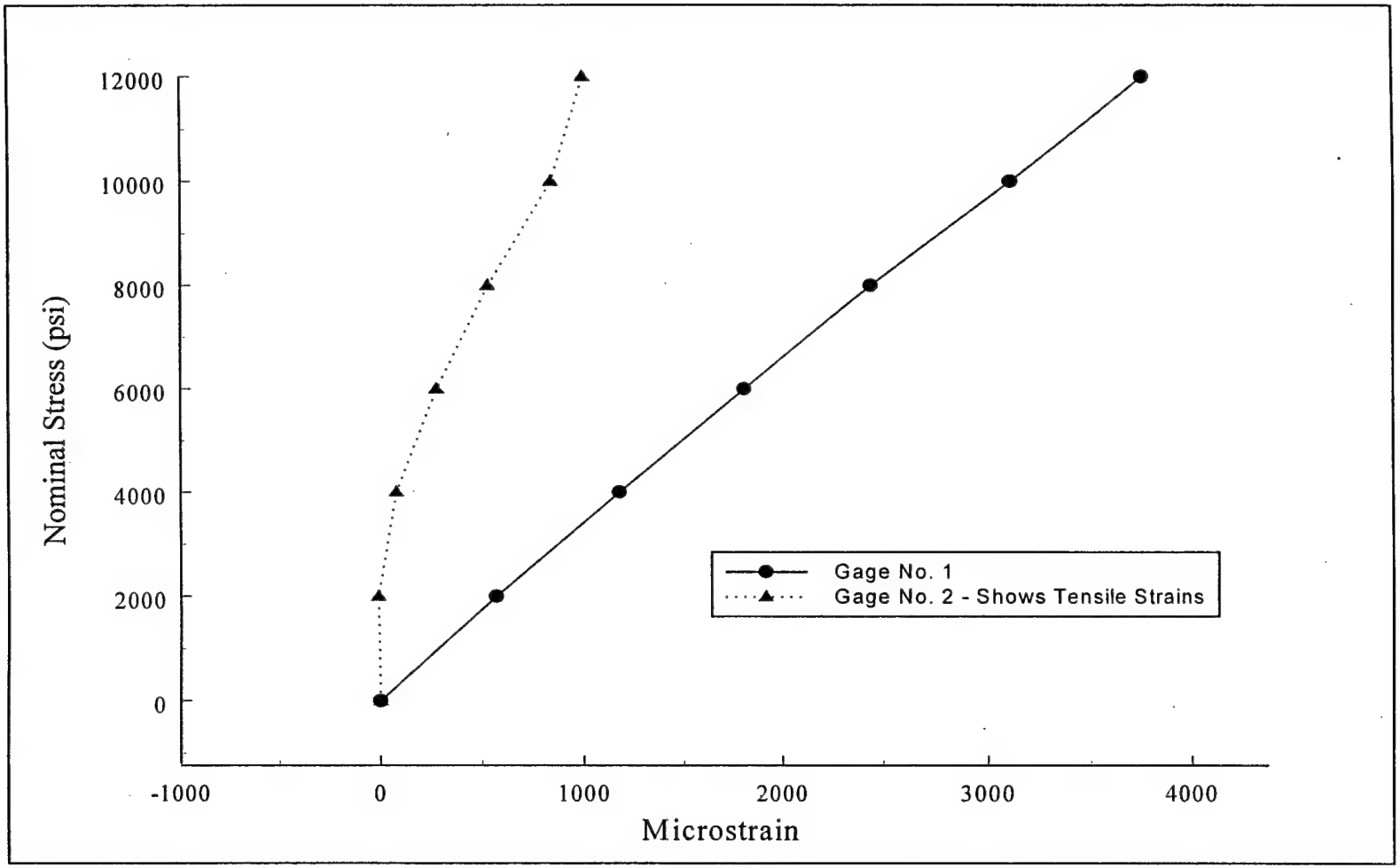

Figure 33 - Strain Gage Readings for Compressive Strength Test of Bonded Joints

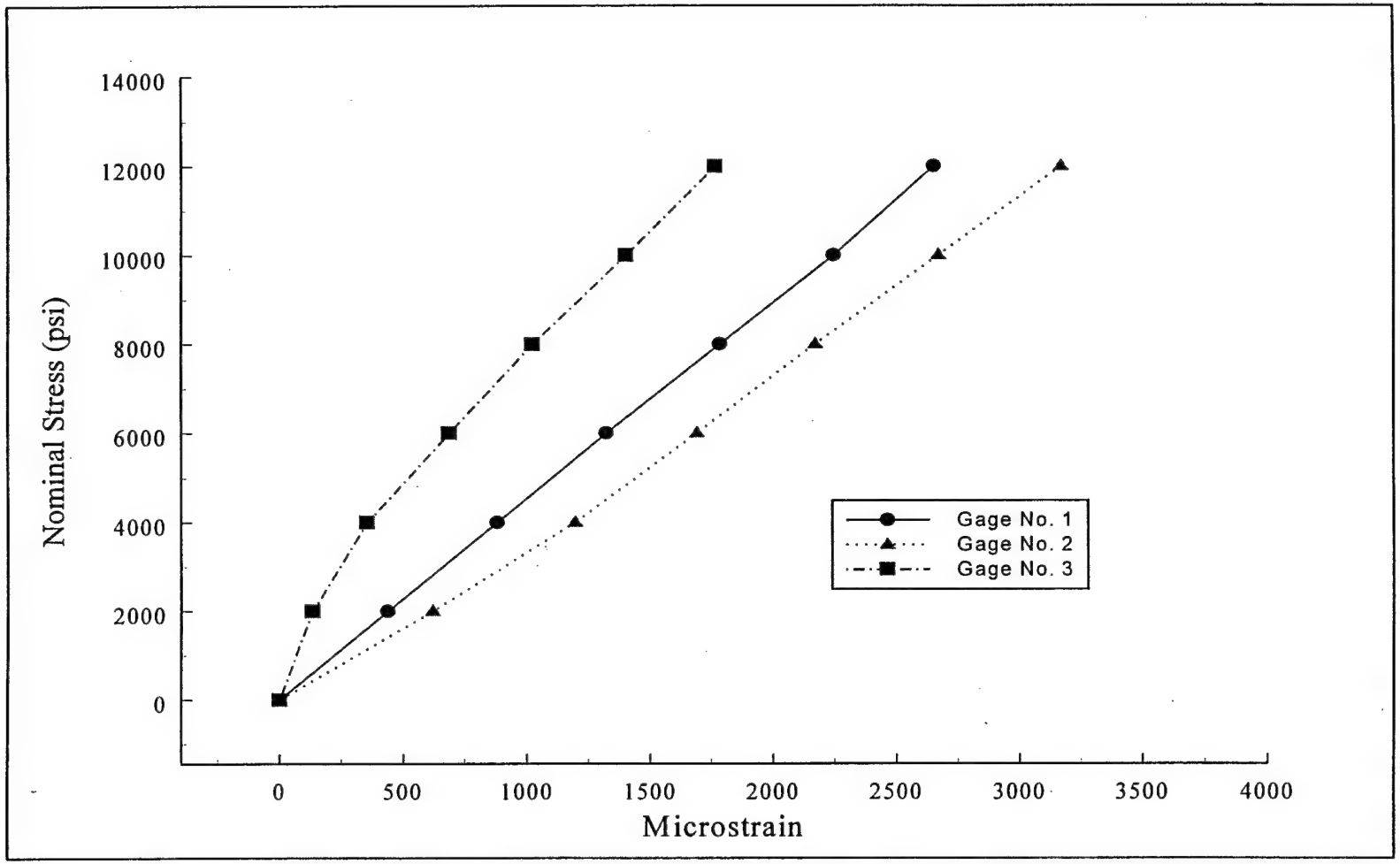

Figure 34 - Strain Gage Readings for Tensile Strength Test of Bolted Joints

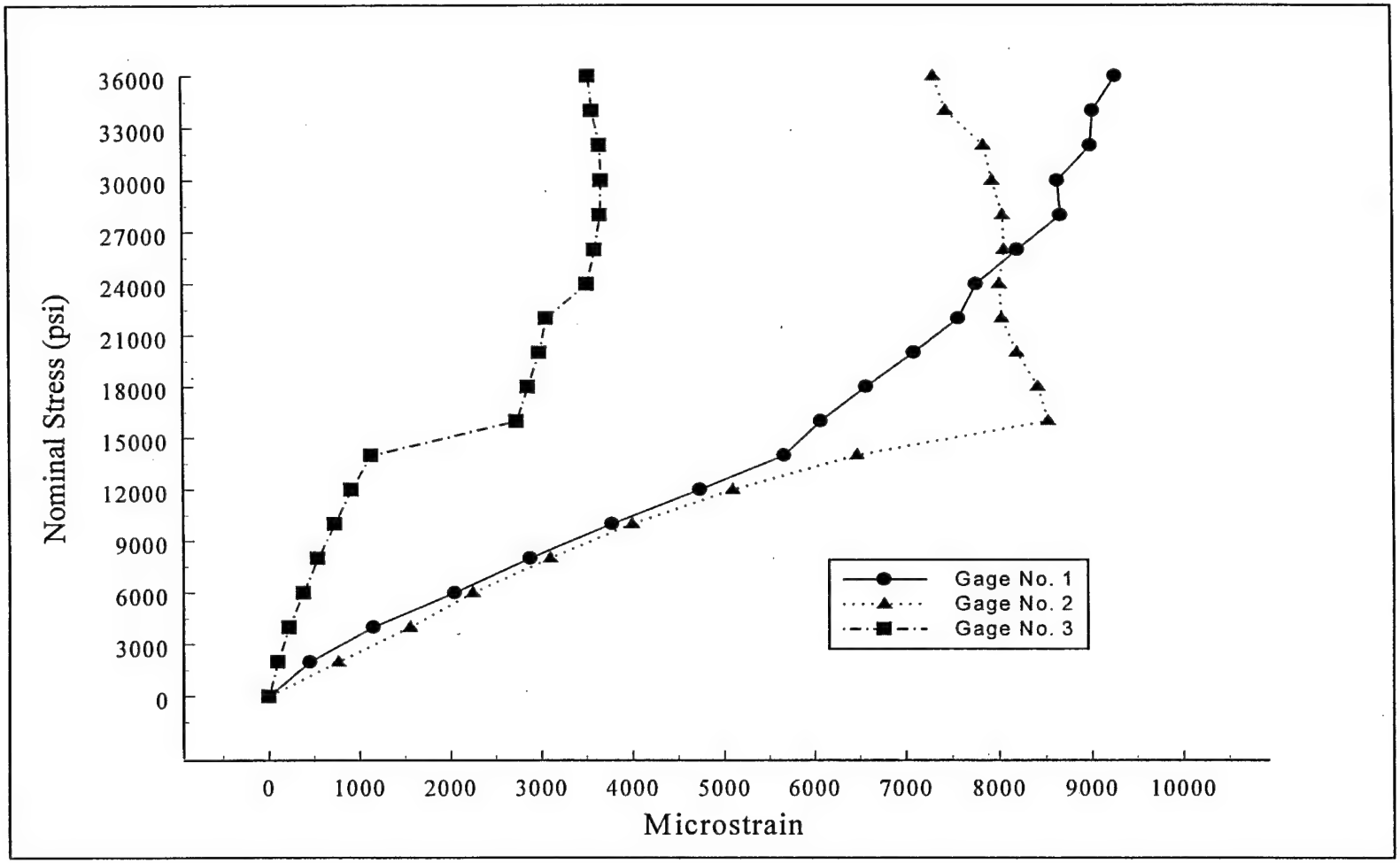

Figure 35 - Strain Gage Readings for Compressive Strength Test of Bolted Joints

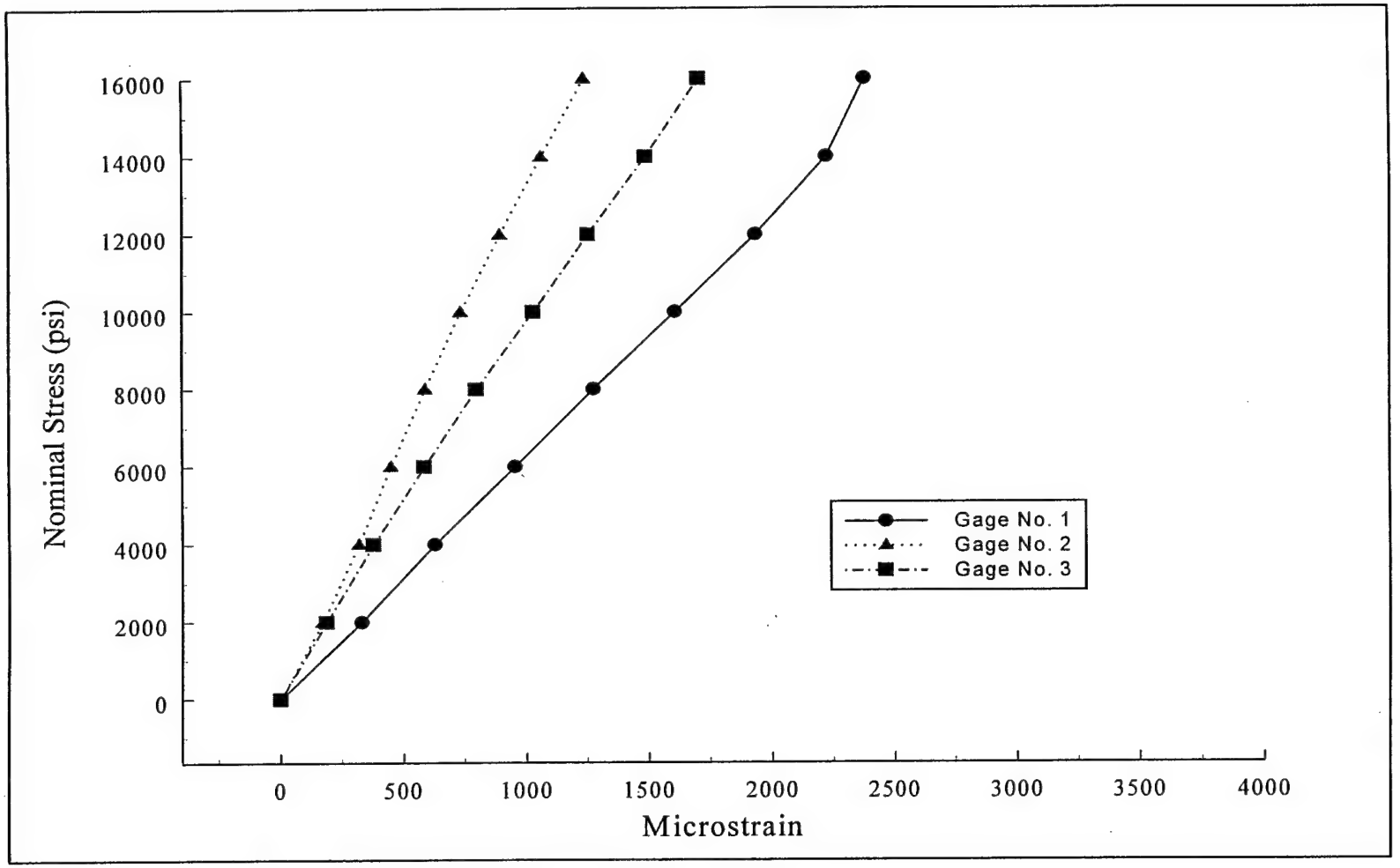

Figure 36 - Strain Gage Readings for Tensile Strength Test of Bolted-Bonded Joints

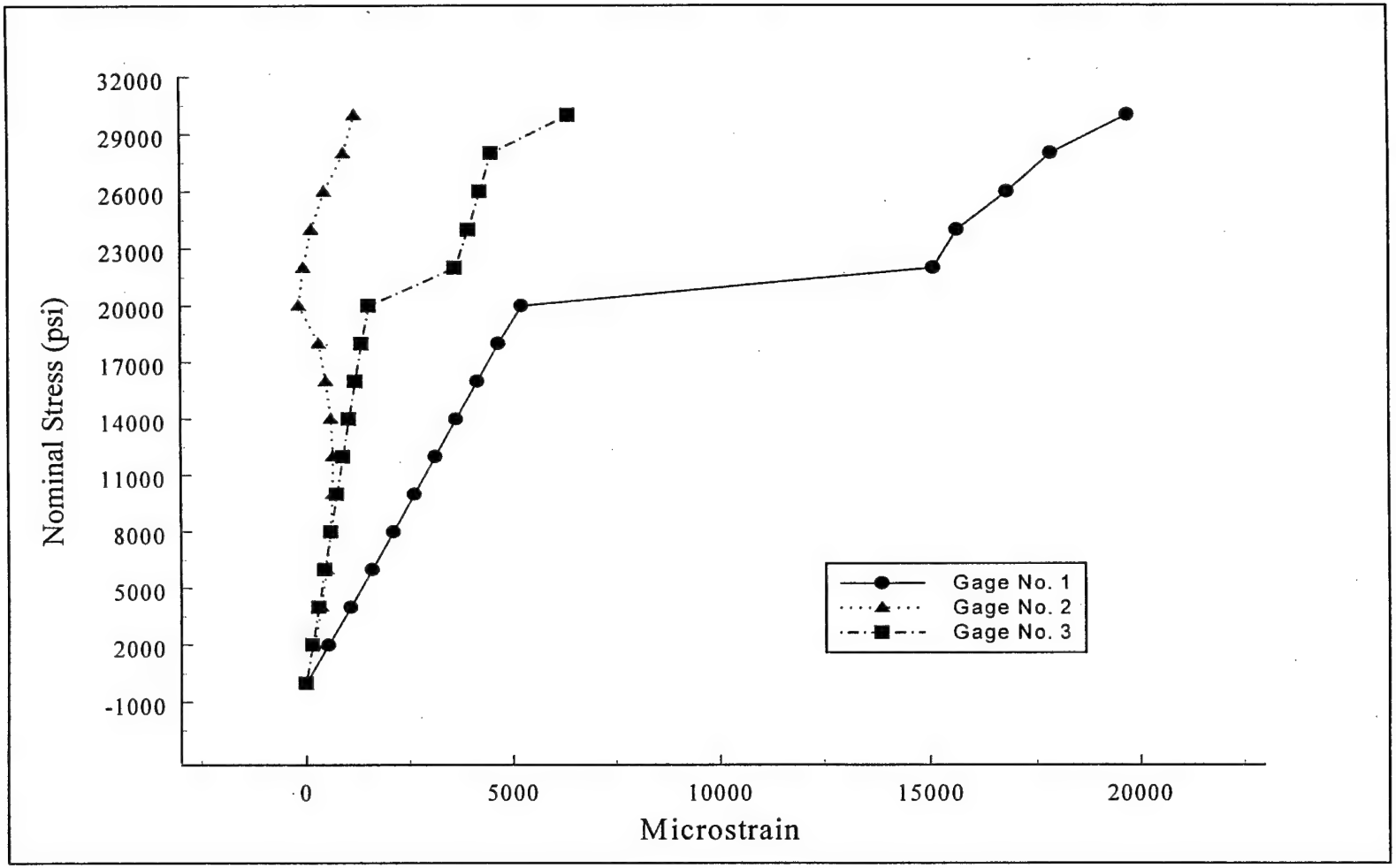

Figure 37 - Strain Gage Readings for Compressive Strength Test of Bolted-Bonded Joints

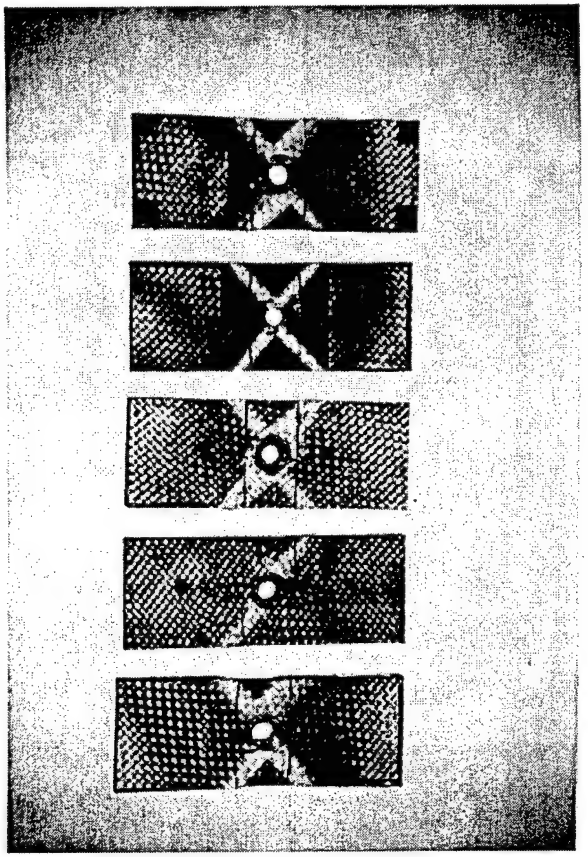

(a) ±45° SPECIMENS

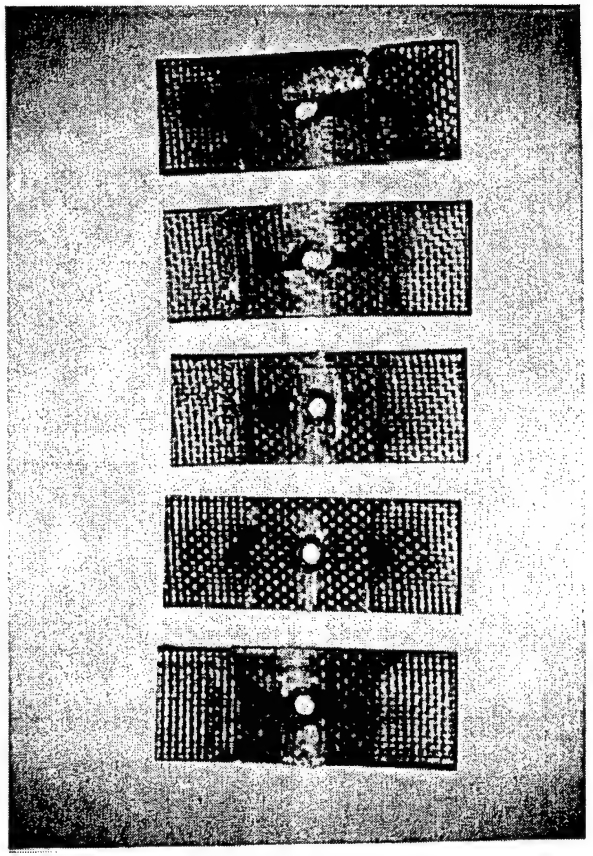

(b) 0/90° SPECIMENS

Figure 38 - Failure Modes for Fatigue Tests of Passive Bearing Case

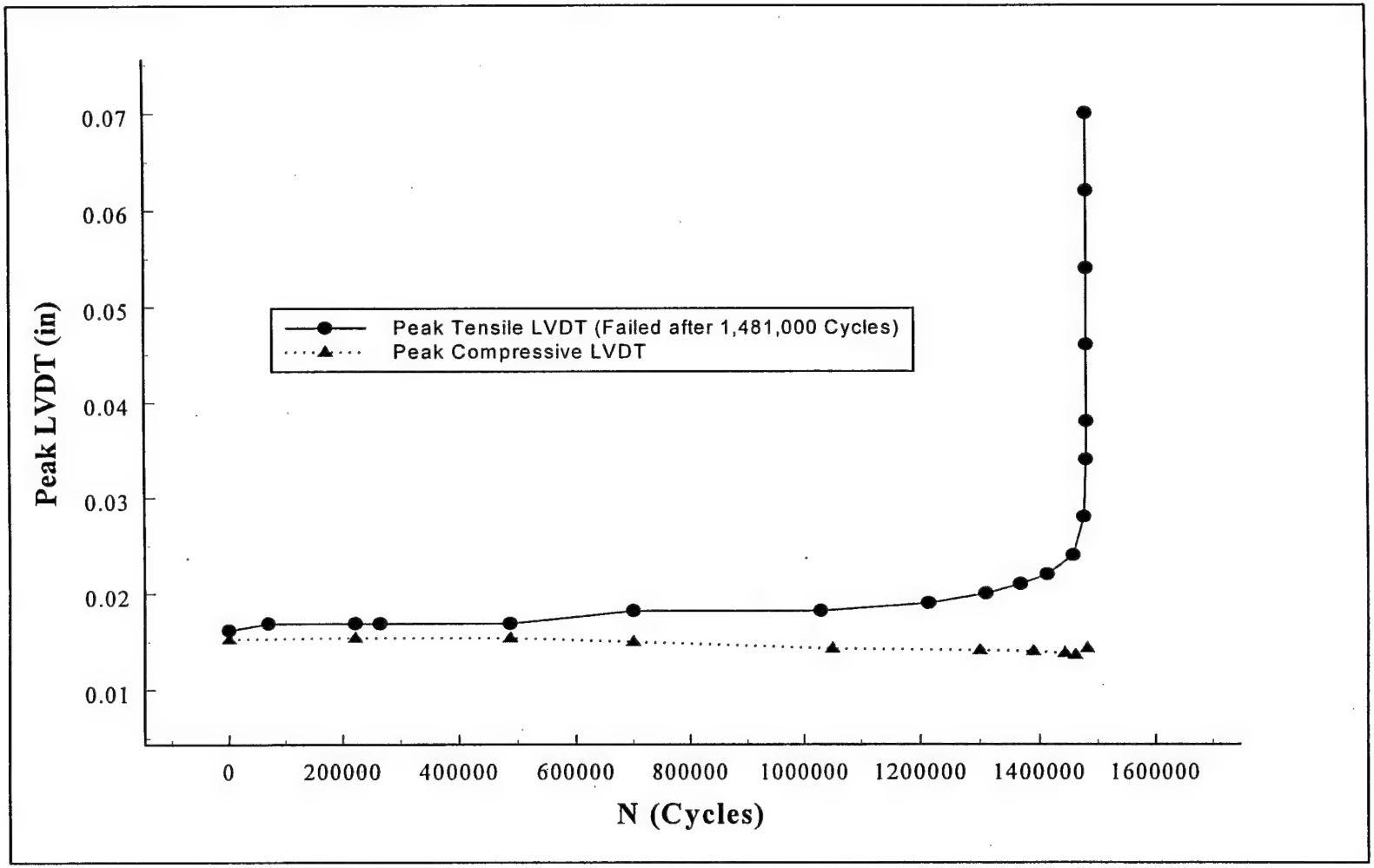

Figure 39 - The Evolution of Deflection During the Fatigue Life of Passive Specimen 6-0750-1: 0/90°, 7.5 ksi

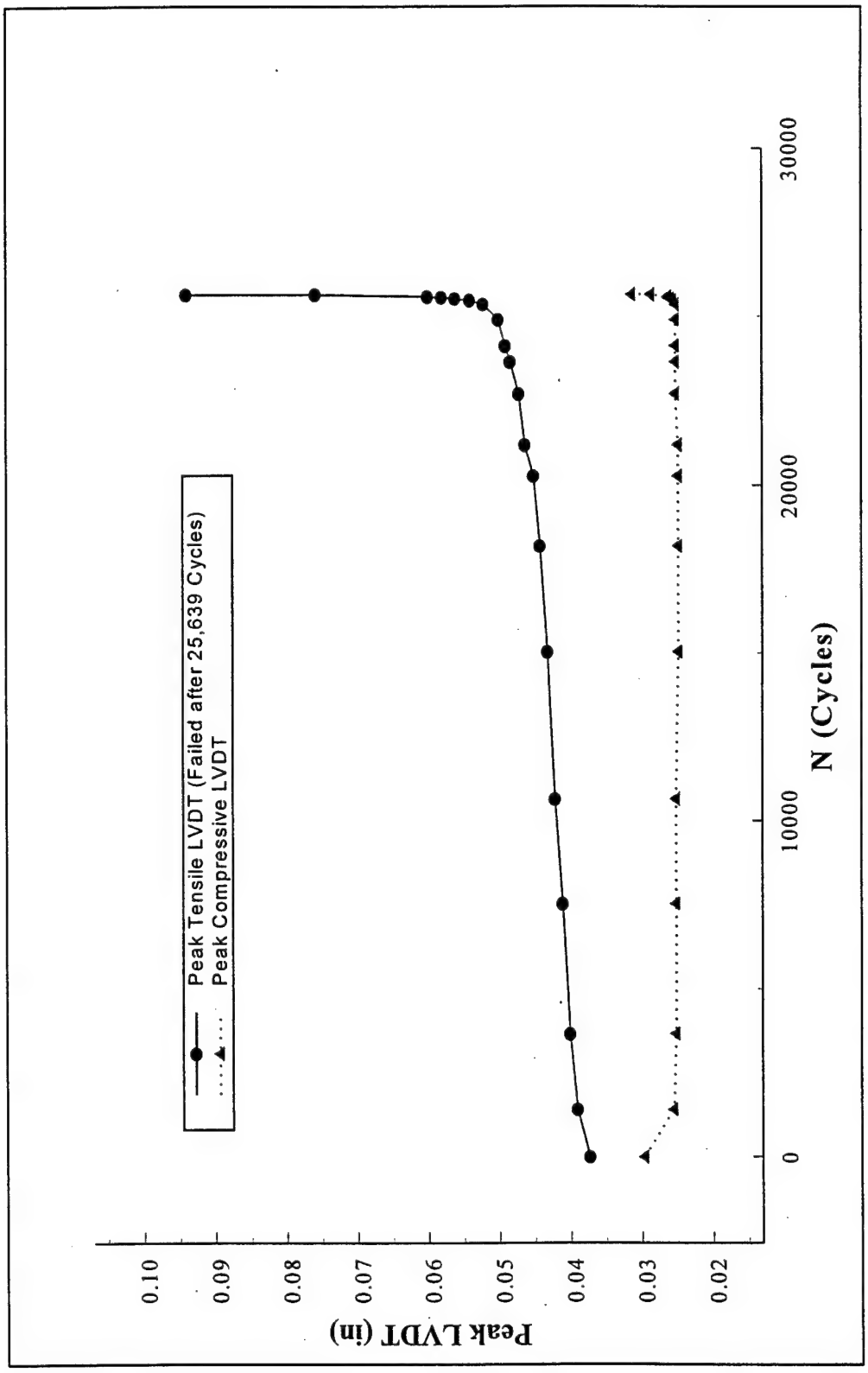

Figure 40 - The Evolution of Deflection During the Fatigue Life of Passive Specimen 6-0750-8: 0/90°, 15 ksi

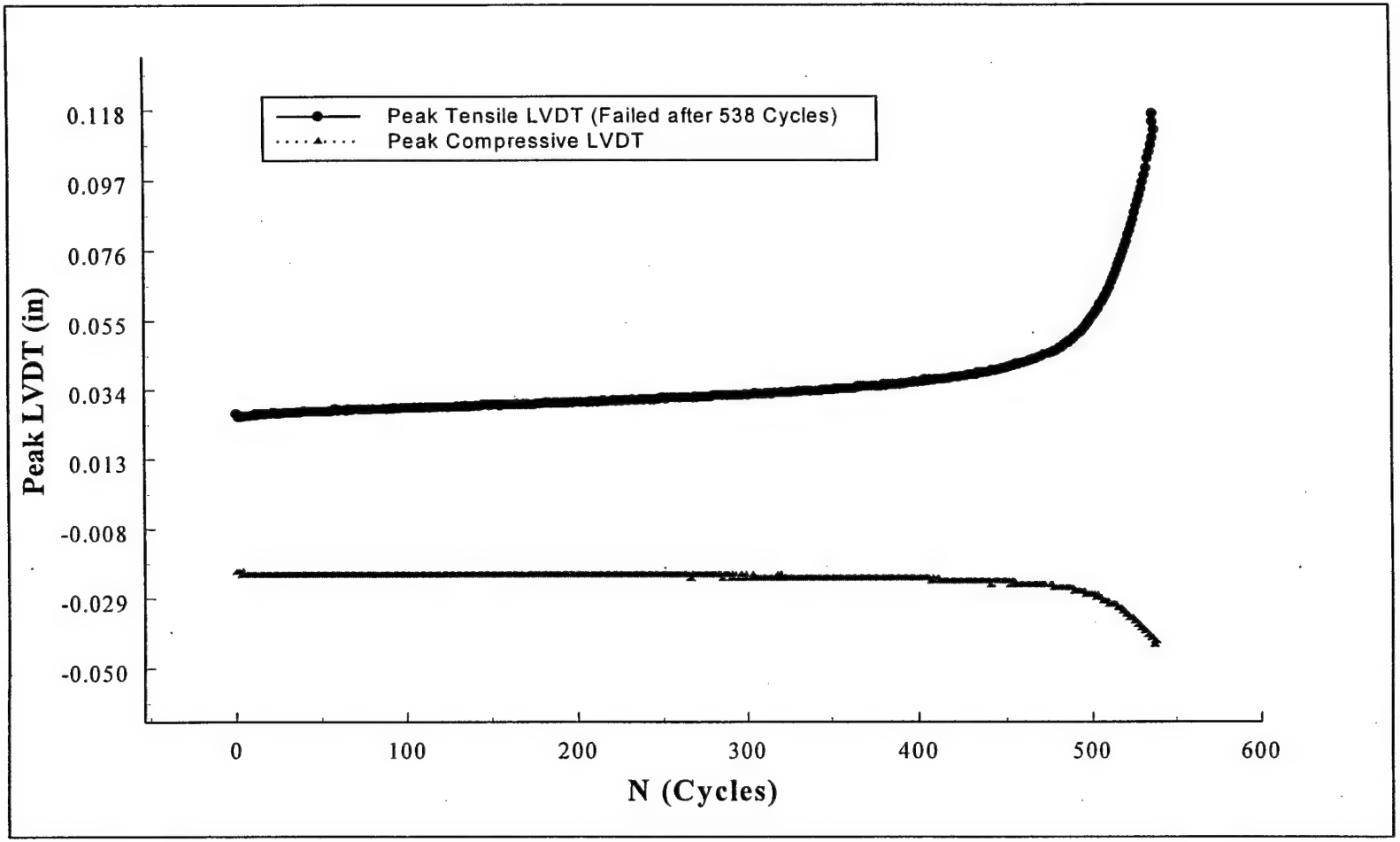

Figure 41 - The Evolution of Deflection During the Fatigue Life of Passive Specimen 9-0750-7: $\pm 45^{\circ}$, 7.5 ksi

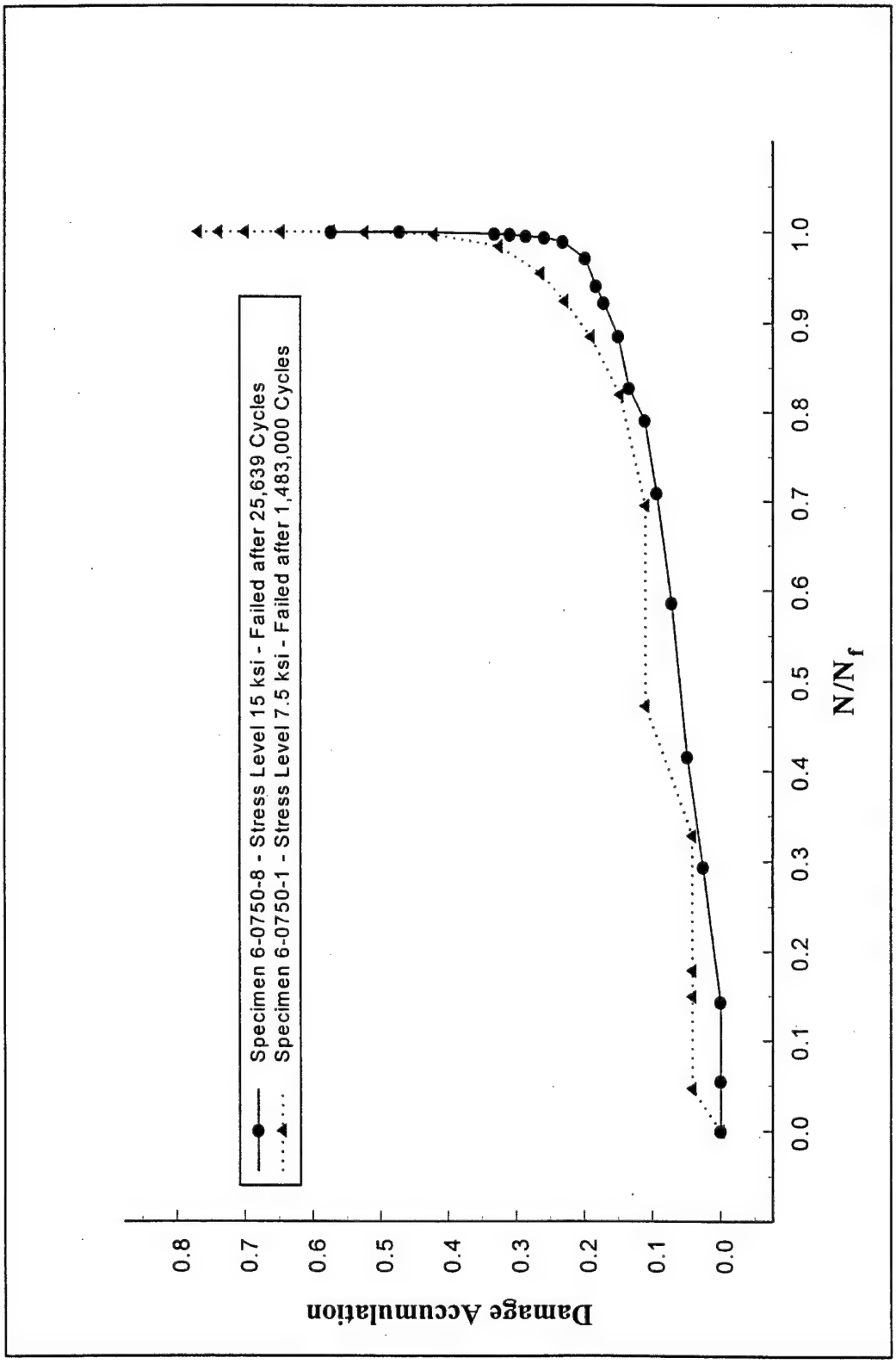

Figure 42 - Constant Amplitude Deflection-Based Fatigue Damage Accumulation in 0/90° FRP Laminates with Holes - Passive Bearing Case

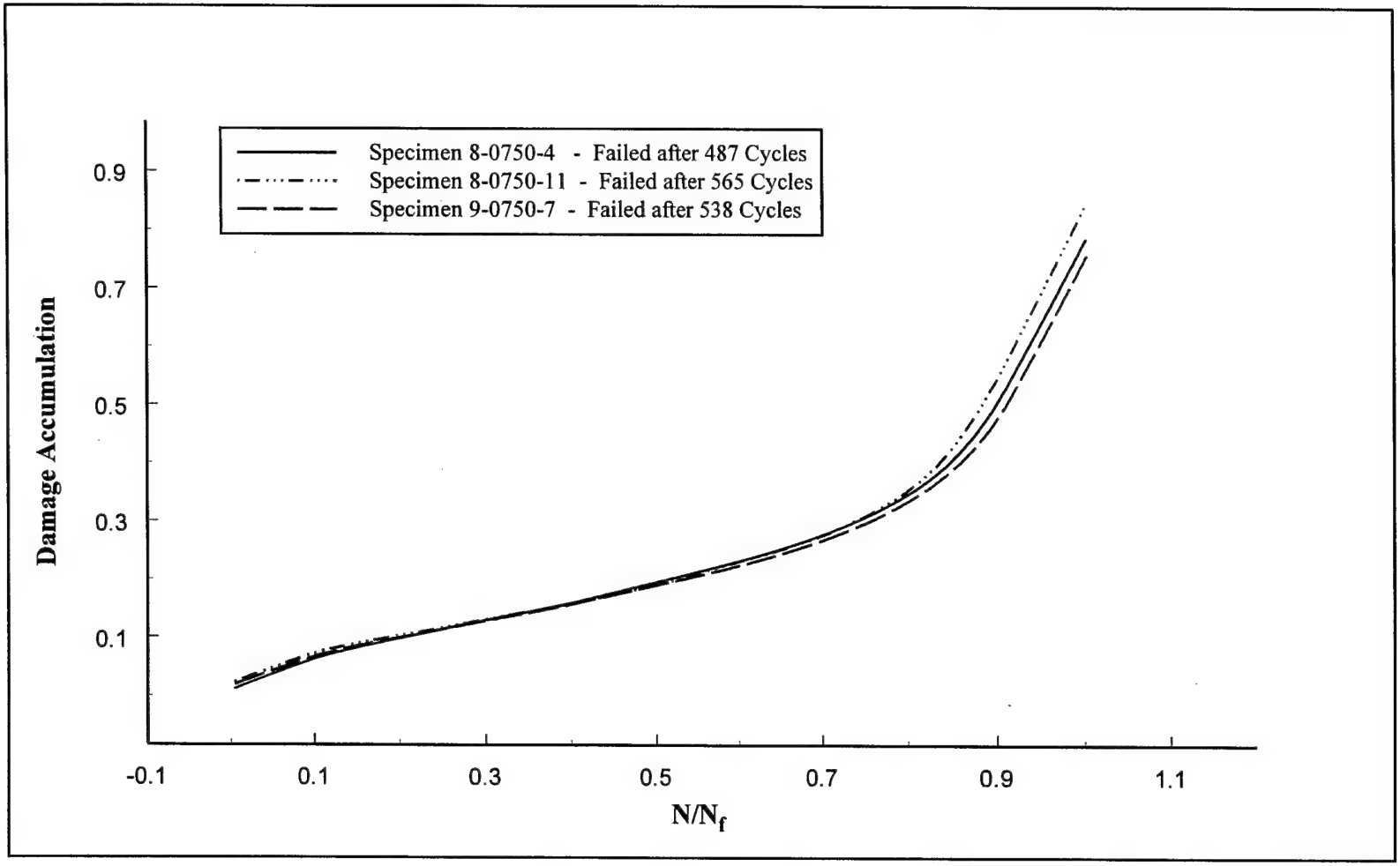

Figure 43 - Constant Amplitude Deflection-Based Fatigue Damage Accumulation in $\pm 45^{\circ}$ FRP Laminates with Holes - Passive Bearing Case

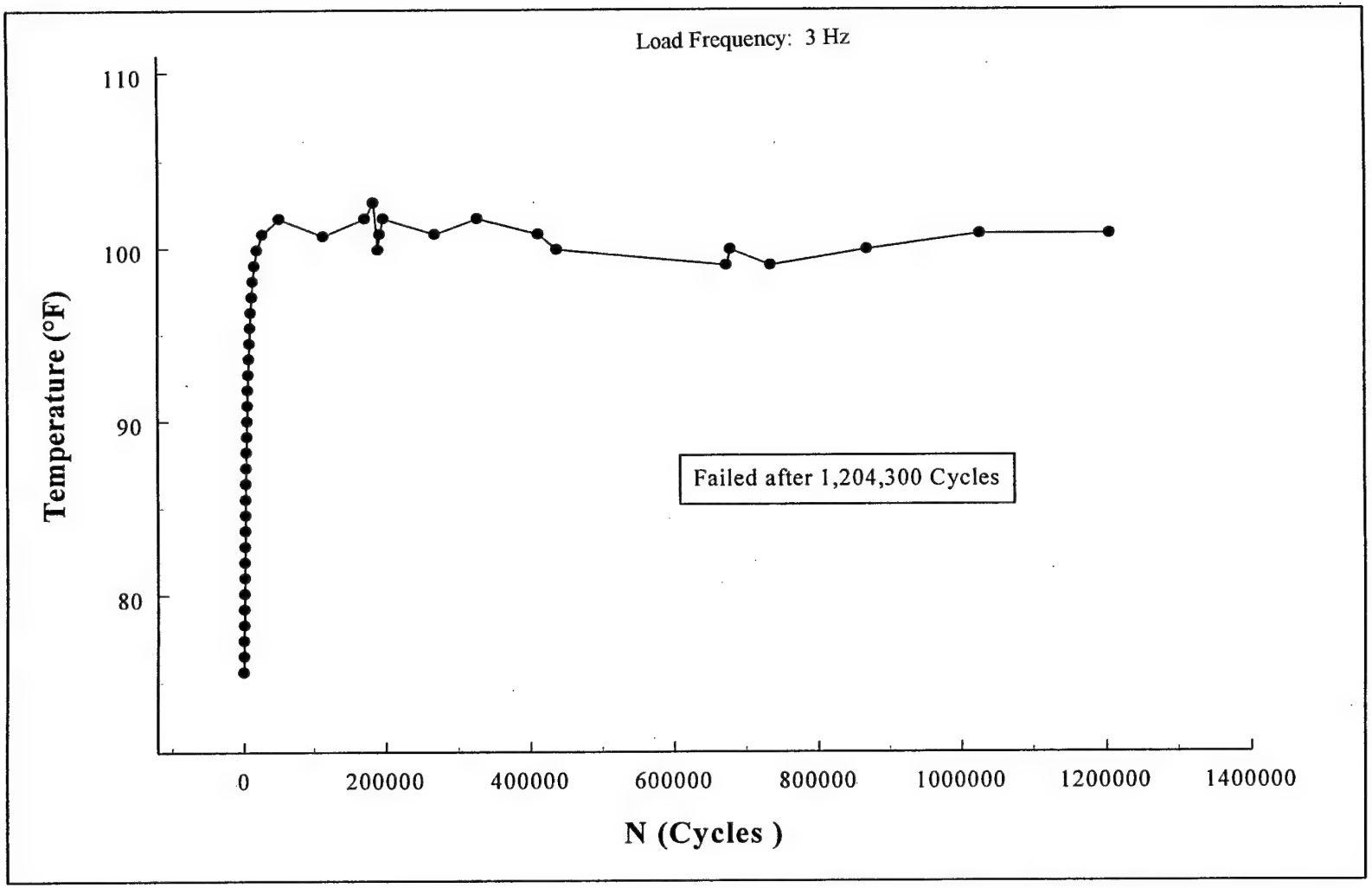

Figure 44 - Temperature Rise During Constant Amplitude Fatigue Tests of Passive Bearing Case; Specimen 8-0750-3: $\pm 45^{\circ}$, 3.5 ksi

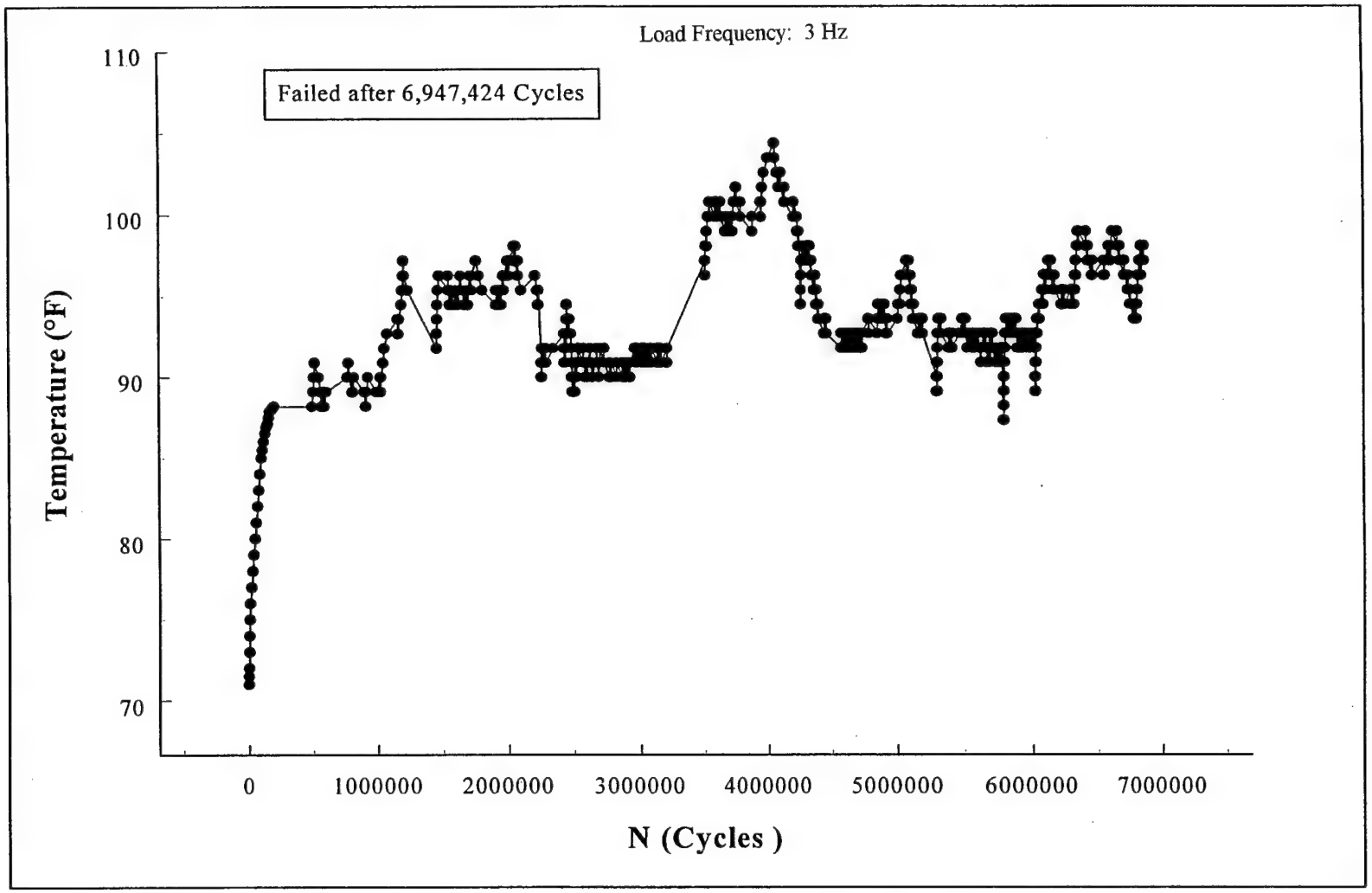

Figure 45 - Temperature Rise During Constant Amplitude Fatigue Tests of Passive Bearing Case; Specimen 9-0750-5: ±45°, 3.5 ksi

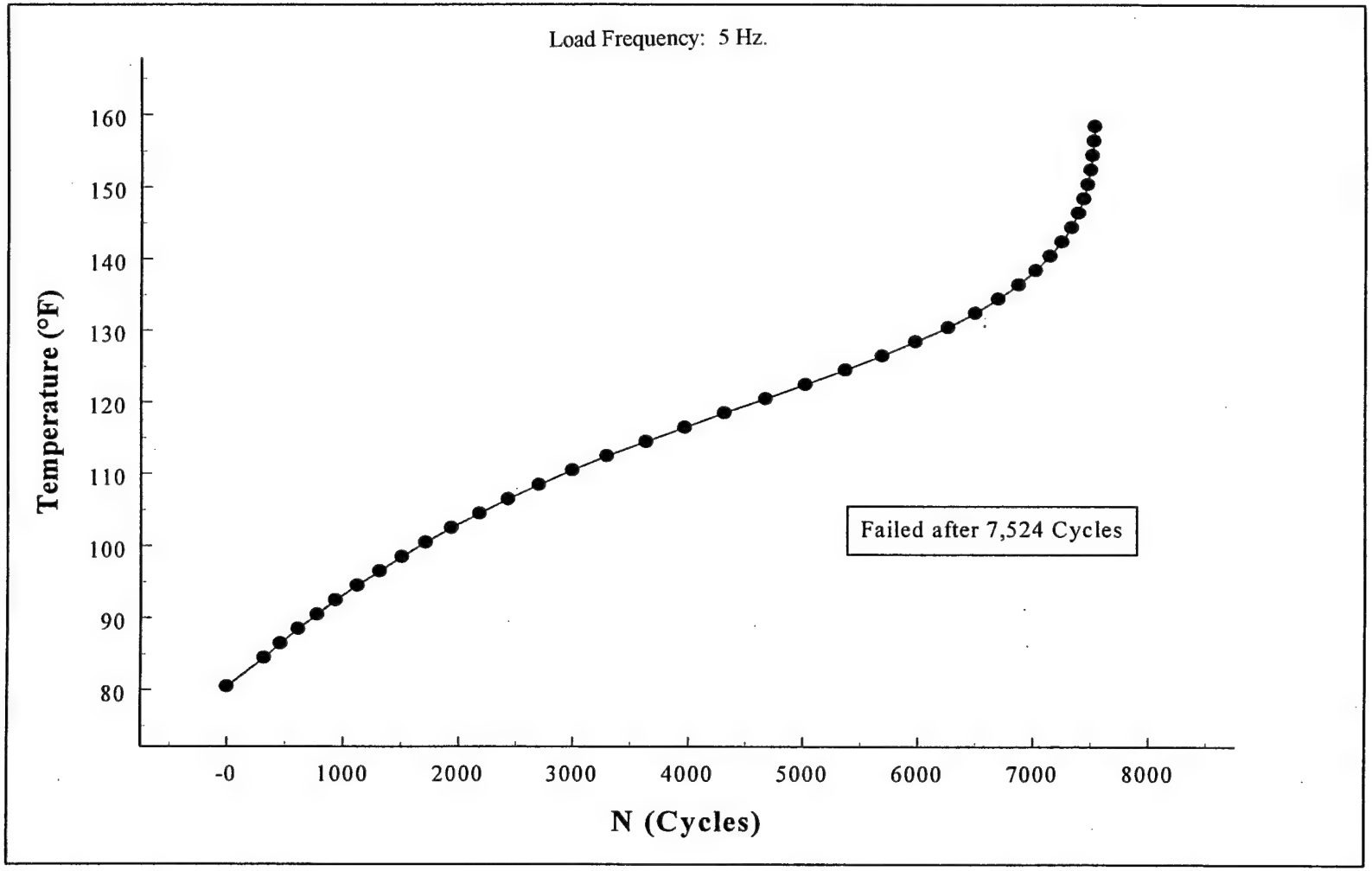

Figure 46 - Temperature Rise During Constant Amplitude Fatigue Tests of Passive Bearing Case; Specimen 9-0750-6: $\pm 45^{\circ}$, 5 ksi

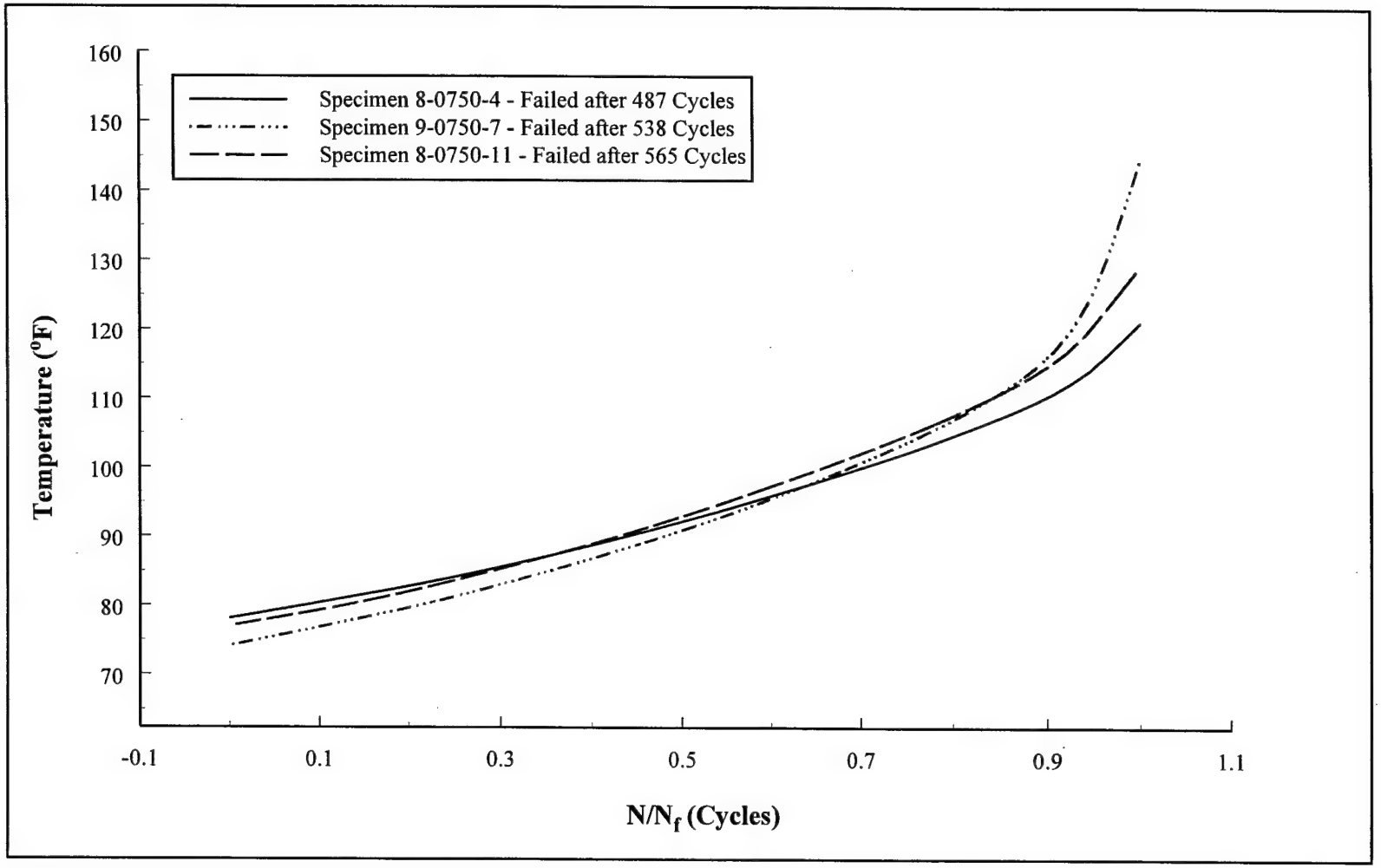

Figure 47 - Temperature Rise During Constant Amplitude Fatigue Tests of Passive Bearing Case; ± 45°, 7.5 ksi

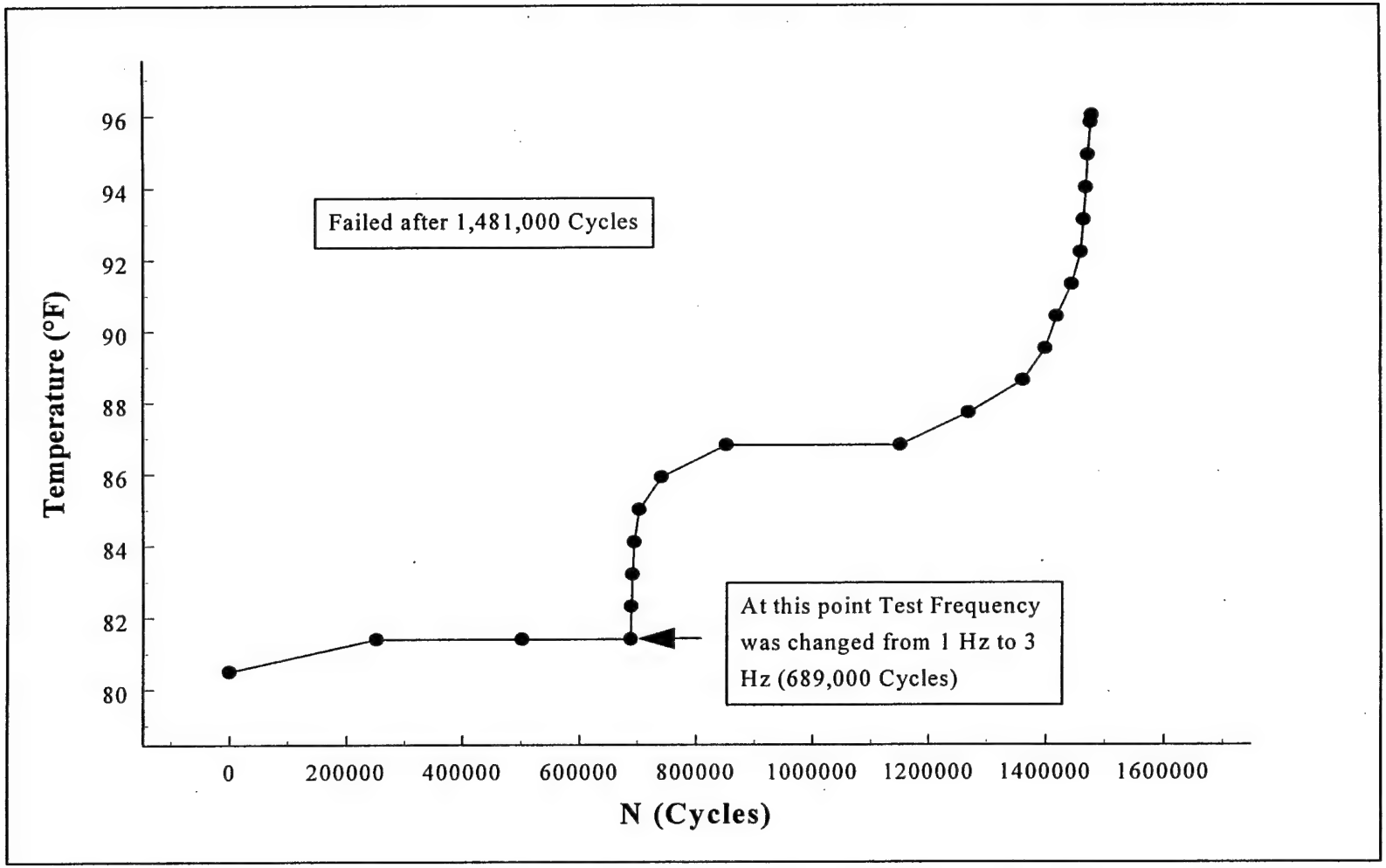

Figure 48 - Temperature Rise During Constant Amplitude Fatigue Tests of Passive Bearing Case; Specimen 6-0750-1: 0/90°, 7.5 ksi

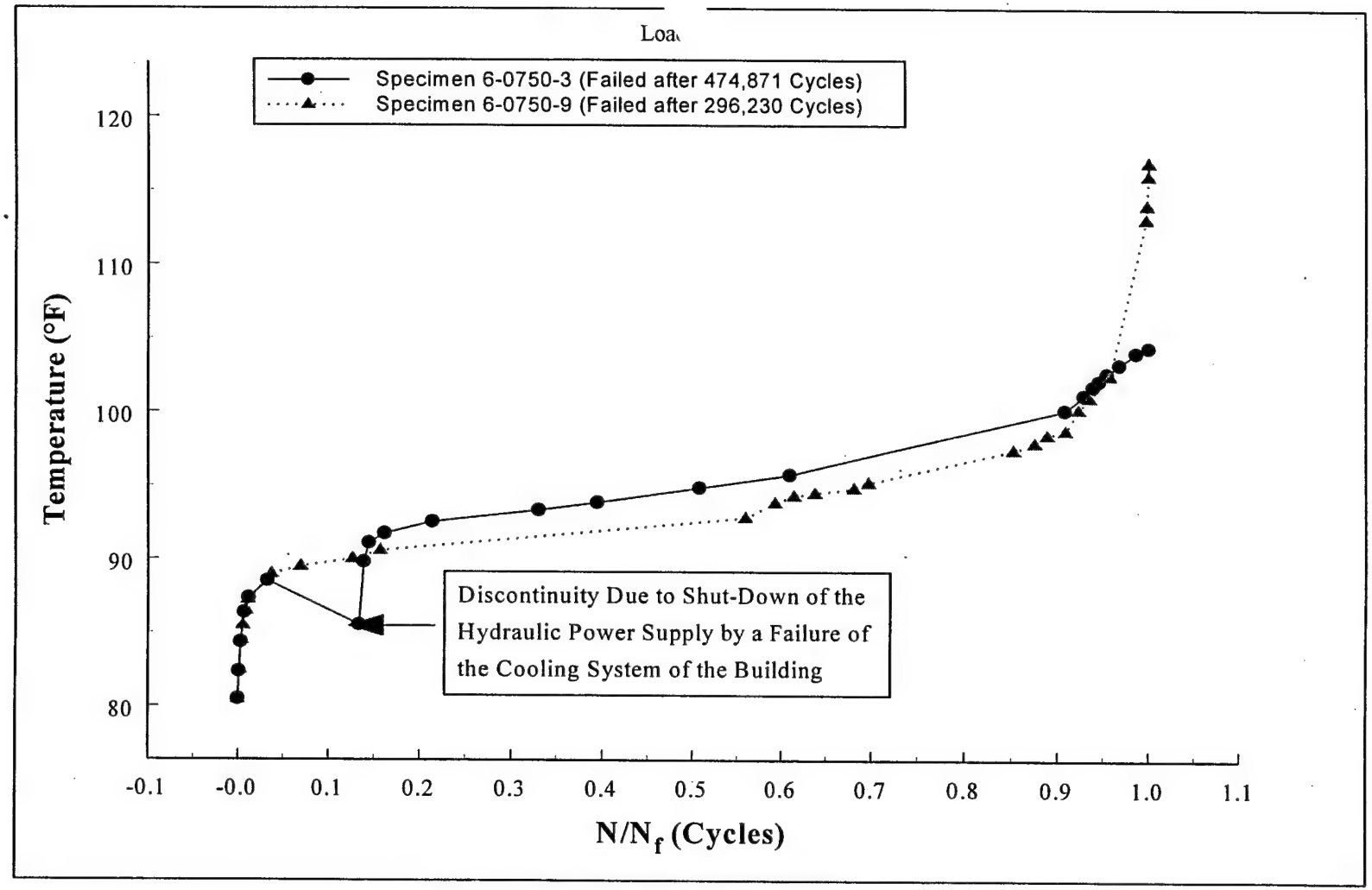

Figure 49 - Temperature Rise During Constant Amplitude Fatigue Tests of Passive Bearing Case; 0/90°, 10 ksi

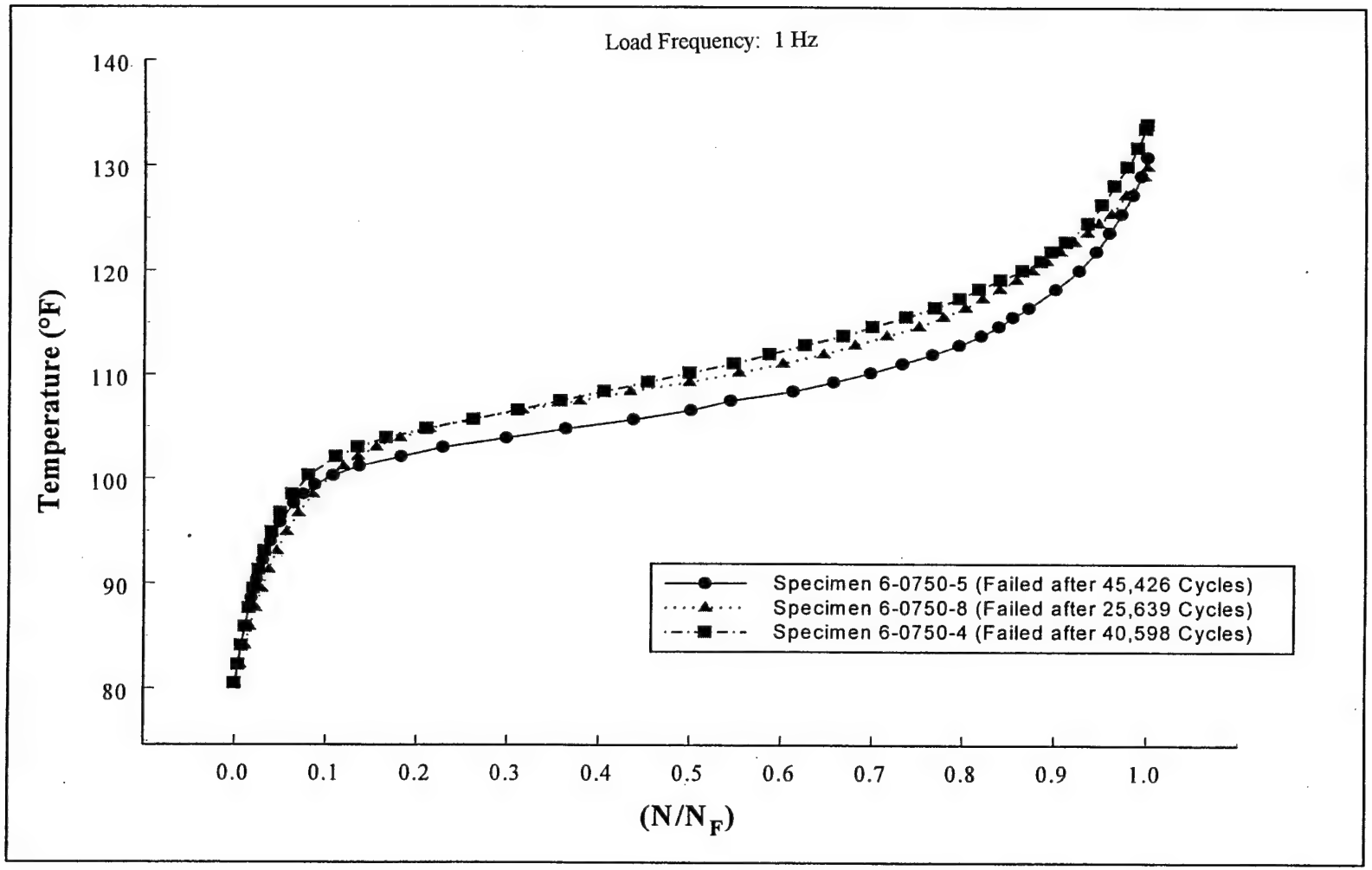

Figure 50 - Temperature Rise During Constant Amplitude Fatigue Tests of Passive Bearing Case; 0/90°, 15 ksi

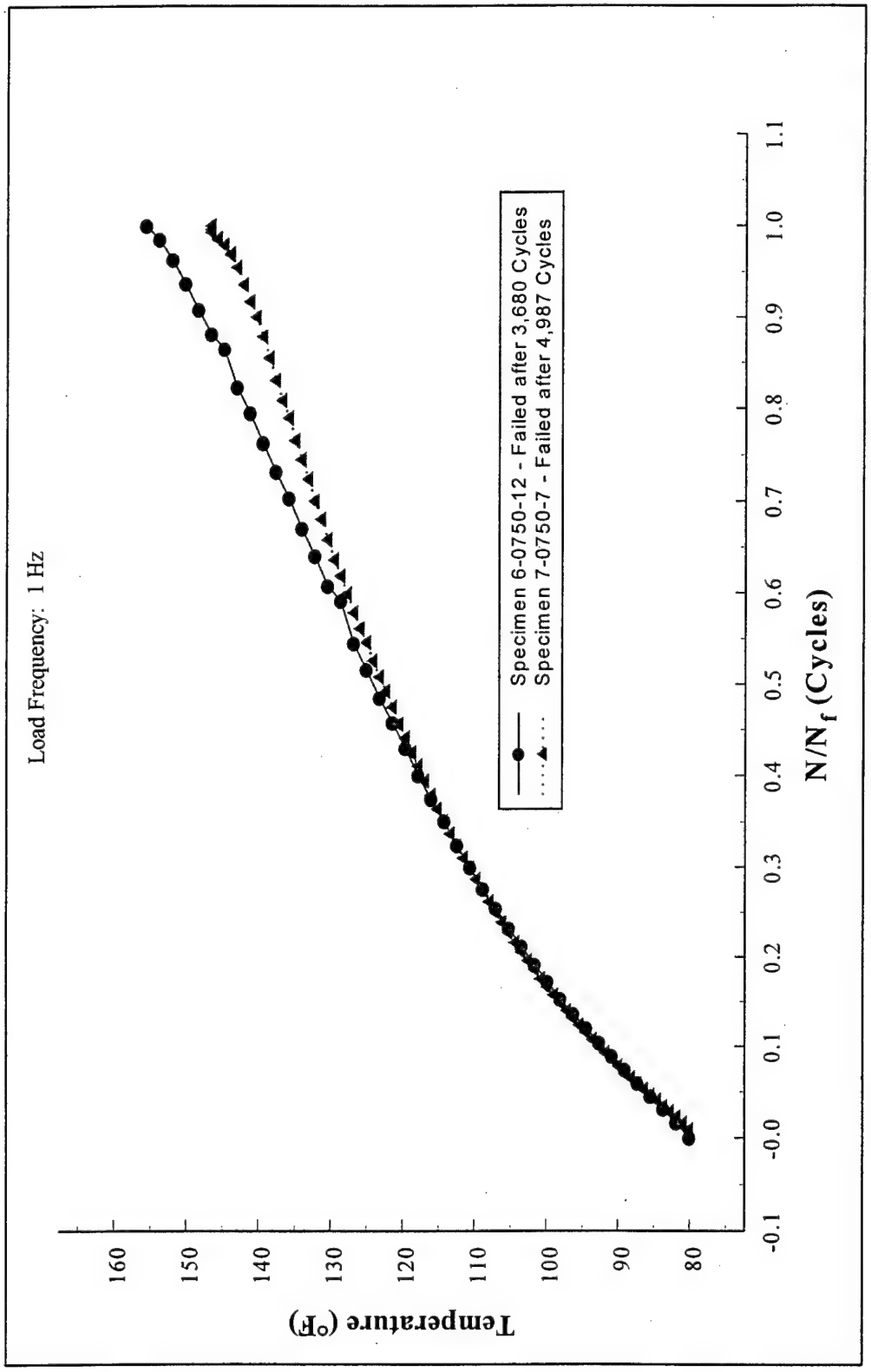

Figure 51 - Temperature Rise During Constant Amplitude Fatigue Tests of Passive Bearing Case; 0/90°, 20 ksi

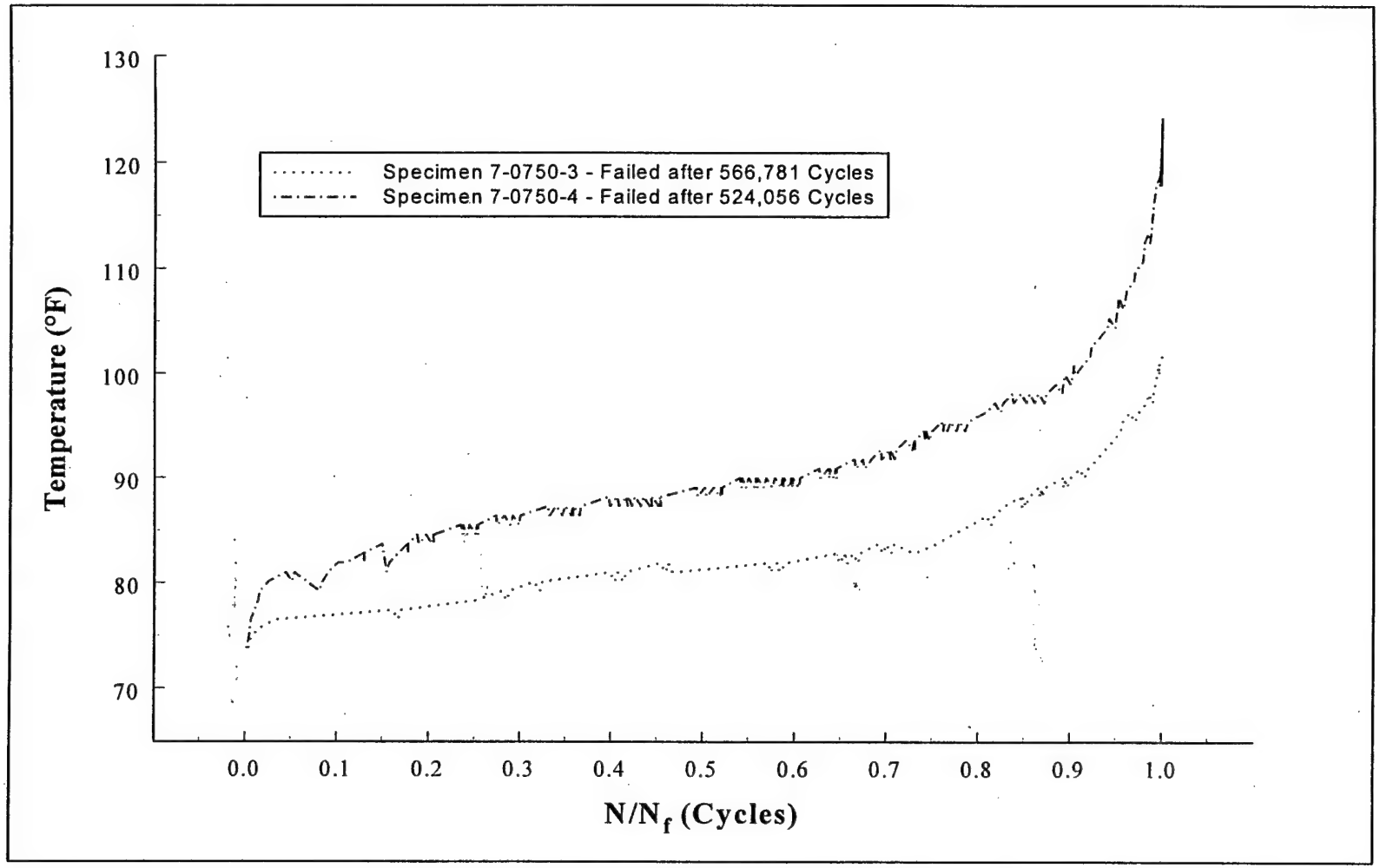

Figure 52 - Temperature Rise During Variable Amplitude Fatigue Tests of Passive Bearing Case; 0/90°, RMS=4.5 ksi

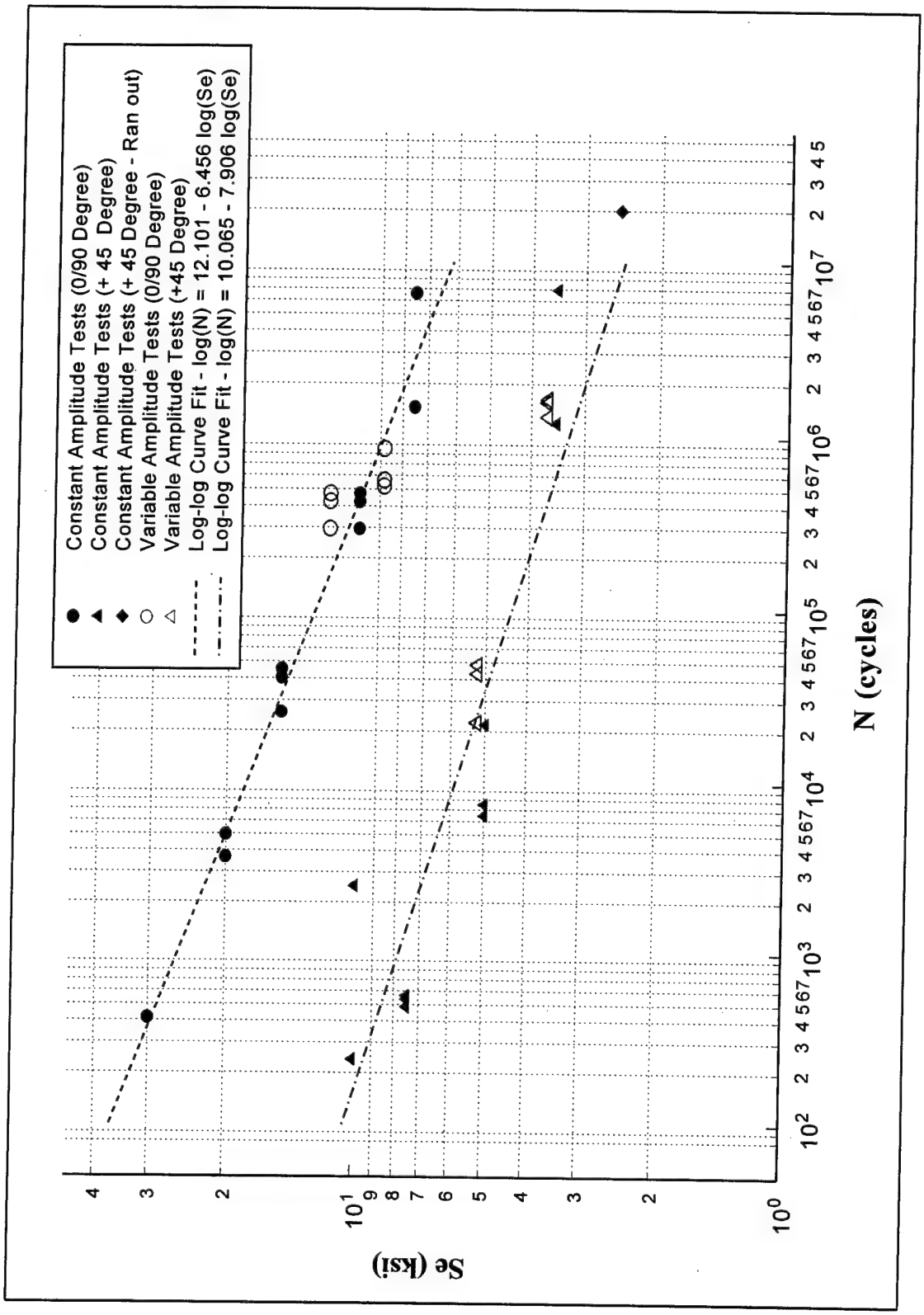

Figure 53 - S-N Curves for Passive Bearing Case (Log-Log Curve Fit)

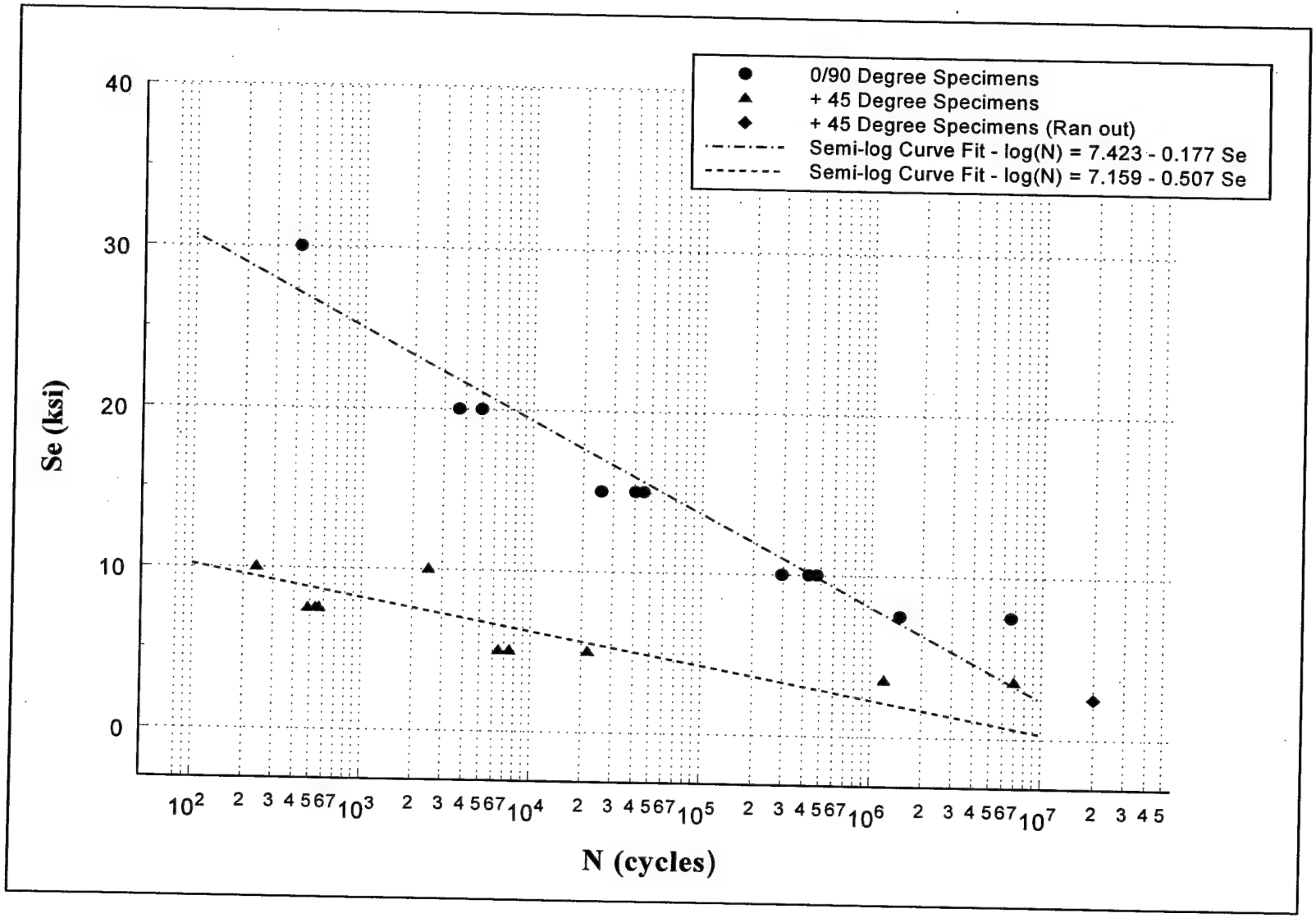

Figure 54 - S-N Curves for Passive Bearing Case (Semi-Log Curve Fit)

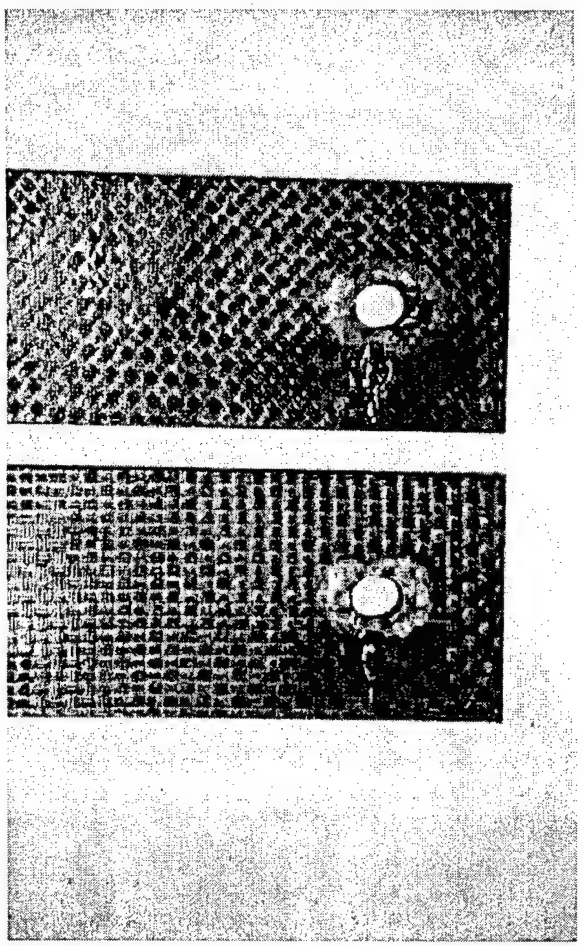

Figure 55 - Fatigue Failure Mode of Active Bearing Specimens (Both Lay-ups)

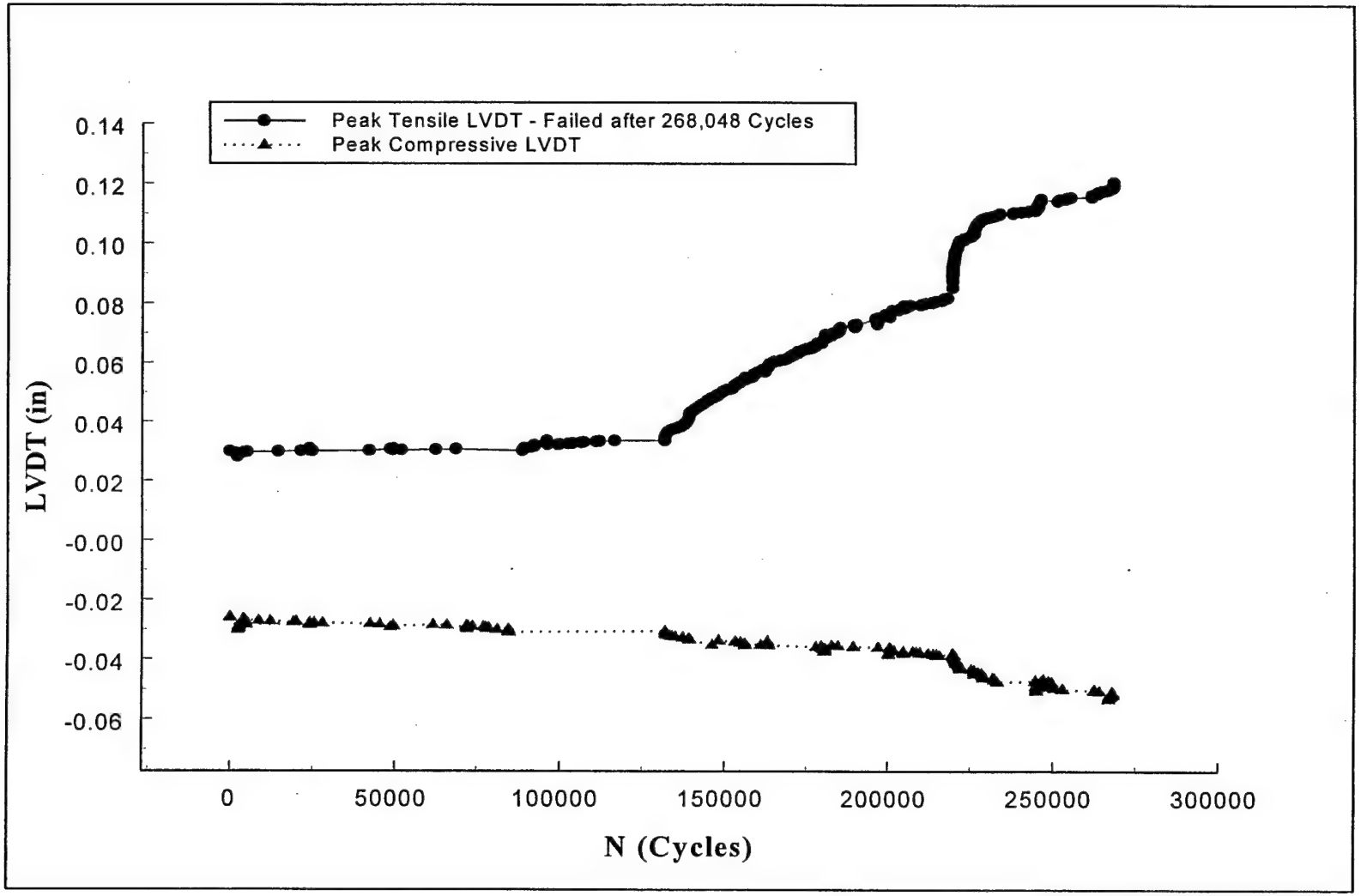

Figure 56 - Evolution of Deflection During the Fatigue Life of Active Bearing Specimens; Specimen 8-0750-2: $\pm 45^{\circ}$, 2.5 ksi, Constant Amplitude

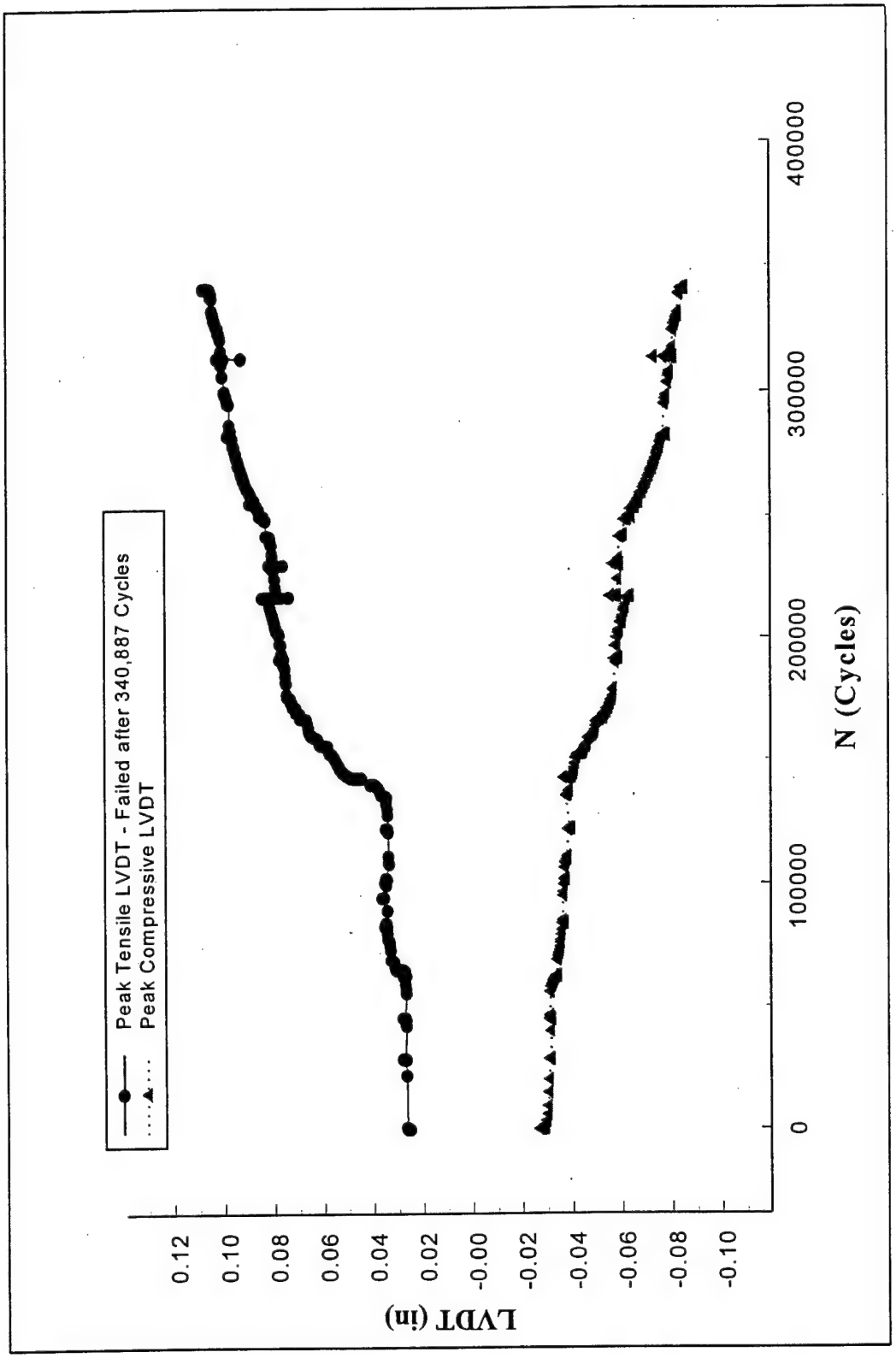

Figure 57 - Evolution of Deflection During the Fatigue Life of Active Bearing Specimens; Specimen 8-0750-4: ± 45°, 2.5 ksi, Constant Amplitude

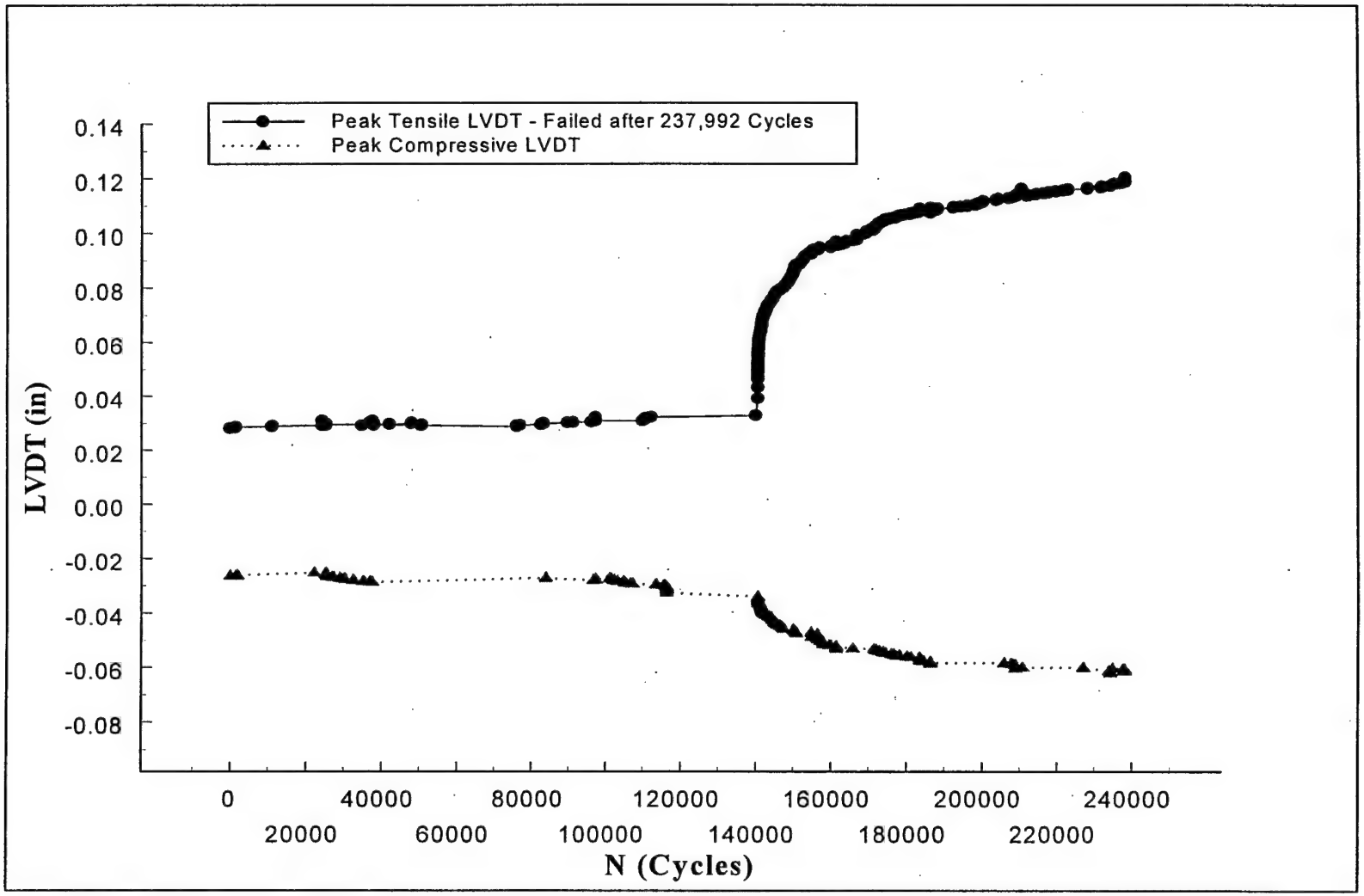

Figure 58 - Evolution of Deflection During the Fatigue Life of Active Bearing Specimens; Specimen 8-0750-1 : $\pm 45^{o}$, 2.5 ksi, Constant Amplitude

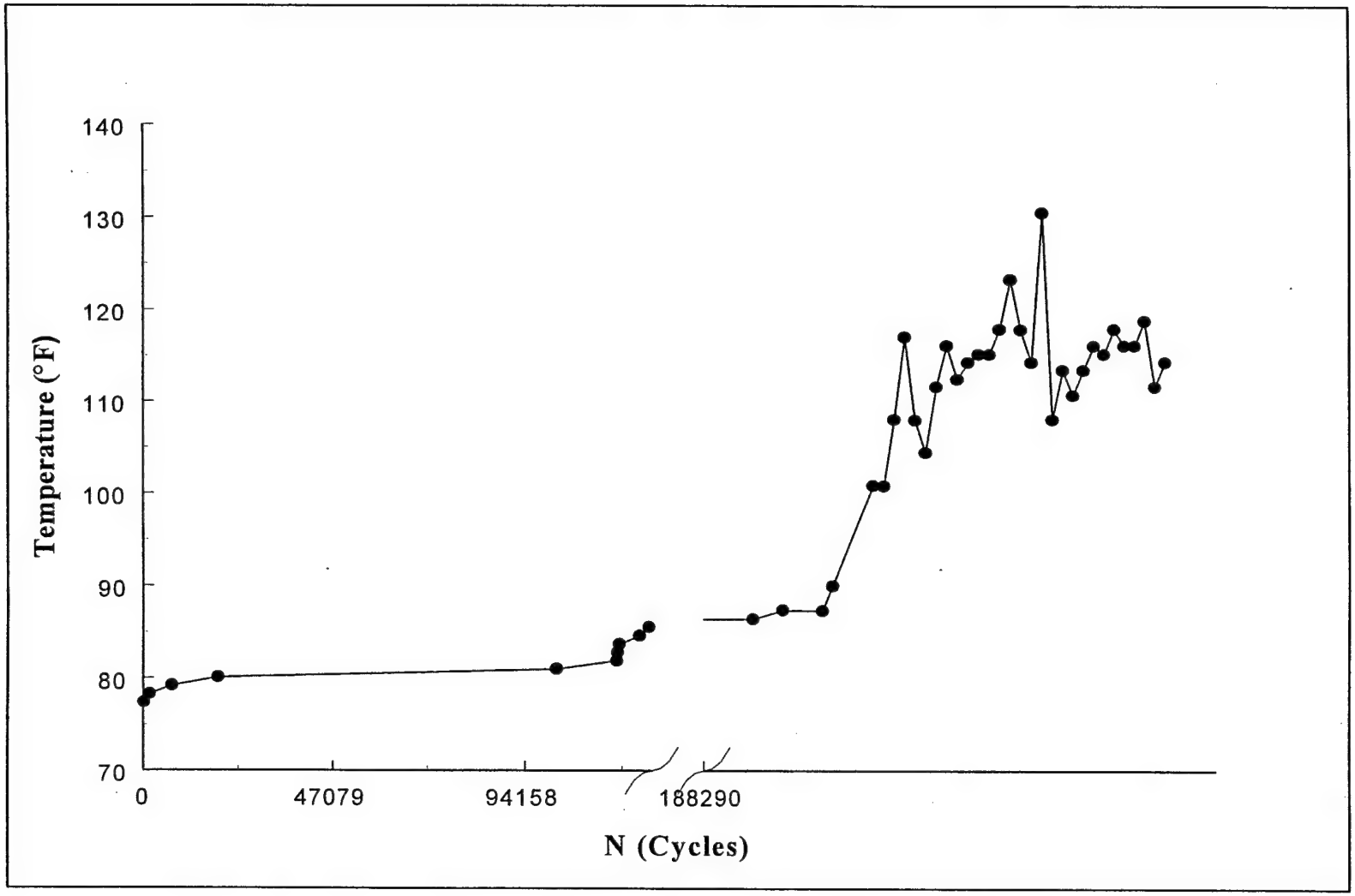

Figure 59 - Temperature Rise During Constant Amplitude Fatigue Testing for ±45° FRP Laminates with Holes (2.5 ksi) - Active Bearing Case - 8-0750-1

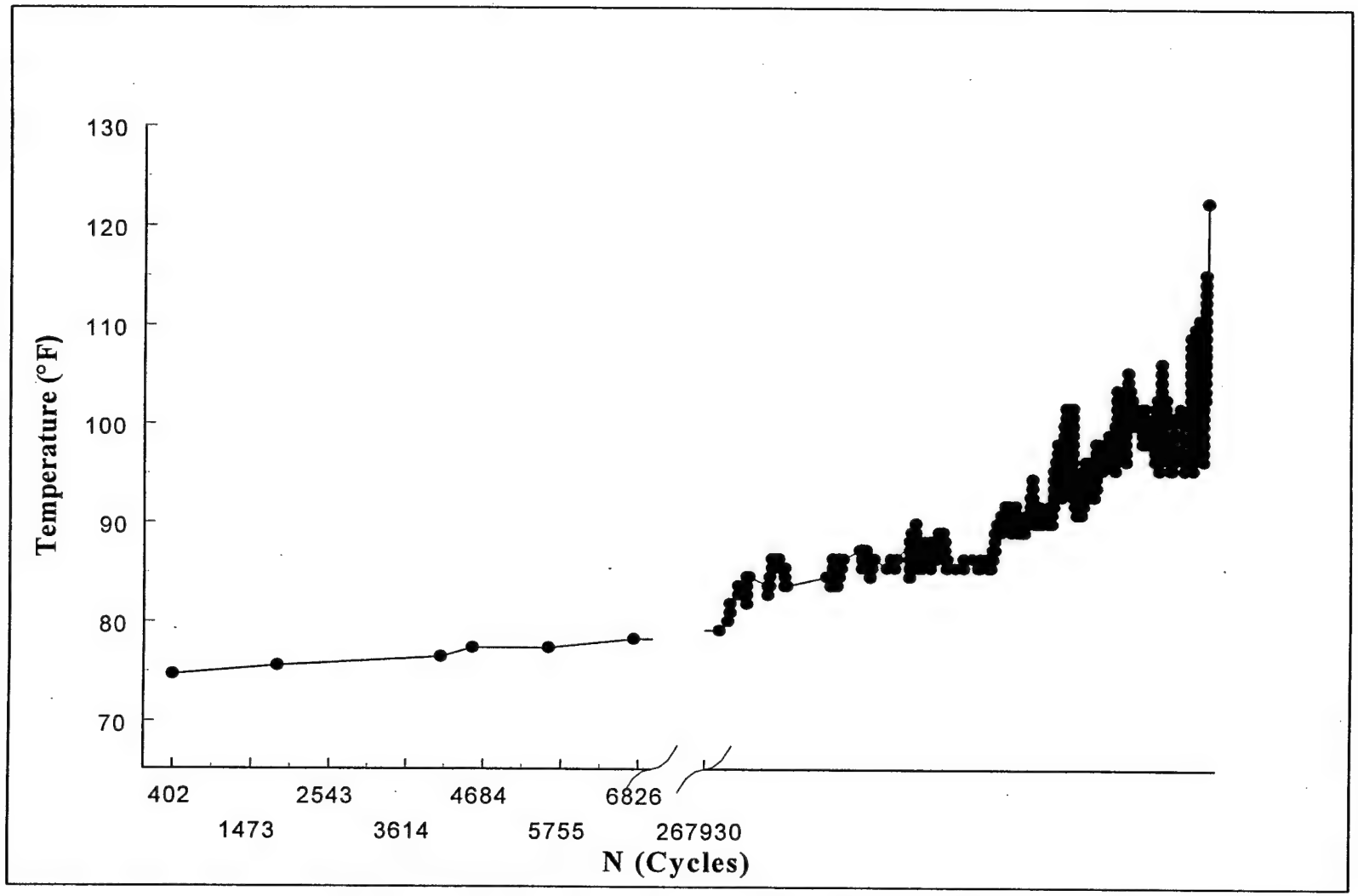

Figure 60 - Temperature Rise During Constant Amplitude Fatigue Testing for ±45° FRP Laminates with Holes (2.5 ksi) - Active Bearing Case - 8-0750-2

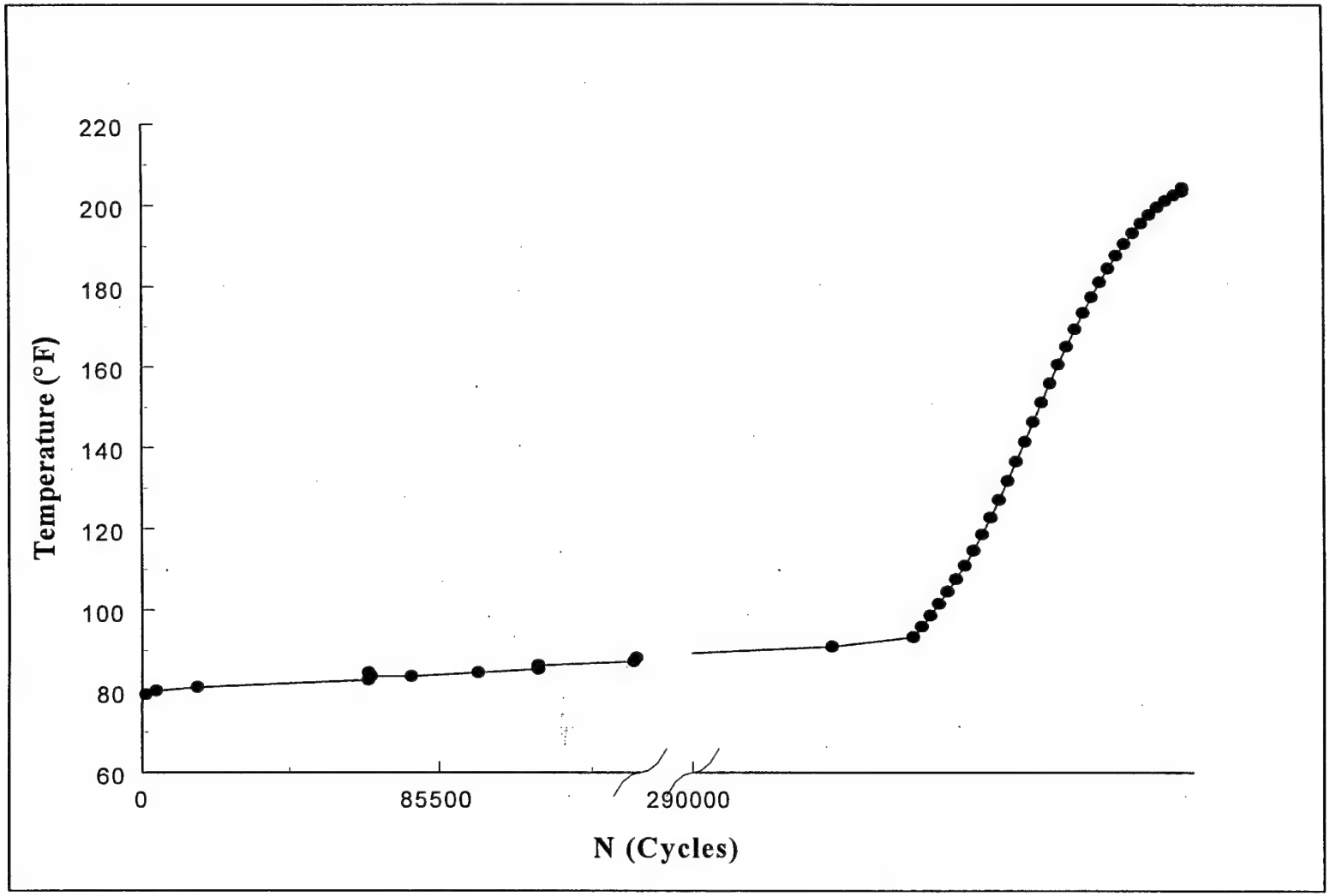

Figure 61 - Temperature Rise During Constant Amplitude Fatigue Testing for ±45° FRP Laminates with Holes (2.5 ksi) - Active Bearing Case - 8-0750-4

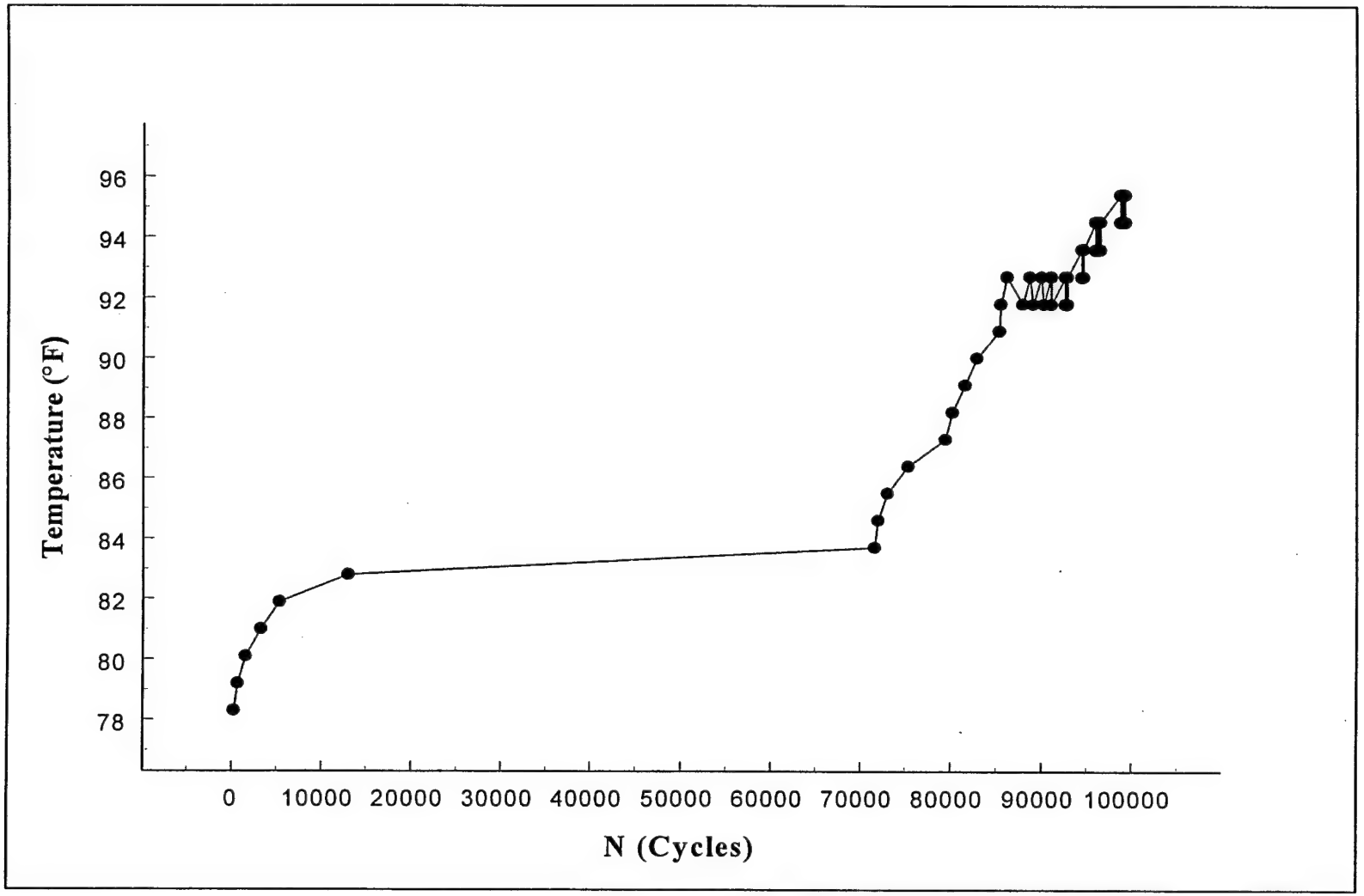

Figure 62 - Temperature Rise During Constant Amplitude Fatigue Testing for ±45° FRP Laminates with Holes (3 ksi) - Active Bearing Case - 7-0750-12

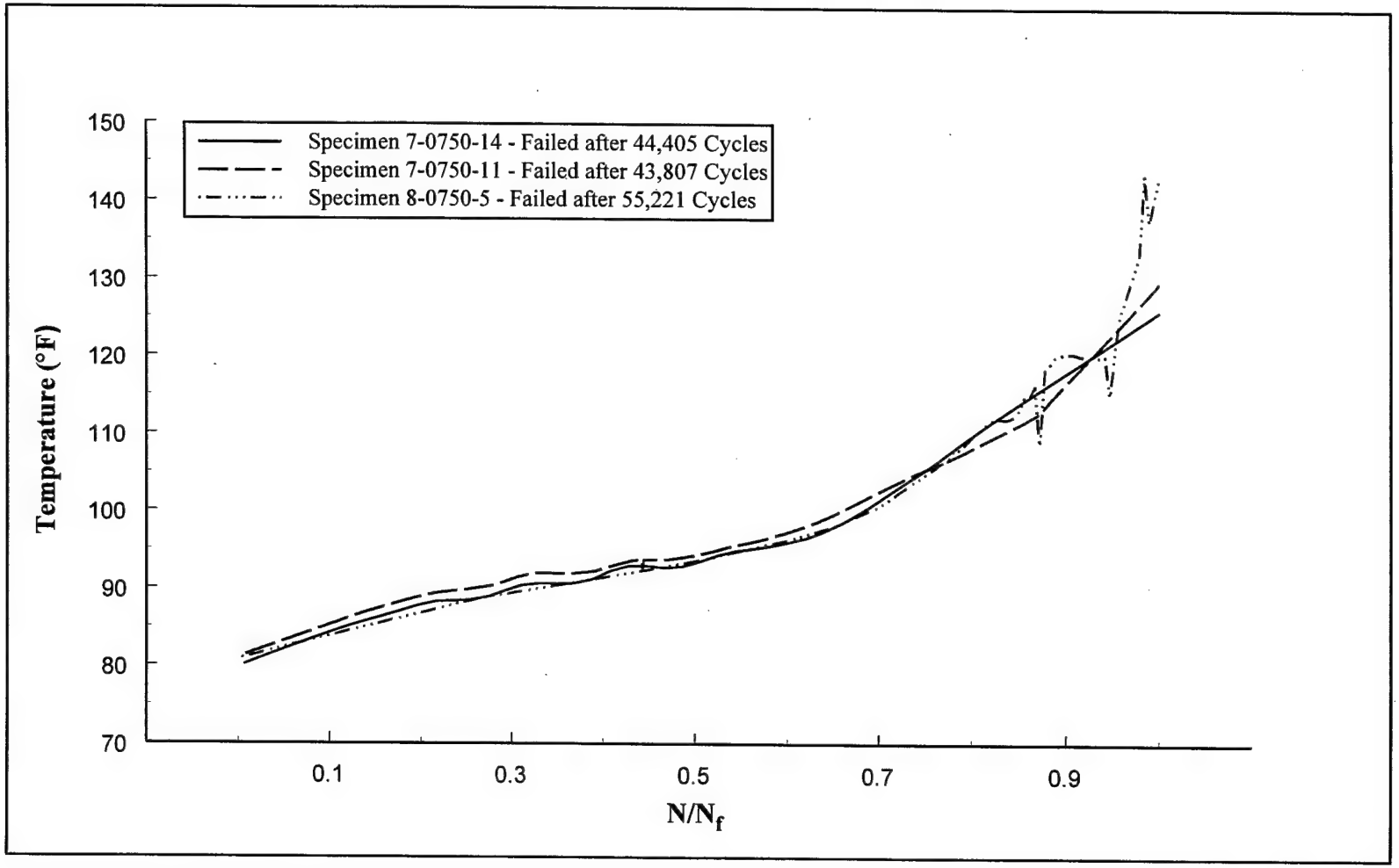

Figure 63 - Temperature Rise During Variable Amplitude Fatigue Testing for ±45° FRP Laminates with Holes (1.75 ksi) - Active Bearing Case

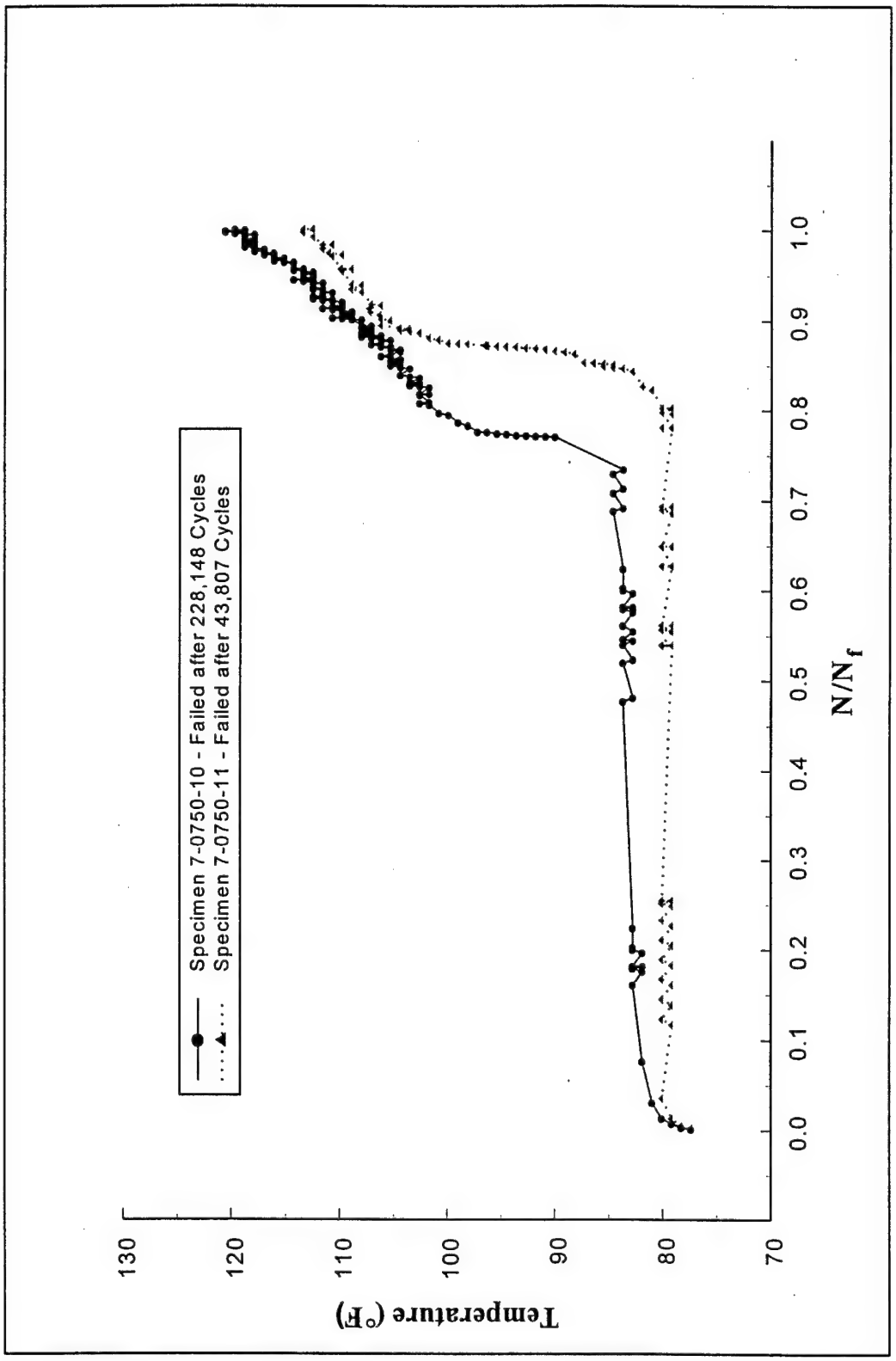

Figure 64 - Temperature Rise During Variable Amplitude Fatigue Testing for ± 45° FRP Laminates with Holes (1.25 ksi) - Active Bearing Case

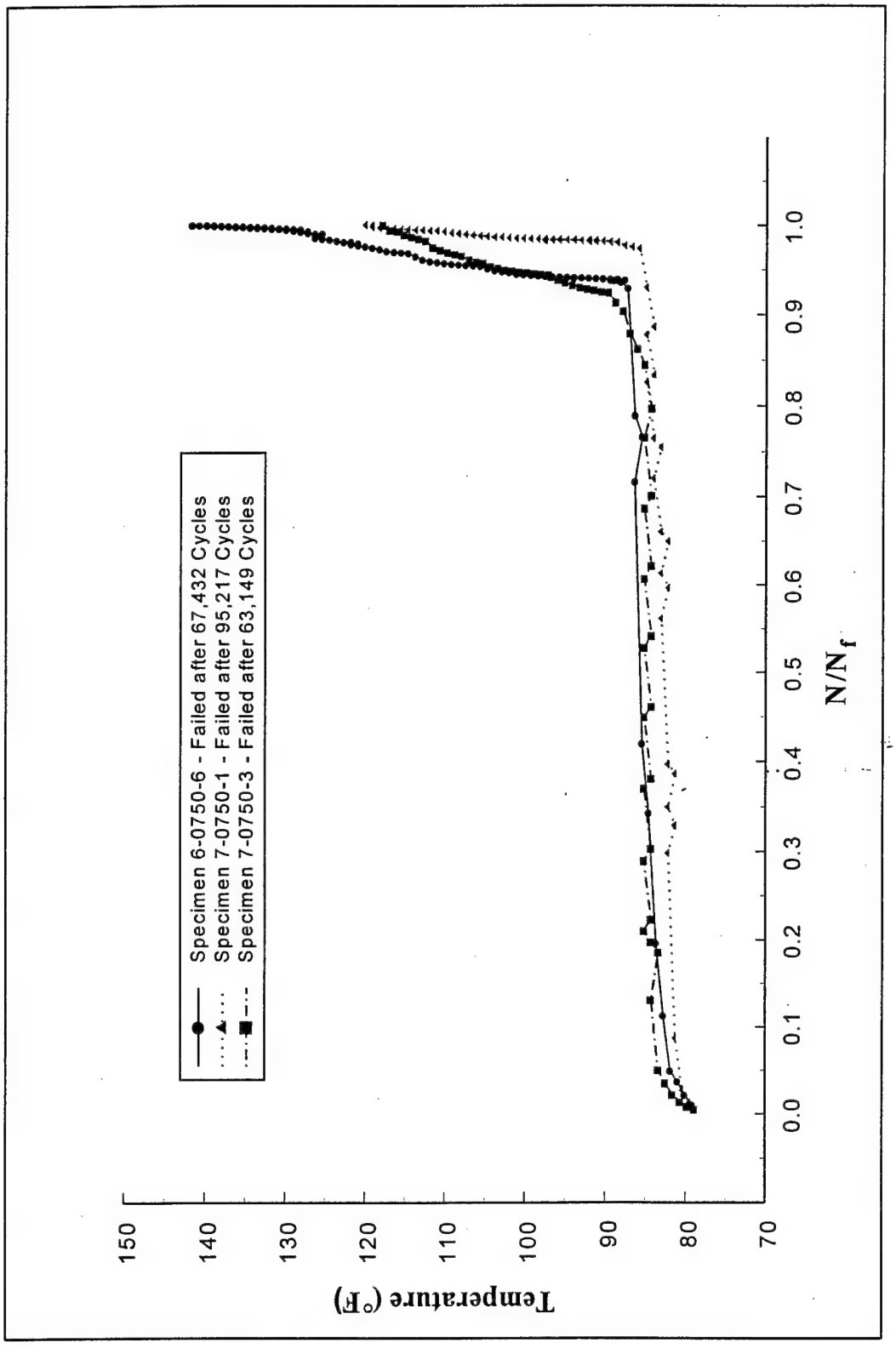

Figure 65 - Temperature Rise During Variable Amplitude Fatigue Testing for 0/90° FRP Laminates with Holes (1.75 ksi) - Active Bearing Case

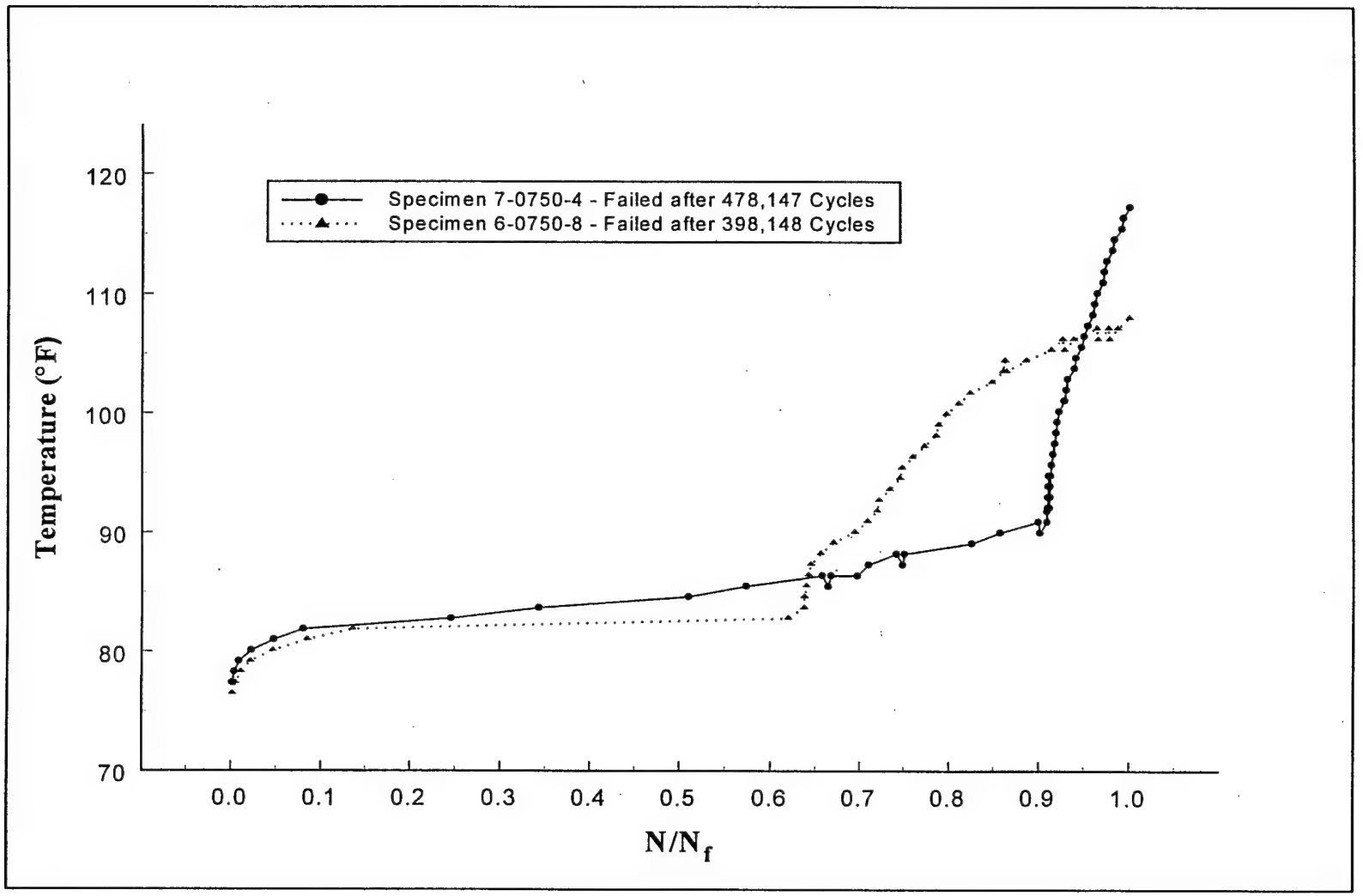

Figure 66 - Temperature Rise During Variable Amplitude Fatigue Testing for 0/90° FRP Laminates with Holes (1.25 ksi) - Active Bearing Case

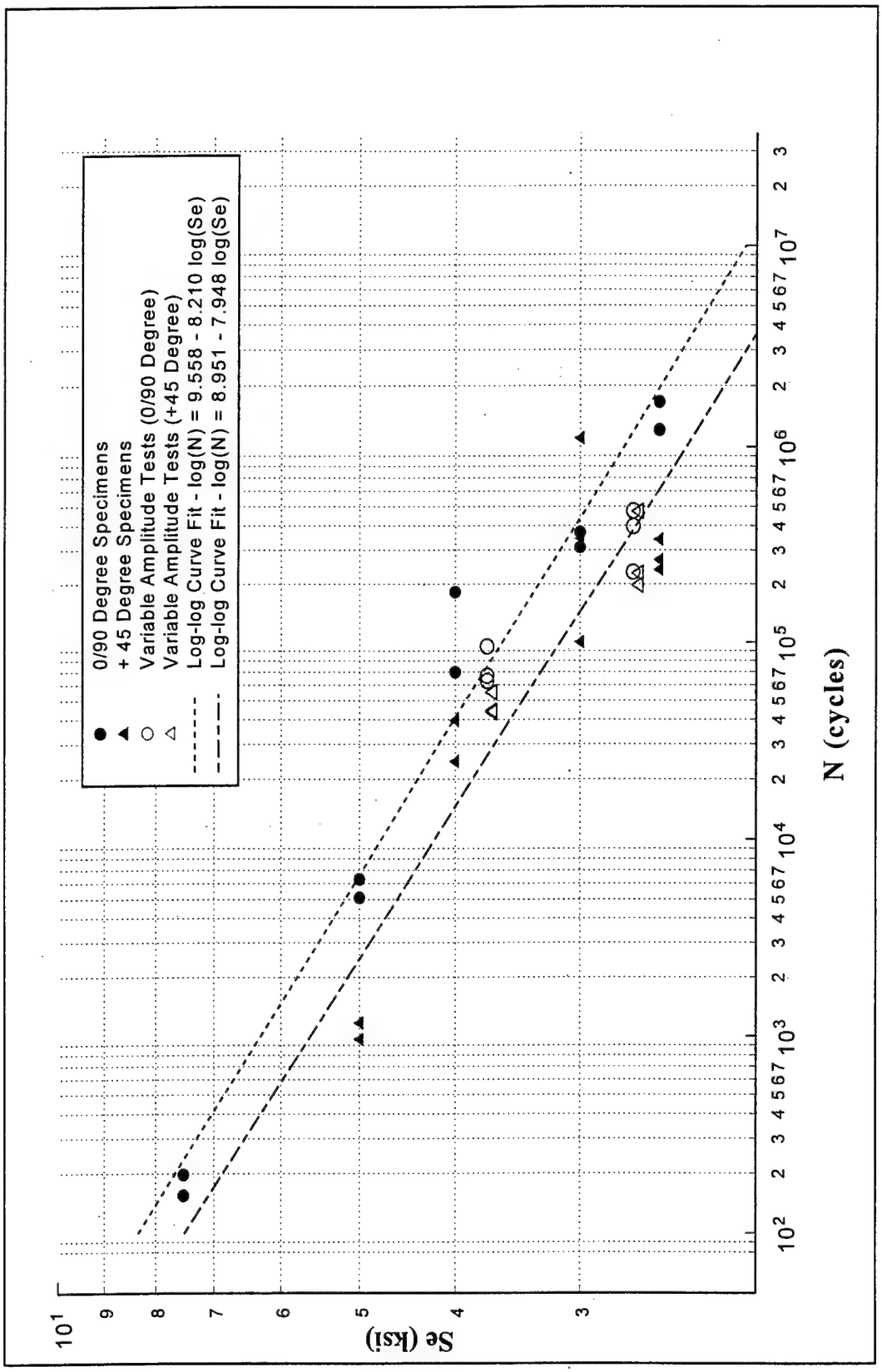

Figure 67 - S-N Curves for Active Bearing Case (Log-Log Curve Fit)

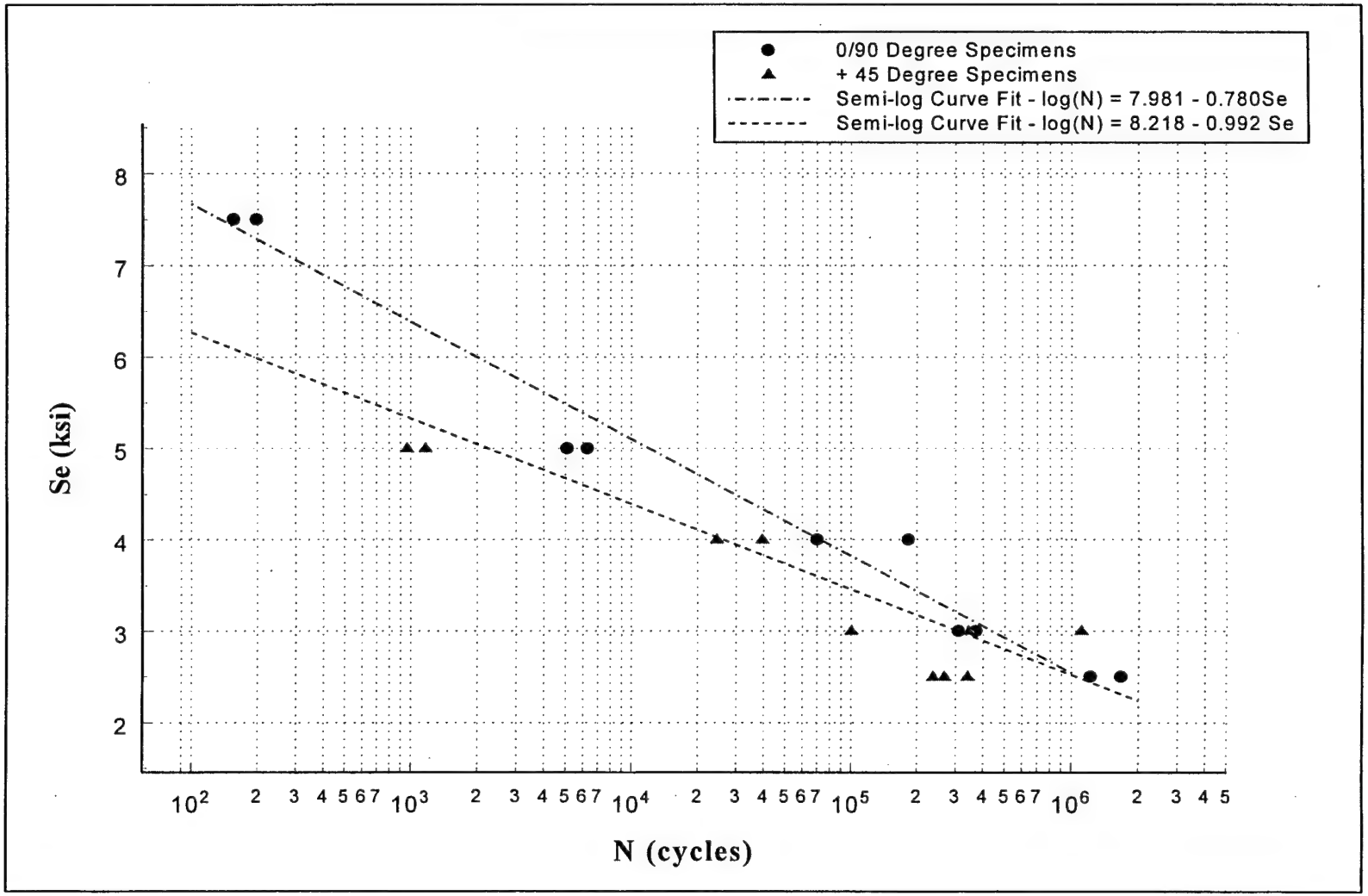

Figure 68 - S-N Curves of Active Bearing Case (Semi-Log Curve Fit)

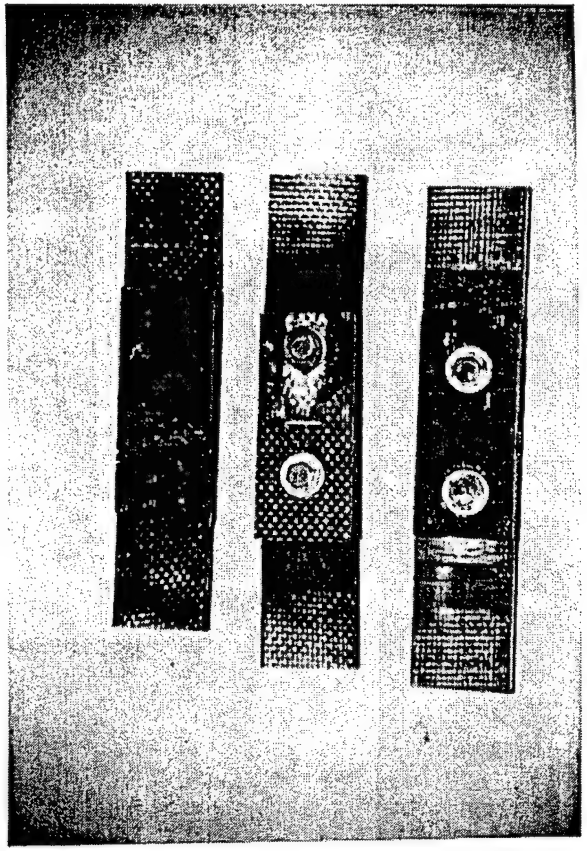

(a) FRONT VIEW

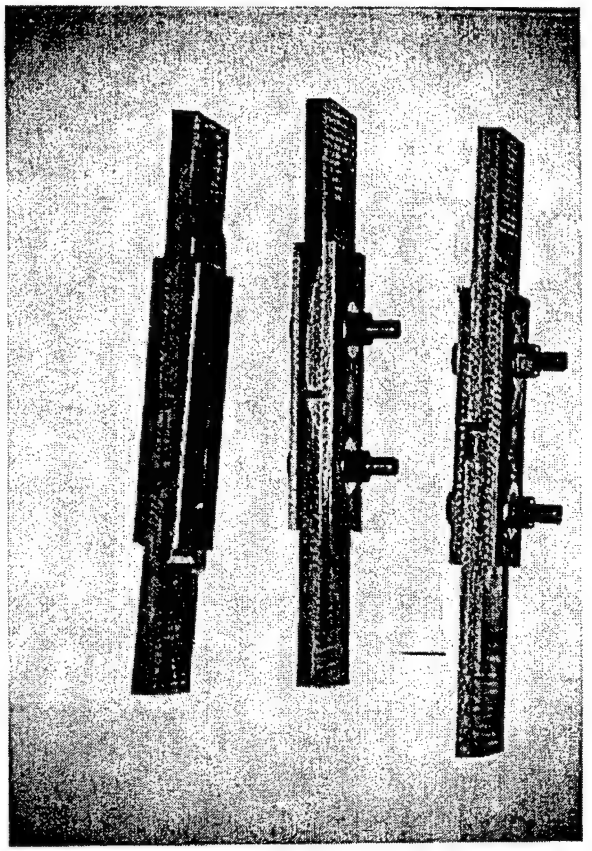

(b) SIDE VIEW

Figure 69 - Appearance of Composite Joints after Fatigue Tests

(FROM LEFT : BONDED, BOLTED, AND BONDED-BOLTED JOINTS)

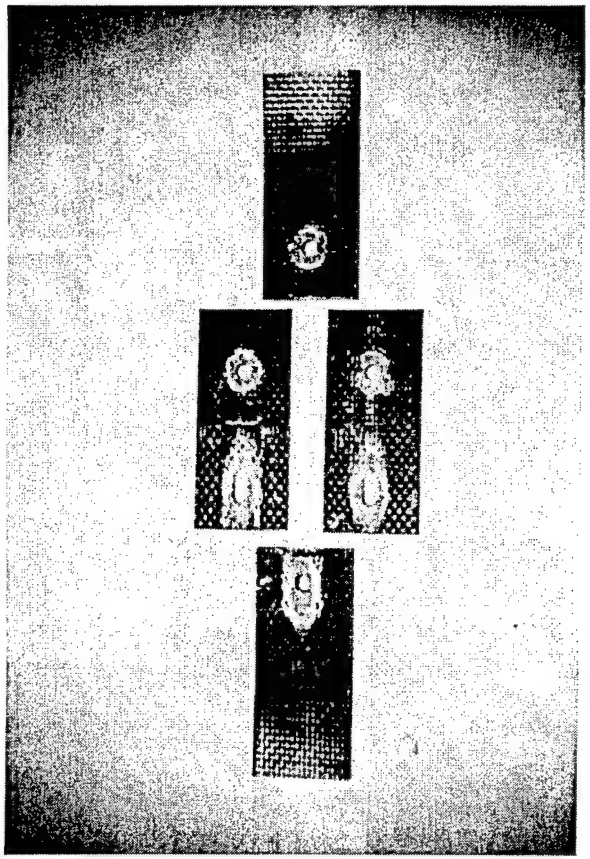

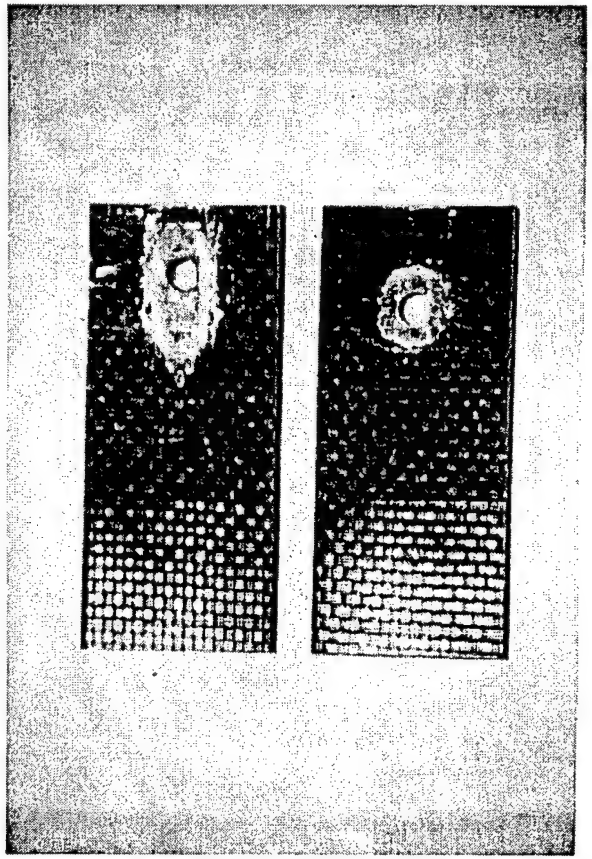

Figure 70 - Disassembled Bolted Joint Showing Partial Shear-Out Failure: Specimen JB-4

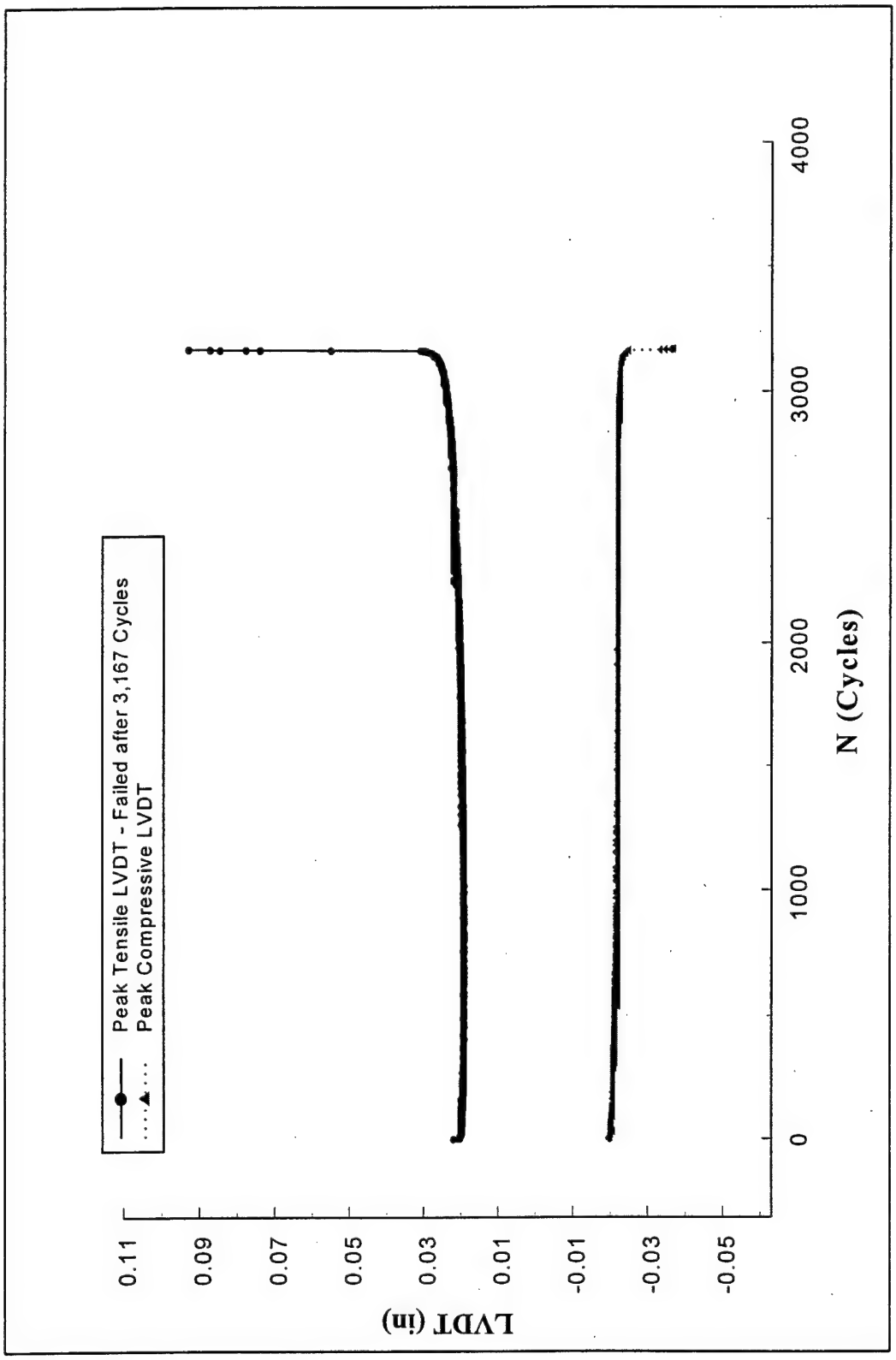

Figure 71 - Evolution of Deflection During the Constant Amplitude Fatigue Tests of Bonded Joints; Specimen JA-5: 5 ksi

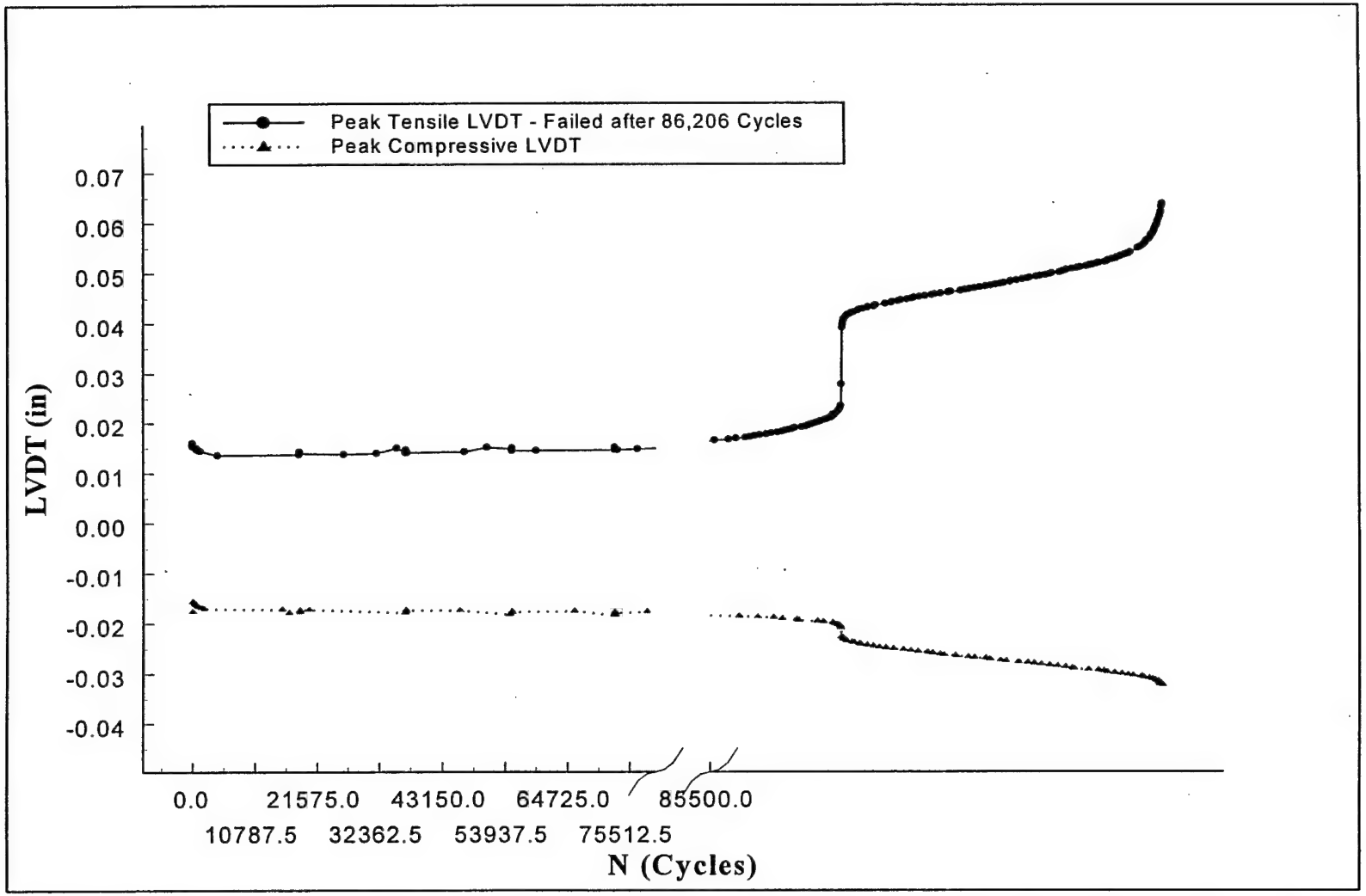

Figure 72 - Evolution of Deflection During the Constant Amplitude Fatigue Tests of Bonded Joints; Specimen JA-18: 4 ksi

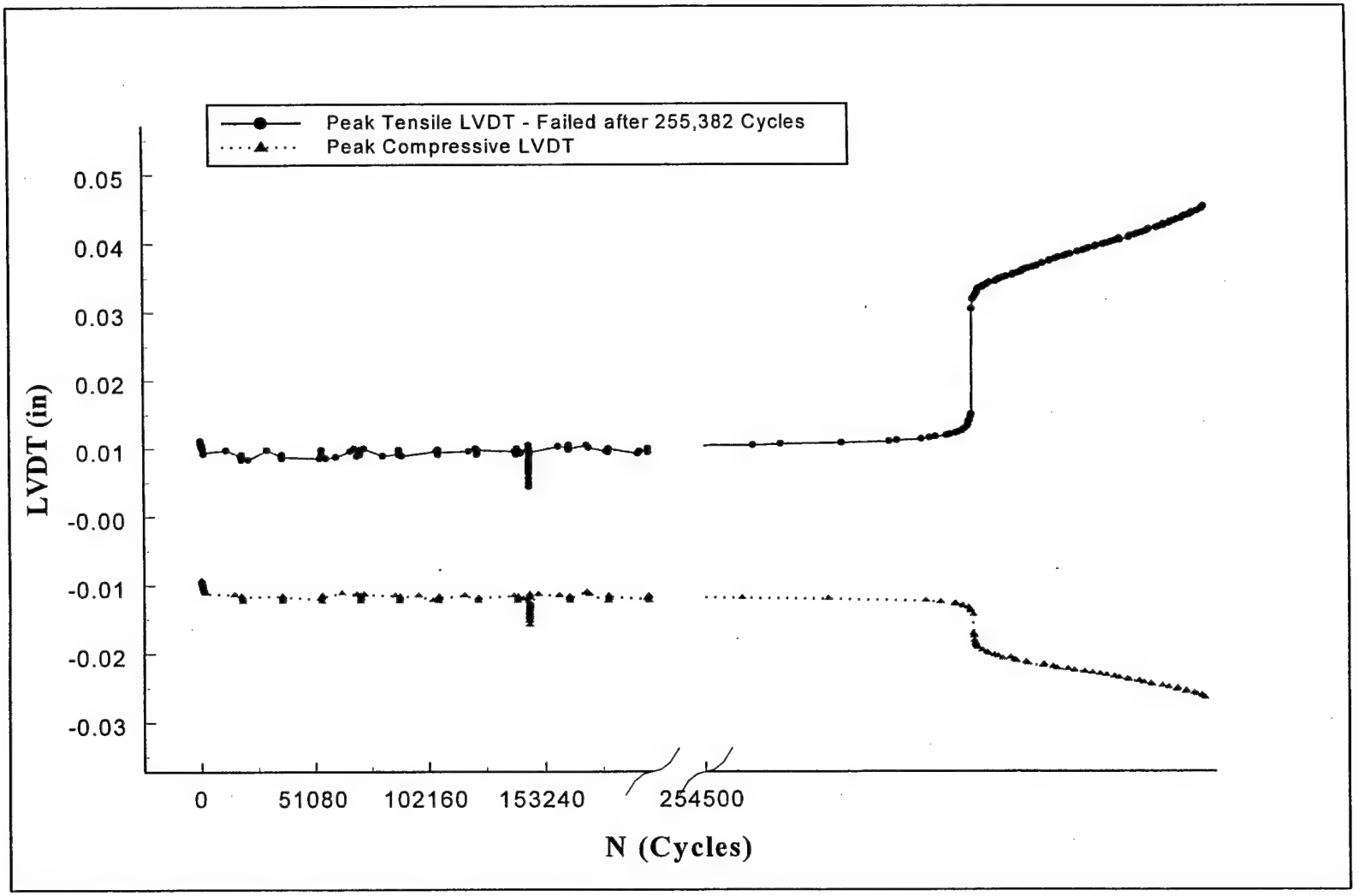

Figure 73 - Evolution of Deflection During the Constant Amplitude Fatigue Tests of Bonded Joints; Specimen JA-8: 3 ksi

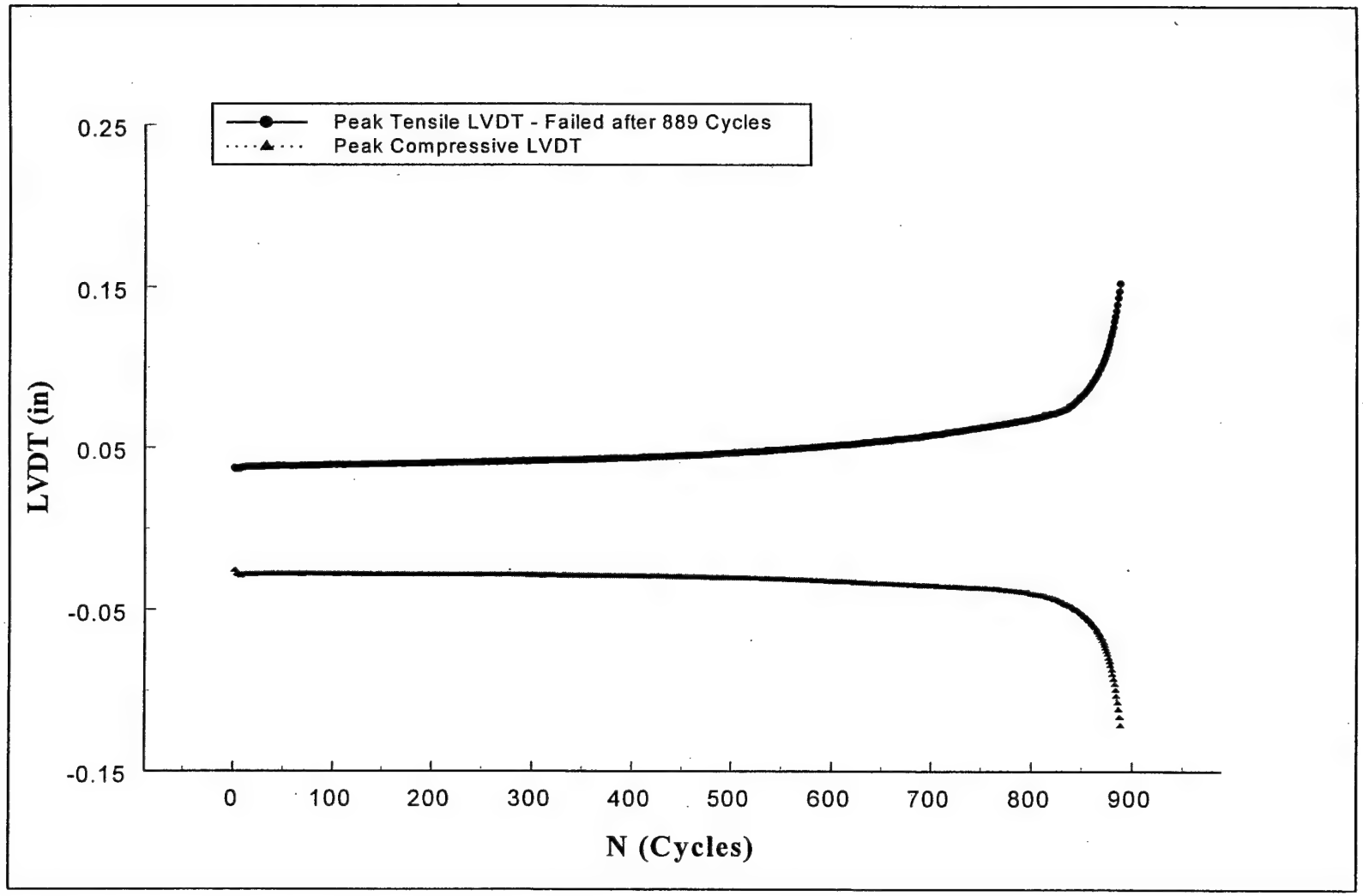

Figure 74 - Evolution of Deflection During the Constant Amplitude Fatigue Tests of Bolted Joints; Specimen JB-5: 5 ksi

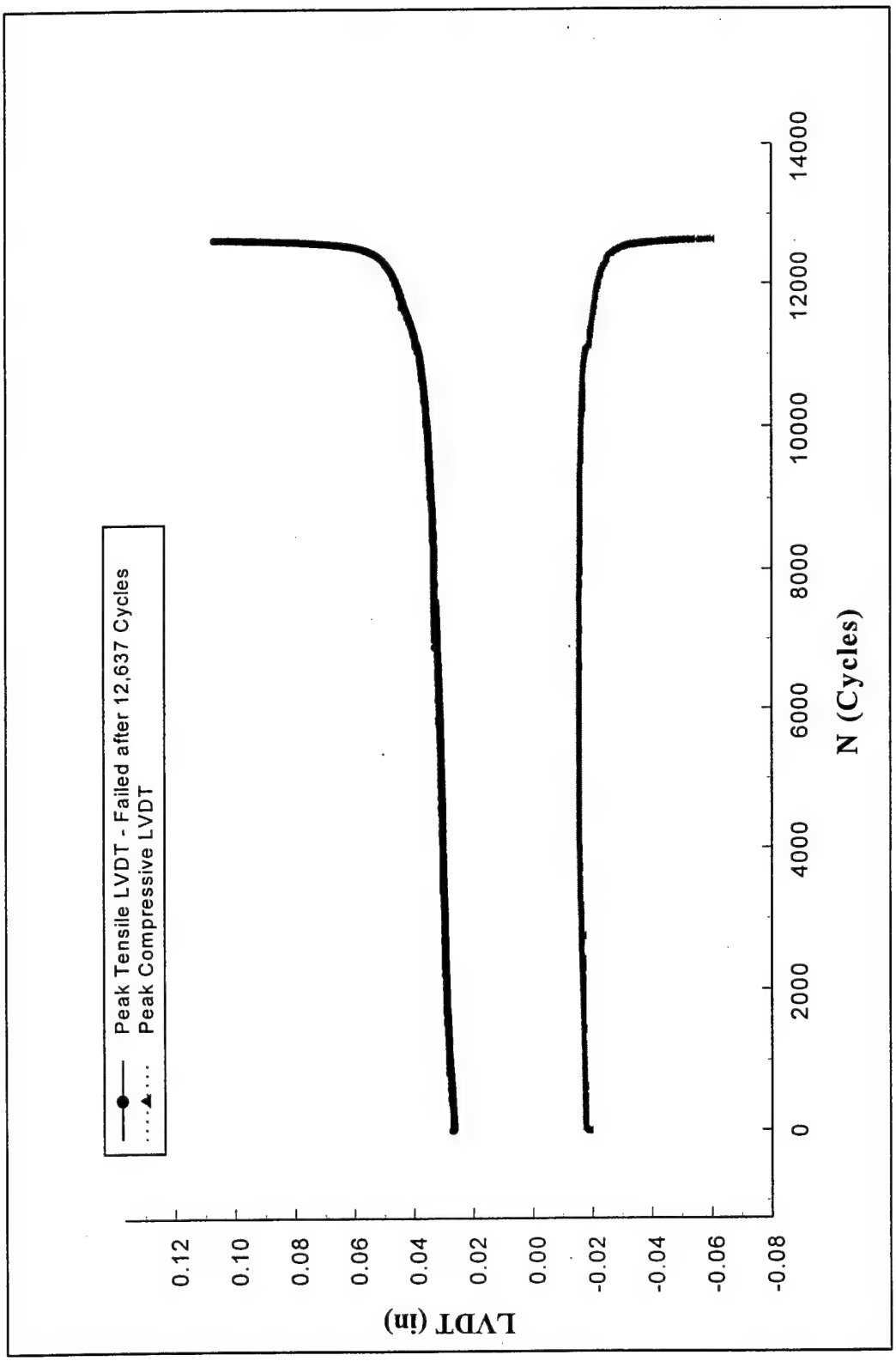

Figure 75 - Evolution of Deflection During the Constant Amplitude Fatigue Tests of Bolted Joints; Specimen JB-11: 3.5 ksi

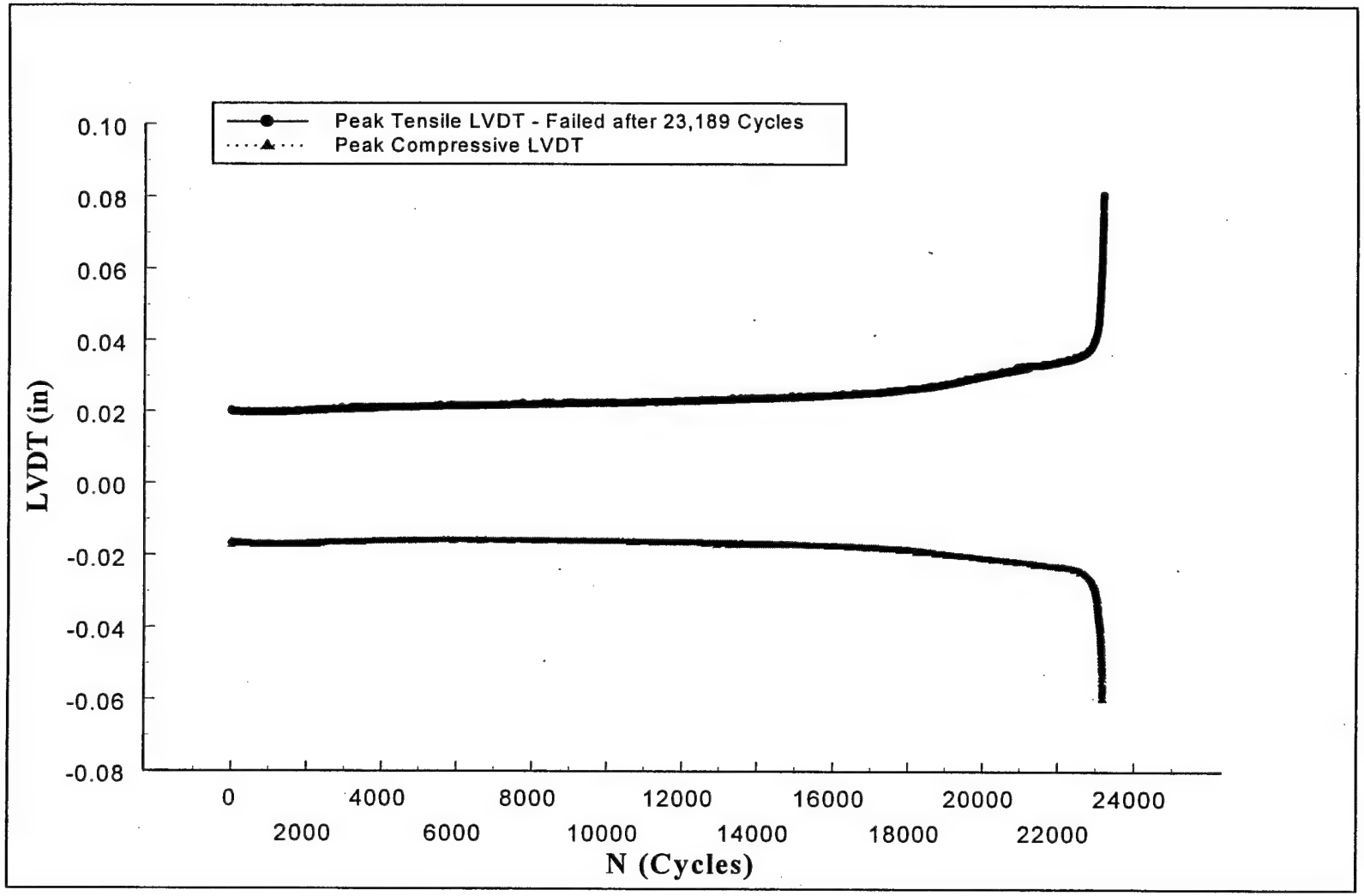

Figure 76 - Evolution of Deflection During the Constant Amplitude Fatigue Tests of Bolted Joints; Specimen JB-13: 3 ksi

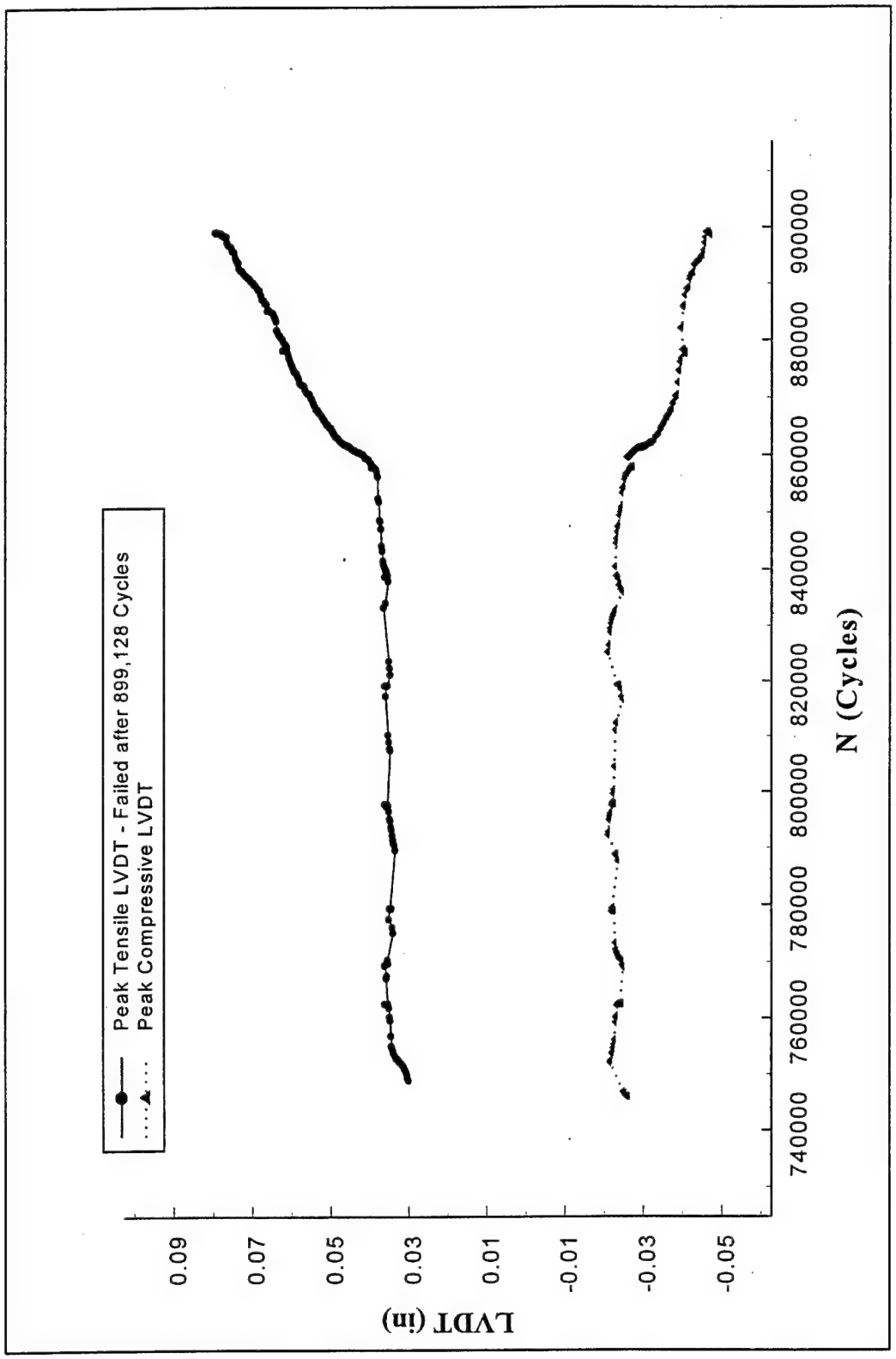

Figure 77 - Evolution of Deflection During the Constant Amplitude Fatigue Tests of Bolted Joints; Specimen JB-14: 3 ksi

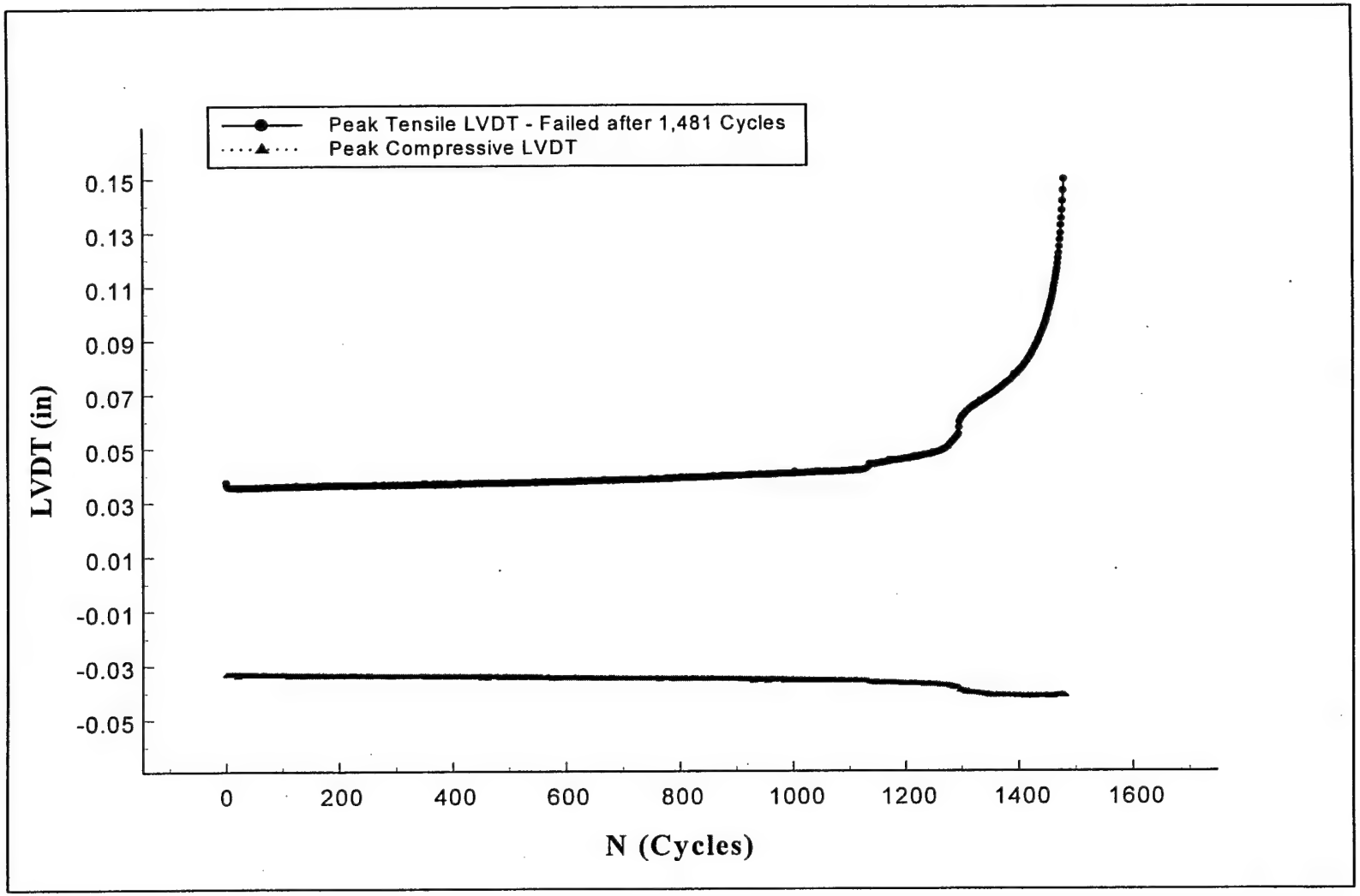

Figure 78 - Evolution of Deflection During the Constant Amplitude Fatigue Tests of Bolted-Bonded Joints; Specimen JAB-13: 9 ksi

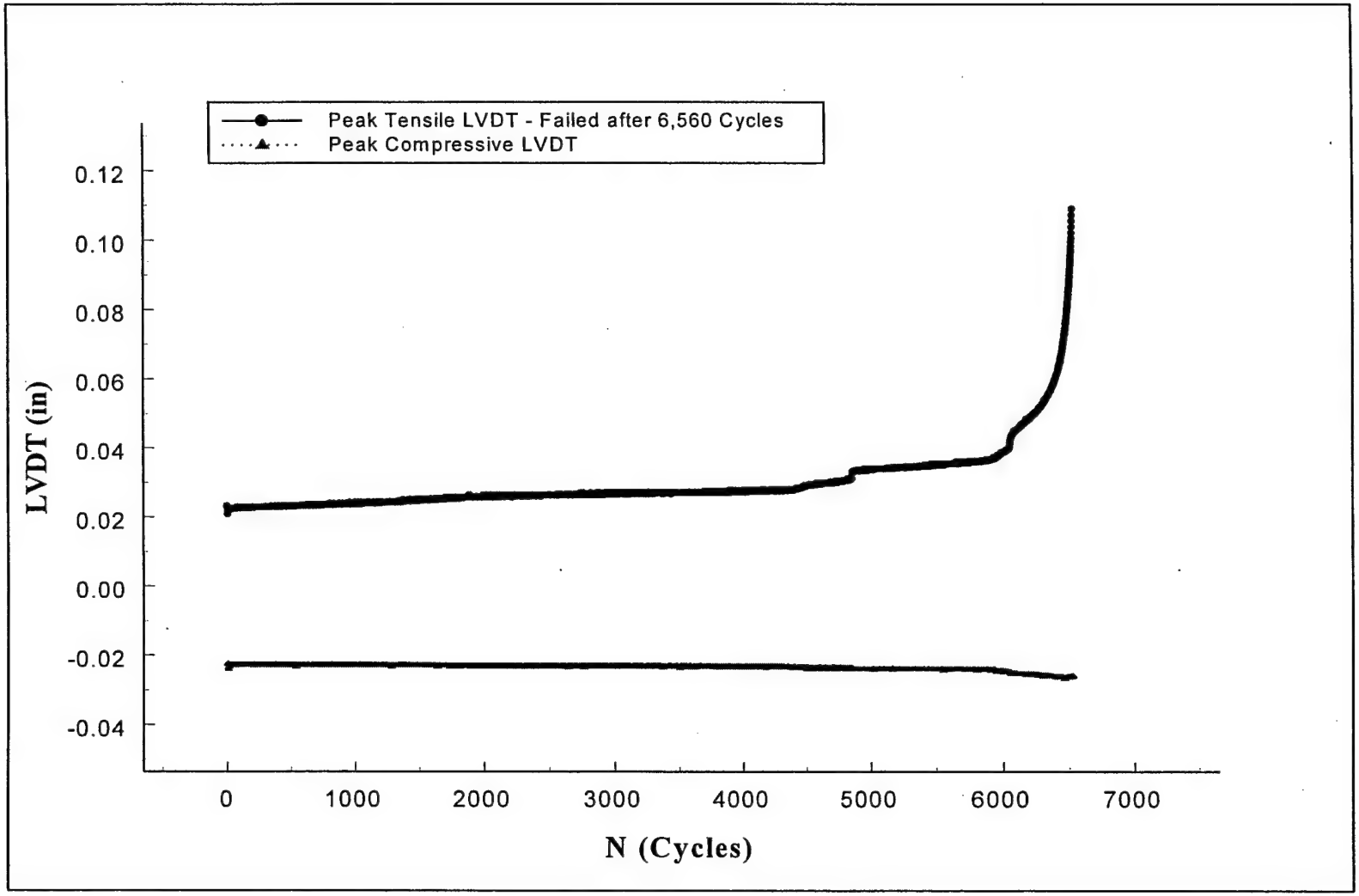

Figure 79 - Evolution of Deflection During the Constant Amplitude Fatigue Tests of Bolted-Bonded Joints; Specimen JAB-3: 7.5 ksi

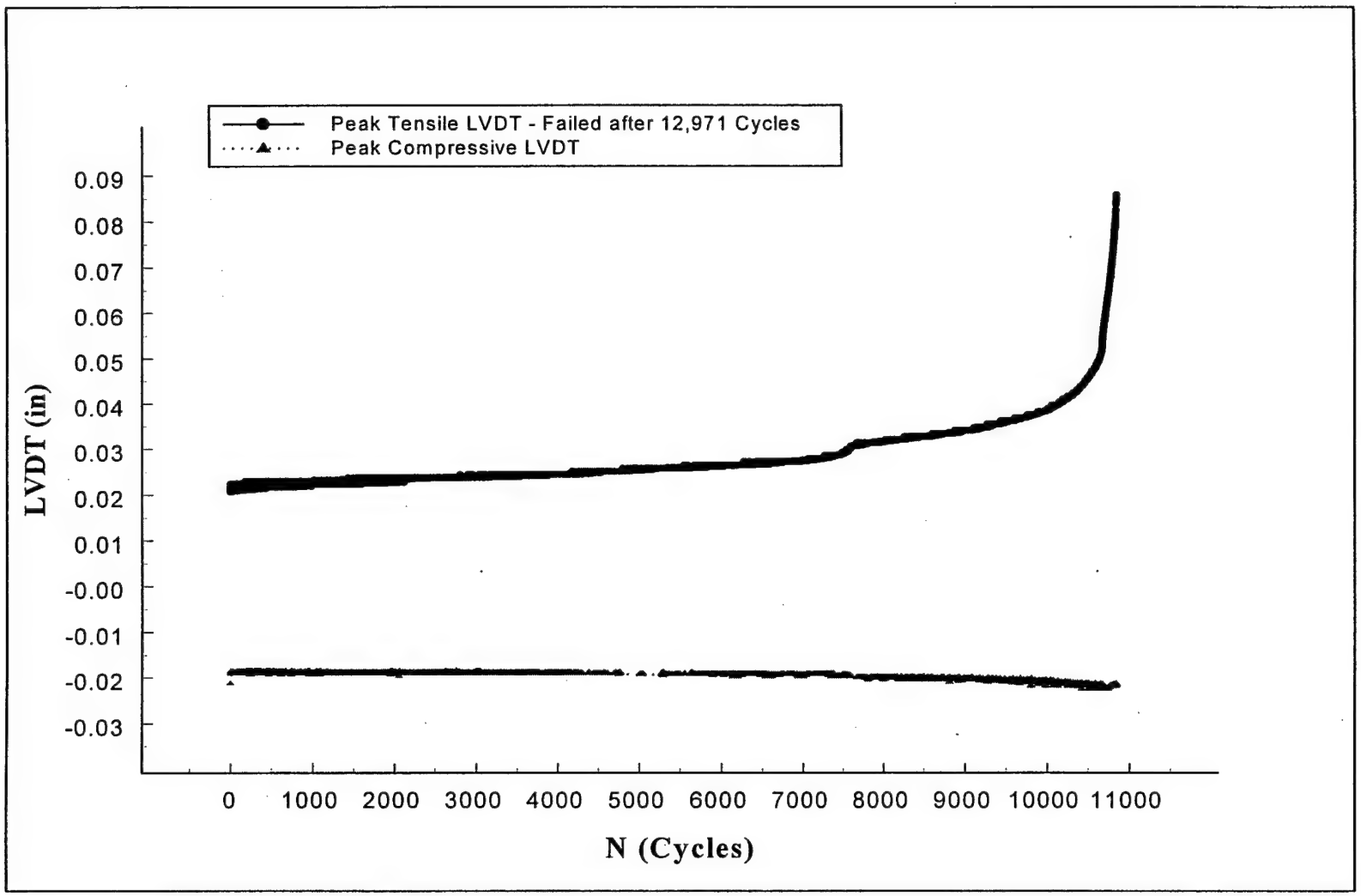

Figure 80 - Evolution of Deflection During the Constant Amplitude Fatigue Tests of Bolted-Bonded Joints; Specimen JAB-7: 6 ksi

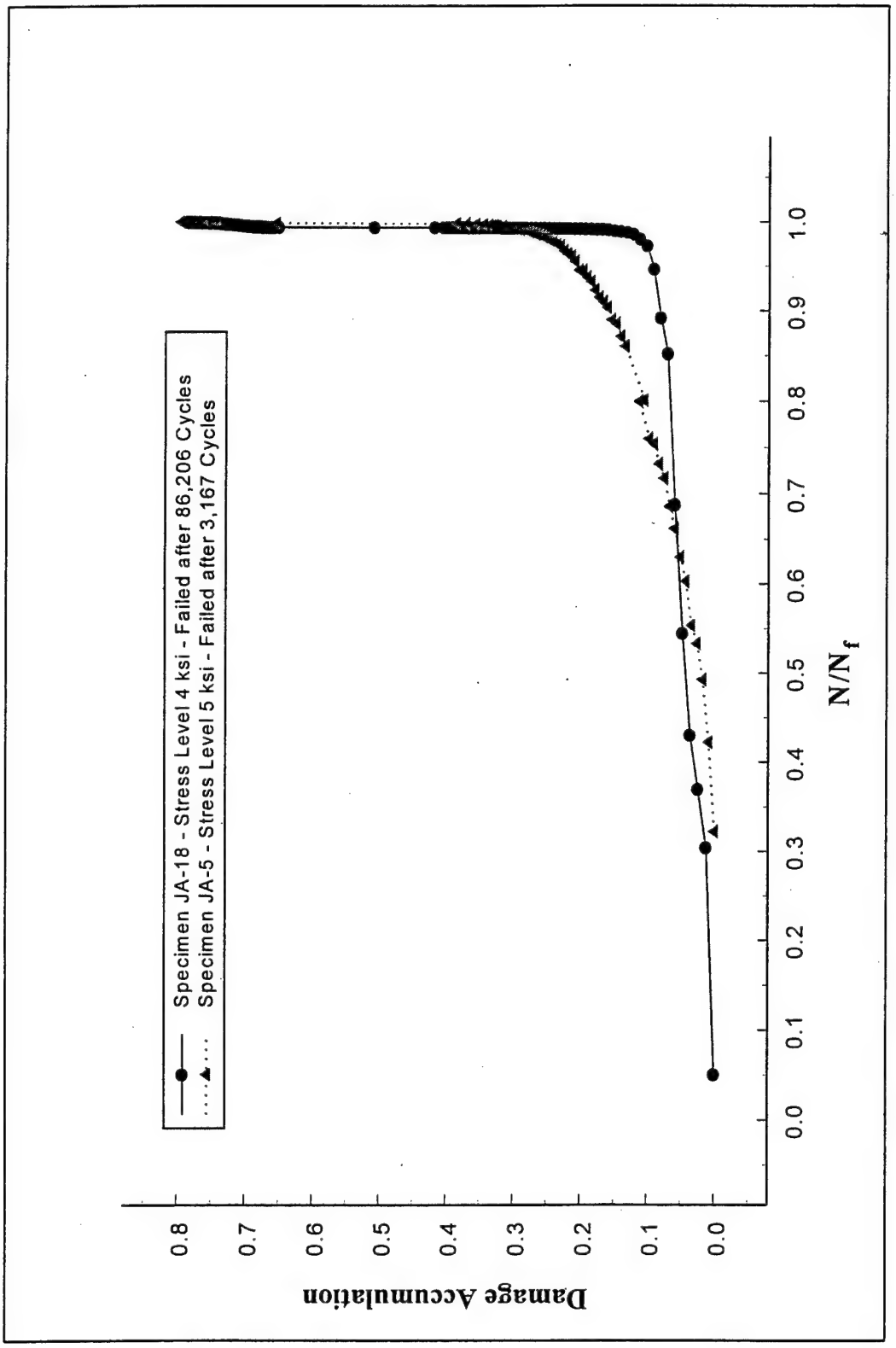

Figure 81 - Constant Amplitude Deflection-Based Fatigue Damage Accumulation in Bonded Joints

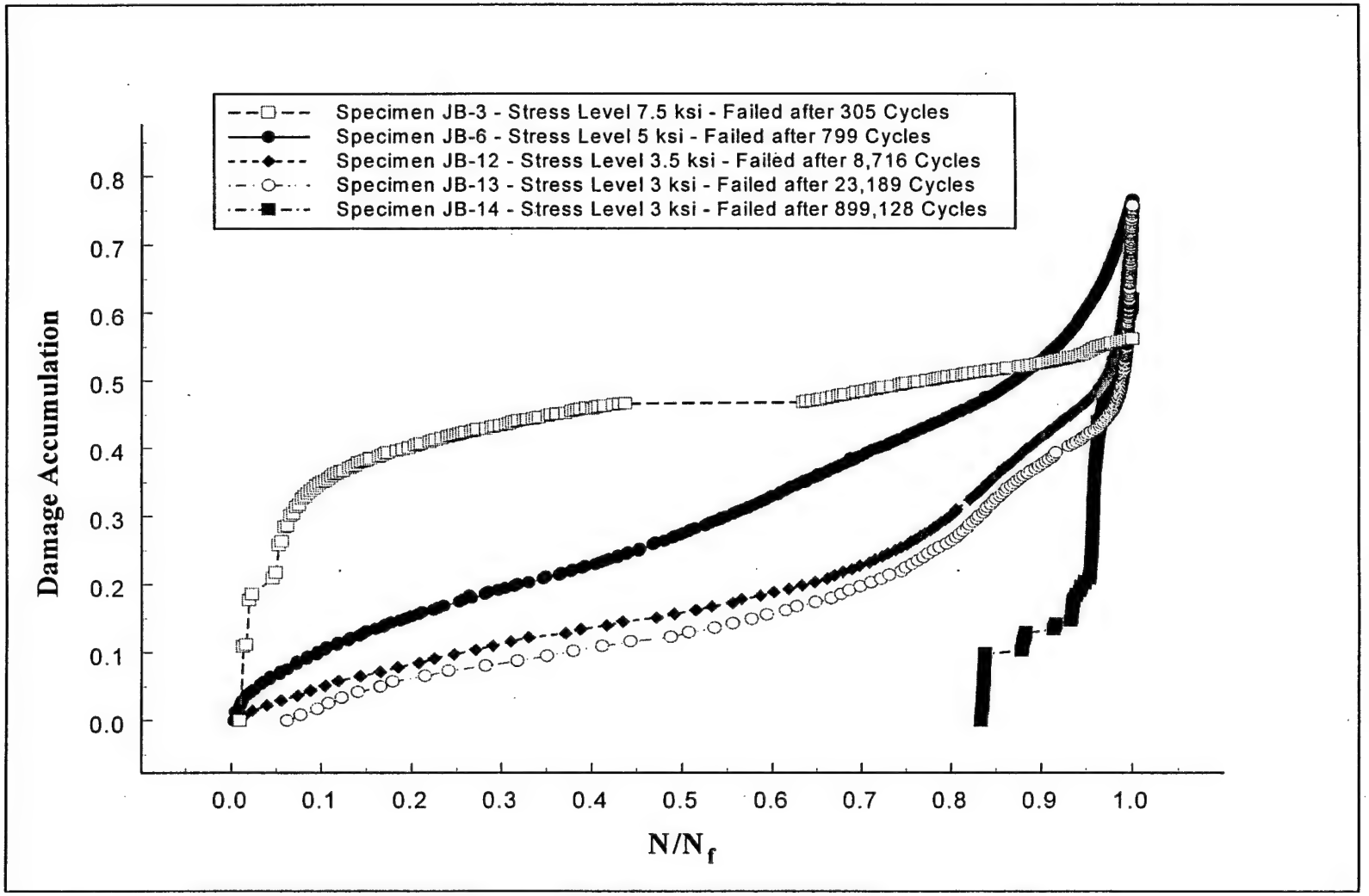

Figure 82 - Constant Amplitude Deflection-Based Fatigue Damage Accumulation in Bolted Joints

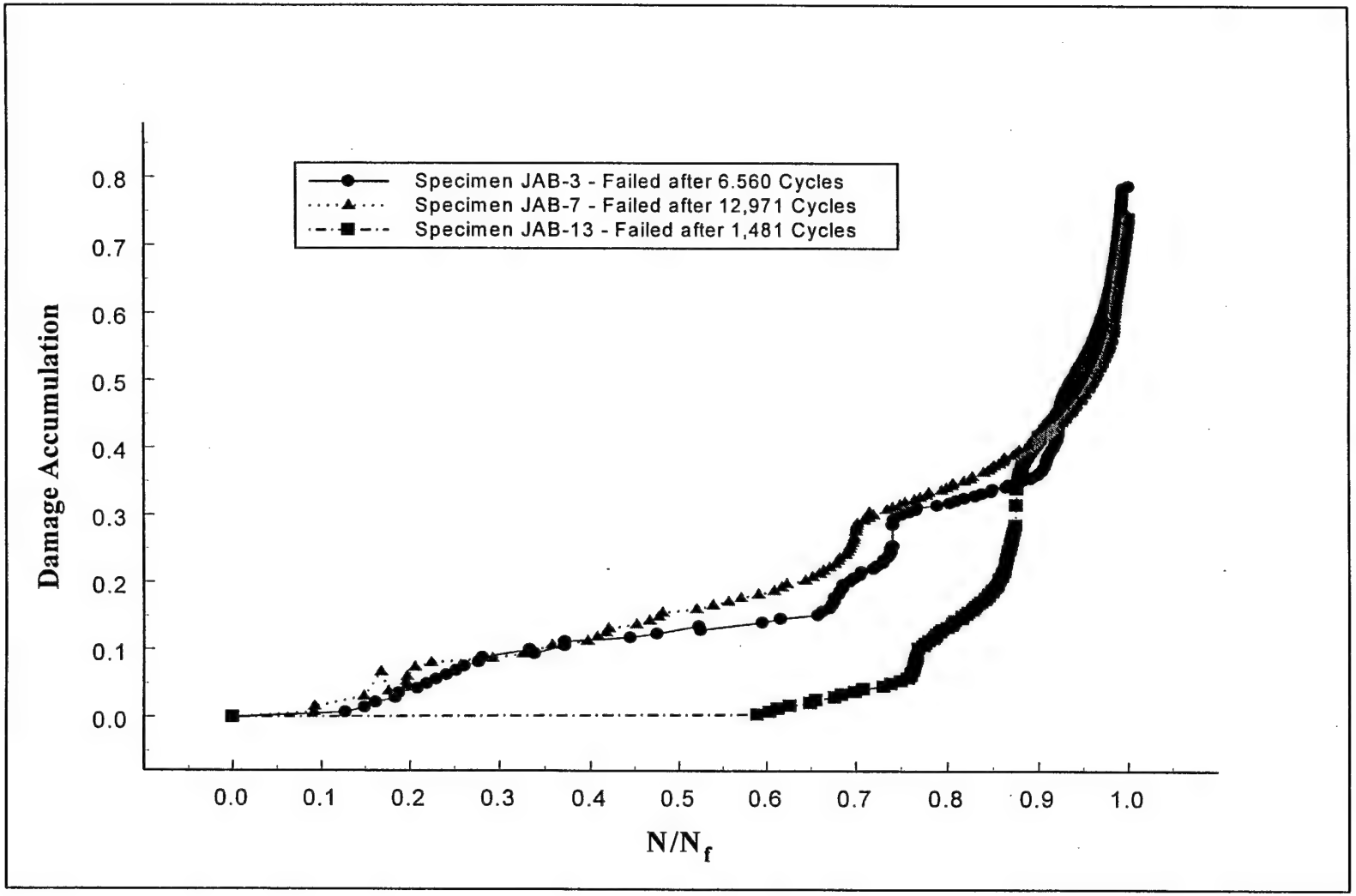

Figure 83 - Constant Amplitude Deflection-Based Fatigue Damage Accumulation in Bolted-Bonded Joints

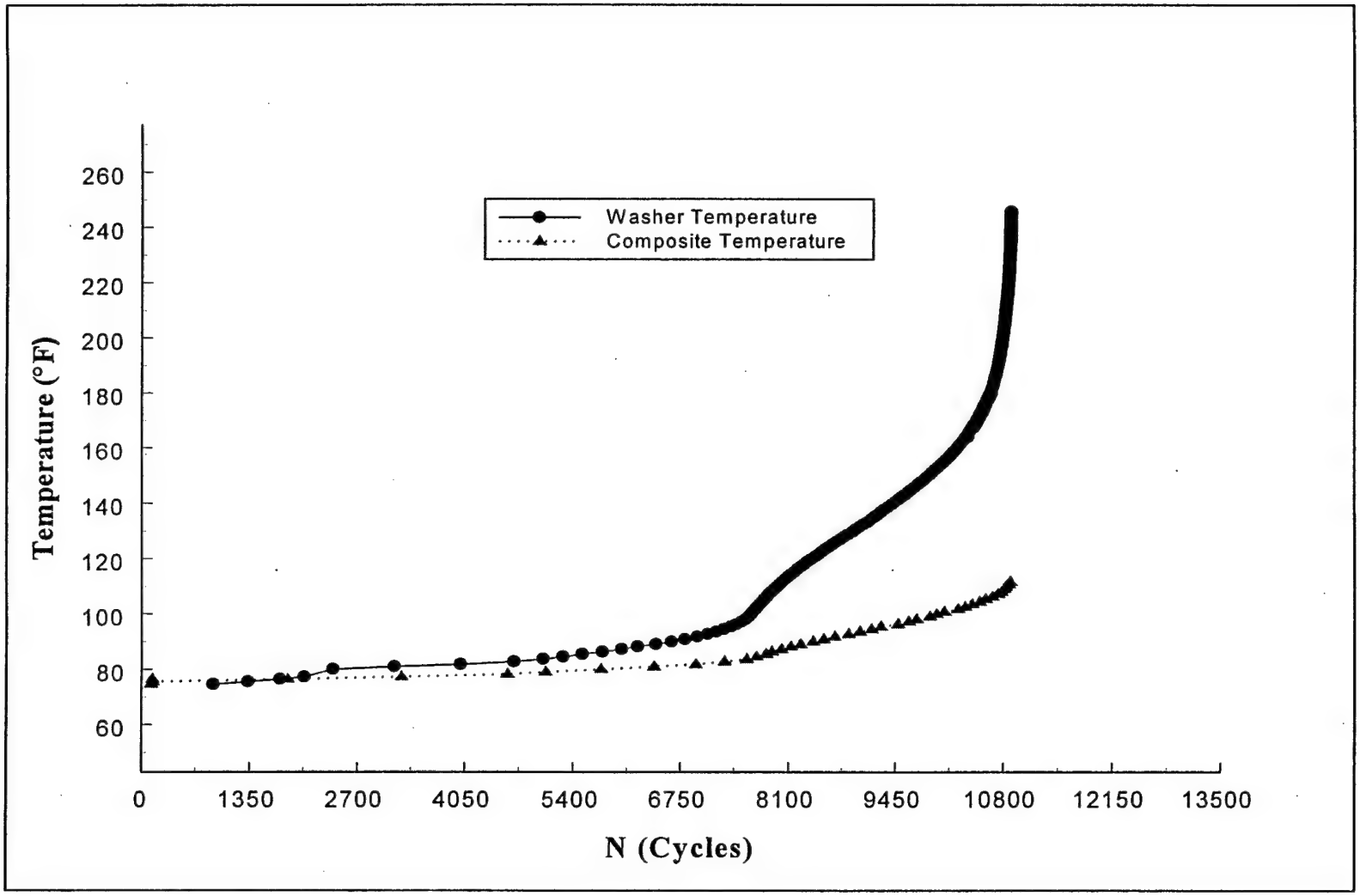

Figure 84 - Temperature Rise During Constant Amplitude Fatigue of a Bolted-Bonded Joint; Specimen JAB-7: 6 ksi

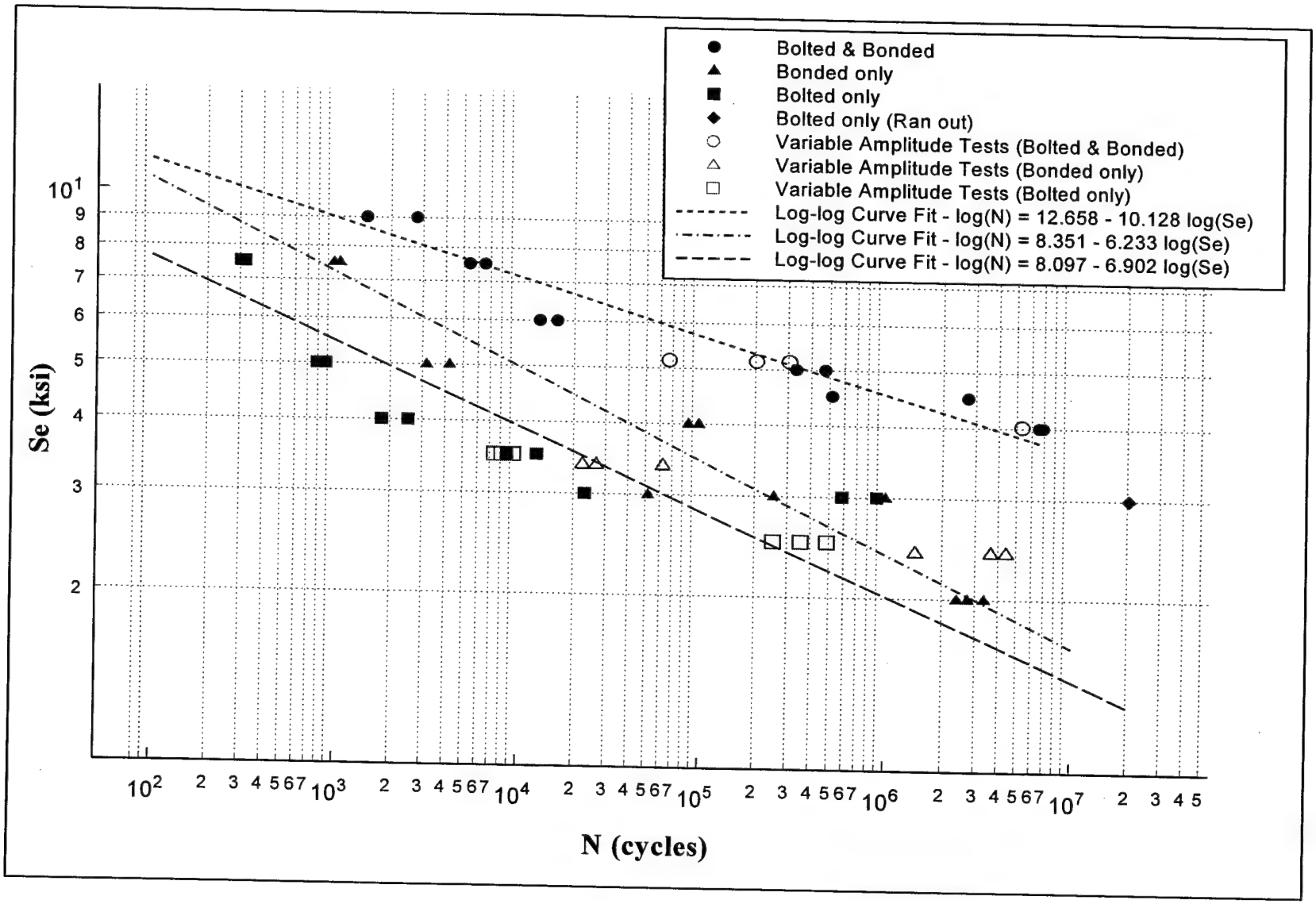

Figure 85 - S-N Curves of FRP Laminate Joints (Log-Log Curve Fit)

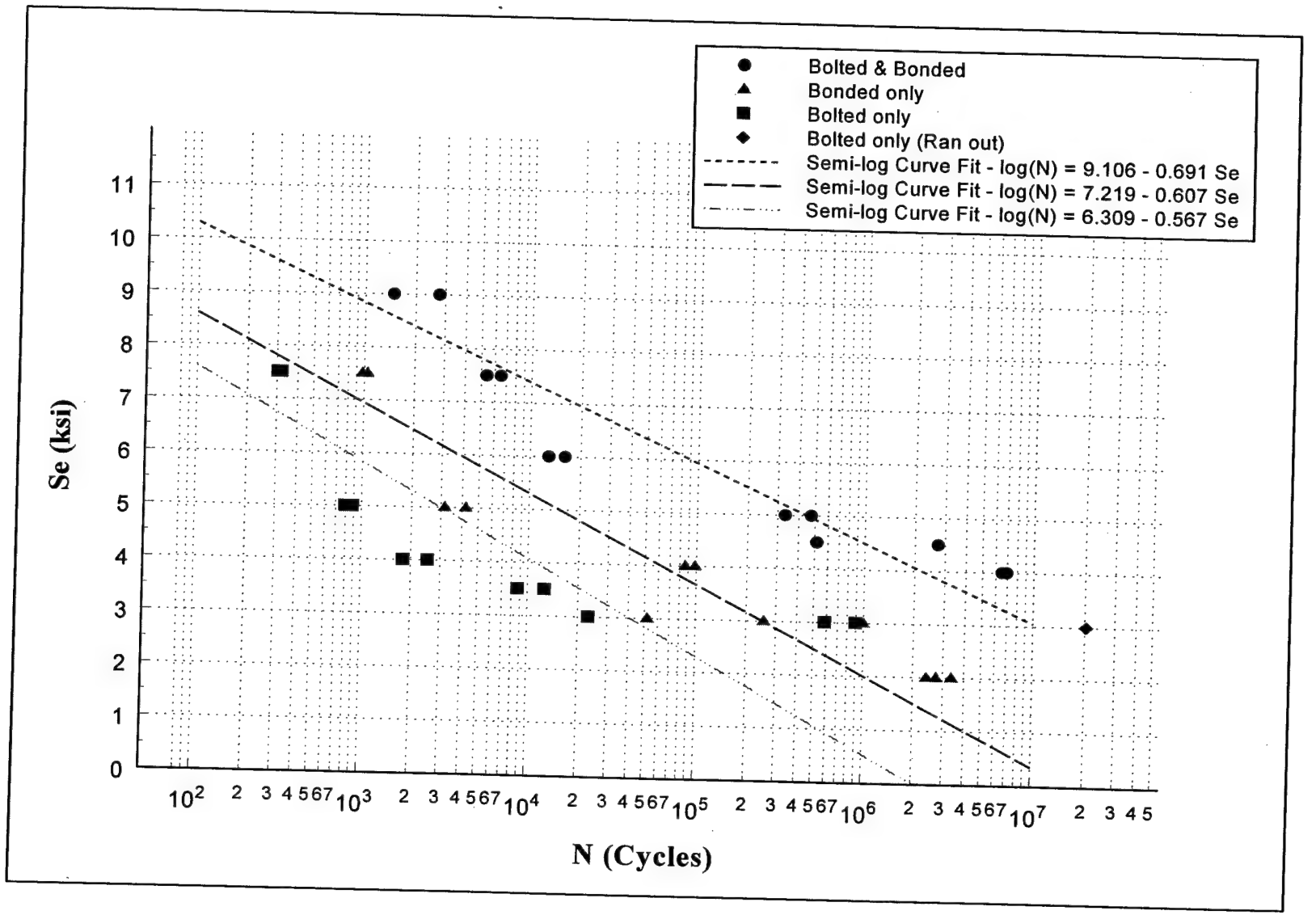

Figure 86 - S-N Curves of FRP Laminate Joints (Semi-Log Curve Fit)

TABLE 1 - STATIC TEST RESULTS FOR COMPOSITE SPECIMENS AND JOINTS

Specimen	Lay-up/Joint Type	Load Type	ID Number	Failure Load (Pounds)	Failure Stress (psi)
Passive Bearing Case	±45°	Tension	9-0750-9	43,110	18,000
			9-0750-11	42,350	18,000
		Compression	9-0750-10	-50,760	-21,570
			9-0750-8	-49,850	-20,500
	0/90°	Tension	6-0750-6	90,830	37,500
			6-0750-7	90,810	38,000
		Compression	6-0750-10	-100,000*	-41,540
Active Bearing Case	±45°	Tension	9-0750-4	27,080	11,220
			9-0750-5	27,770	11,590
		Compression	9-0750-8	-31,600	-13,210
			9-0750-6	-29,500	-11,940
	0/90°	Tension	6-0750-10	25,940	11,010
			6-0750-9	27,490	11,790
		Compression	6-0750-12	-40,720	-17,000
			6-0750-11	-40,820	-16,890
Joints	Bonded only	Tension	JA-1	36,180	14,000
		Compression	JA-2	-31,860	-12,630
	Bolted only	Tension	JB-1	33,630	13,960
		Compression	JB-2	-90,490	-36,000
	Bonded & Bolted	Tension	JAB-1	39,130	16,430
		Compression	JAB-2	-73,600	-31,100

* Suspended after exceeding the maximum capacity of the testing machine.

TABLE 2 - CONSTANT AMPLITUDE FATIGUE TESTS OF FRP LAMINATES - PASSIVE BEARING CASE

Lay-up	Identification No.	Max. Stress Level (ksi)	Max. Load Level (lbs)	Load Frequency (Hz)	Failure Criterion (x Initial LVDT)	Cycles to Failure	Additional Data Collected	
							LVDT	Temp.
±45°	9-0750-4	2.5	5,858	1 & 3*	4	20,000,000 +	--	--
	8-0750-6	2.5	5,864	3	4	19,100,000 +	--	--
	8-0750-3	3.5	8,112	3	4	1,204,300	--	✓
	9-0750-5	3.5	8,281	3	4	6,946,300	✓	✓
	8-0750-7	5	12,113	1	4	21,800	--	--
	9-0750-1	5	12,023	3	4	6,500	--	--
	9-0750-6	5	12,424	5	4	7,530	--	✓
	8-0750-4	7.5	17,914	1	4	490	✓	✓
	8-0750-11	7.5	17,924	1	4	570	✓	✓
	9-0750-7	7.5	17,773	1	4	540	✓	✓
	9-0750-2	10	24,000	4	6	2,500	--	--
	9-0750-3	10	24,305	3	6	240	--	--

+ Indicates test was suspended without failure

*After 1,969,795 cycles the load frequency was changed to 3 Hz.

Note: All ±45° specimens developed X-Shaped damage bands along the principal material directions in the gage section. These damage bands may be due to shear (mode II) cracking of the laminates.

TABLE 2 (con't) - CONSTANT AMPLITUDE FATIGUE TESTS OF FRP LAMINATES - PASSIVE BEARING CASE

Lay-up	Identification No.	Max. Stress Level (ksi)	Max. Load Level (lbs)	Load Frequency (Hz)	Failure Criterion (x Initial LVDT)	Cycles to Failure	Additional Data Collected	
							LVDT	Temp.
0/90°	6-0750-1	7.5	17,607	1&3**	4	1,483,000	✓	✓
	6-0750-11	7.5	17,740	3	4	6,636,000	--	--
	6-0750-2	10	23,594	3	4	426,600	--	--
	6-0750-3	10	23,858	1	4	474,900	✓	✓
	6-0750-9	10	23,638	1	4	296,200	✓	✓
	6-0750-4	15	35,833	1	4	40,600	✓	✓
	6-0750-5	15	35,870	1	4	45,400	✓	✓
	6-0750-8	15	34,642	1	4	25,600	✓	✓
	6-0750-12	20	47,365	1	4	3,680	✓	✓
	7-0750-7	20	45,828	1	4	4,990	✓	✓
	7-0750-1	30	71,616	4	2	420	--	--

**After 689,045 cycles the load frequency was changed to 3 Hz.

Note: All 0/90° Specimens developed mode I cracks starting from the middle of the bolt holes and propagating perpendicular to the loading direction.

TABLE 3 - VARIABLE AMPLITUDE FATIGUE TESTS OF FRP LAMINATES - PASSIVE BEARING CASE

Lay-up	Identification No.	RMS (ksi)	Max-Min Stress	Max. Load Level (lbs)	Load Frequency (Hz)	Failure Criterion (x Initial LVDT)	Cycles to Failure	Additional Data Collected
								Temperature
±45°	8-0750-2	1.75	±7.597	17,758	3	4	1,580,300	--
	8-0750-8	1.75	±7.597	17,828	3	4	1,641,300	--
	8-0750-10	1.75	±7.597	18,016	3	4	1,309,500	--
	8-0750-1	2.5	±10.854	25,277	1	4	43,200	--
	8-0750-5	2.5	±10.854	25,682	1	4	48,500	--
	8-0750-9	2.5	±10.854	25,540	1	4	22,600	--
0/90°	7-0750-2	4.5	±19.536	46,577	3	4	857,500	--
	7-0750-3	4.5	±19.536	46,017	3	4	566,800	✓
	7-0750-4	4.5	±19.536	46,011	3	4	524,100	✓
	6-0750-8	6	±26.048	60,945	3	4	426,600	✓
	7-0750-5	6	±26.048	60,653	3	4	474,900	--
	7-0750-6	6	±26.048	61,159	3	4	296,200	✓

TABLE 4 - CONSTANT AMPLITUDE FATIGUE TESTS OF FRP LAMINATES - ACTIVE BEARING CASE

Lay-up	Identification No.	Max. Stress Level (ksi)	Max. Load Level (lbs)	Load Frequency (Hz)	Failure Criterion (x Initial LVDT)	Cycles to Failure	Additional Data	
							LVDT	Temp.
±45°	8-0750-1	2.5	5,790	1	4	238,000	✓	✓
	8-0750-2	2.5	5,849	1	4	268,000	✓	✓
	8-0750-4	2.5	5,867	1	4	340,900	✓	✓
	7-0750-12	3	7,275	1	4	100,300	✓	✓
	8-0750-3	3	7,103	1	4	344,700	--	--
	9-0750-1	3	7,205	1	4	1,104,600	--	--
	9-0750-2	4	9,910	1	4	24,600	--	--
	9-0750-7	4	10,054	1	4	39,500	--	--
	7-0750-9	5	12,323	1	4	1,170	--	--
	9-0750-3	5	12,433	1	4	970	--	--

TABLE 4 (con't) - CONSTANT AMPLITUDE FATIGUE TESTS OF FRP LAMINATES - ACTIVE BEARING CASE

Lay-up	Identification No.	Max. Stress Level (ksi)	Max. Load Level (lbs)	Load Frequency (Hz)	Failure Criterion (x Initial LVDT)	Cycles to Failure	Additional Data	
							LVDT	Temp.
0/90°	7-0750-2	2.5	6,137	1	4	1,675,000	--	--
	7-0750-5	2.5	5,832	1	4	1,218,400	--	--
	6-0750-1	3	7,041	1	4	310,900	--	--
	7-0750-8	3	6,952	1	4	371,900	--	--
	7-0750-6	4	9,611	1	4	70,300	--	--
	7-0750-7	4	9,450	1	4	183,000	--	--
	6-0750-4	5	11,624	1	4	5,120	--	--
	6-0750-5	5	11,647	1	4	6,320	--	--
	6-0750-2	7.5	17,236	1	4	155	--	--
	6-0750-3	7.5	17,617	1	4	200	--	--

TABLE 5 - VARIABLE AMPLITUDE FATIGUE TESTS OF FRP LAMINATES - ACTIVE BEARING CASE

Lay-up	Identification No.	RMS (ksi)	Max-Min Stress (ksi)	Max. Load Level (lbs)	Load Frequency (Hz)	Failure Criterion (x Initial LVDT)	Cycles to Failure	Additional Data Collected
								Temperature
±45°	7-0750-10	1.25	±5.426	12,910	3	4	228,100	✓
	7-0750-13	1.25	±5.426	12,929	3	4	198,100	✓
	8-0750-7	1.25	±5.426	12,753	3	4	474,500	✓
	7-0750-11	1.75	±7.597	18,971	3	4	43,800	✓
	7-0750-14	1.75	±7.597	18,428	3	4	44,400	✓
	8-0750-5	1.75	±7.597	18,268	3	4	55,500	✓
0/90°	6-0750-7	1.25	±5.426	12,751	3	4	231,700	✓
	6-0750-8	1.25	±5.426	12,570	3	4	398,100	✓
	7-0750-4	1.25	±5.426	12,742	3	4	478,100	✓
	6-0750-6	1.75	±7.597	18,434	3	4	67,400	✓
	7-0750-1	1.75	±7.597	18,676	3	4	95,200	✓
	7-0750-3	1.75	±7.597	18,169	3	4	63,100	✓

TABLE 6 - CONSTANT AMPLITUDE FATIGUE TESTS OF FRP JOINTS

Joint Type	Identification Name	Max. Stress Level (ksi)	Max. Load Level (lbs)	Load Frequency (Hz)	Failure Criterion (x Initial LVDT)	Cycles to Failure	Additional Data	
							LVDT	Temp.
Bonded	JA - 9	2	5,044	2	4	2,411,800	✓	--
	JA - 10	2	5,042	2	4	3,369,600	--	--
	JA - 20	2	5,035	2	4	2,748,500	✓	--
	JA - 7	3	7,735	1	4	51,900	--	--
	JA - 8	3	7,591	1	4	255,400	✓	--
	JA - 19	3	7,735	1	4	1,000,300	✓	--
	JA - 17	4	10,134	1	4	98,600	✓	--
	JA - 18	4	10,170	1	4	86,200	✓	--
	JA - 5	5	12,806	1	4	3,170	✓	--
	JA - 6	5	12,846	1	4	4,220	✓	--
	JA - 3	7.5	18,737	3	4	980	--	--
	JA - 4	7.5	18,764	3	4	1,060	--	--

TABLE 6 (con't) - CONSTANT AMPLITUDE FATIGUE TESTS OF FRP JOINTS

Joint Type	Identification Name	Max. Stress Level (ksi)	Max. Load Level (lbs)	Load Frequency (Hz)	Failure Criterion (x Initial LVDT)	Cycles to Failure	Additional Data	
							LVDT	Temp.
Bolted	JB - 7	3	7,607	1	4	589,400	--	--
	JB - 8	3	7,019	1	4	20,000,000 +	✓	--
	JB -13	3	7,307	1	4	23,200	✓	--
	JB -14	3	7,319	1	4	899,100	✓	--
	JB - 11	3.5	8,617	1	4	12,600	✓	--
	JB -12	3.5	8,409	1	4	8,720	✓	--
	JB - 9	4	9,623	1	4	1,810	--	--
	JB - 10	4	9,464	1	4	2,530	--	--
	JB - 5	5	11,795	1	4	890	✓	--
	JB - 6	5	11,695	1	4	800	✓	--
	JB - 3	7.5	17,774	3	3	305	✓	--
	JB - 4	7.5	17,793	0.5	4	320	✓	--

+ Indicates test was suspended without failure.

TABLE 6 (con't) - CONSTANT AMPLITUDE FATIGUE TESTS OF FRP JOINTS

Joint Type	Identification Name	Max. Stress Level (ksi)	Max. Load Level (lbs)	Load Frequency (Hz)	Failure Criterion (x Initial LVDT)	Cycles to Failure	Additional Data	
							LVDT	Temp.
Bonded & Bolted	JAB - 9	4	9,511	1	4	6,964,000	--	--
	JAB - 10	4	9,667	1	4	6,578,900	✓	--
	JAB - 11	4.5	10,958	1	4	517,800	--	--
	JAB - 12	4.5	10,765	1	4	2,733,500	✓	--
	JAB - 5	5	11,878	1	4	475,900	✓	--
	JAB - 6	5	11,775	1	4	333,500	✓	--
	JAB - 7	6	14,463	1	4	13,000	✓	✓
	JAB - 8	6	14,191	1	4	16,200	✓	--
	JAB - 3	7.5	17,850	0.5	4	6,560	✓	--
	JAB - 4	7.5	17,692	0.5	4	5,420	✓	--
	JAB - 13	9	21,331	1	4	1,480	✓	--
	JAB -14	9	21,331	1	4	2,780	✓	--

TABLE 7 - VARIABLE AMPLITUDE FATIGUE TESTS OF FRP JOINTS

Joint Type	I.D. No.	RMS (ksi)	Max-Min Stress (ksi)	Max. Load Level (lbs)	Load Freq. (Hz)	Failure Criterion (x Initial LVDT)	Cycles to Failure
Bonded only	JA - 14	1.25	±5.426	13,812	3	4	3,654,300
	JA - 15	1.25	±5.426	13,912	3	4	1,441,900
	JA - 16	1.25	±5.426	13,839	3	4	4,419,200
	JA - 11	1.75	±7.597	19,949	3	4	62,500
	JA - 12	1.75	±7.597	19,103	3	4	22,500
	JA - 13	1.75	±7.597	19,306	3	4	26,700
Bolted only	JB - 18	1.25	±5.426	13,116	3	4	253,900
	JB - 19	1.25	±5.426	13,060	3	4	492,500
	JB - 20	1.25	±5.426	13,161	3	4	356,700
	JB - 15	1.75	±7.597	18,671	3	4	7,520
	JB - 16	1.75	±7.597	18,407	3	4	9,390
	JB - 17	1.75	±7.597	18,357	3	4	8,220
Bonded & Bolted	JAB - 18	1.75	±7.597	19,279	3	4	5,343,100
	JAB - 19	1.75	±7.597	18,070	3	4	11,934,700
	JAB - 20	1.75	±7.597	17,986	3	4	9,977,000
	JAB - 15	2.25	±9.765	23,169	3	4	203,100
	JAB - 16	2.25	±9.765	22,900	3	4	305,700
	JAB - 17	2.25	±9.765	24,664	3	4	67,400

TABLE 8 - COMPARISON OF RAYLEIGH FATIGUE LIVES WITH TEST RESULTS

Specimen	Lay-up/Joint Type	RMS level (ksi)	Experimental (Geom. Mean)	Rayleigh approximation with log-log S-N curve	Rayleigh approximation with semi-log S-N curve
Passive Bearing Case	±45°	1.75	1,503,200	401,800	348,100
		2.5	36,200	24,000	27,900
	0/90°	4.5	633,900	1,015,000	1,064,200
		6.0	391,500	158,400	217,100
Active Bearing Case	±45°	1.25	277,800	418,100	391,700
		1.75	47,600	28,800	5,600
	0/90°	1.25	353,300	1,194,600	1,365,800
		1.75	74,000	75,400	87,000
Joints	Bonded only	1.25	2,855,600	925,300	979,200
		1.75	33,500	113,600	148,300
	Bolted only	1.25	354,600	225,500	129,800
		1.75	8,340	22,100	26,100
	Bonded & Bolted	1.75	8,600,700	3,510,200	3,789,200
		2.25	161,100	275,400	234,500

REFERENCES

Amijima, S., Tanimoto, T., and Matsuoka, T., [1982], "Study on Frequency Dependence of Fatigue Life of FRP,"*Journal of the Society of Materials Science*, Japan, v 31, n 351, pp.1156-1161.

Davis, J. W., McCarthy, J. A., and Schrub, J. N., [1964], "The Fatigue Resistance of Reinforced Plastics," *In Materials in Design Engineering*, pp. 87-91.

Hahn, H. T., and Kim, R.Y., [1976], "Fatigue Behavior of Composite Laminates," *Journal of Composite Materials*, 10, 156-180.

Halpin, J. C., Jerina, K. L., and Johnson, T. A., [1973], "Characteristics of Composites for the Purpose of Reliability Prediction," *In Analysis of Test Methods for High Modulus Fibers and Composites, ASTM STP 521.*

Hashin, Z. and A. Rotem, [1978], "A Cumulative Damage Theory of Fatigue Failures," *Mater. Sci. Engng.*, (34), pp. 147-160.

Hashin, Z., [1985], "Cumulative Damage Theory for Composite Materials: Residual Life and Residual Strength Method," *Composites Science and Technology*, 23, 1-19.

Howson, J. C., Rymill, R. J., and Pinzelli, R. F., [1992], "Fatigue Performance of Marine Laminates Reinforced with Kevlar Aramid Fibers," *Composites International Conference and Exhibition*, Paris.

Hwang, W., and Han, H. S., [1986a], "Cumulative Damage Models and Multi-Stress Fatigue Life Prediction," *Journal of Composite Materials*, 20, 125-153.

Hwang, W., and Han, K. S., [1986b], "Fatigue of Composites-Fatigue Modulus Concept and Life Prediction," *Journal of Composite Materials*, 20, 154-165.

Hwang, W., Lee, C. S., Park, H. C., and K. C. Han, [1995], "Single and Multi-Stress Level Fatigue Life Prediction of Glass/Epoxy Composites," *Journal of Advanced Materials*, 3-9.

Lee, L.J., Fu., K.E., and Yang, J.N., [1996], "Prediction of Fatigue Damage and Life for Composite Laminates Under Service Loading Spectra," *Composite Science and Technology*, 56, pp. 635-648.

Mandell, J. and Meier, Urs, [1983], "Effects of Stress Ratio, Frequency, and Loading Time on the Tensile Fatigue of Glass-Reinforced Epoxy," *ASTM STP 813*, pp. 55-77.

Miles, J.W., [1954], "On Structural Fatigue Under Random Loading", *Journal of Aeronautical Science*, pp. 753-762.

Miner, M.A., [1945], "Cumulative Damage in Fatigue", *Journal of Applied Mechanics*, Volume 12.

Miyano, Y., et al., [1994], "Loading Rate and Temperature Dependence on Flexural Fatigue Behavior of a Satin Woven CFRP Laminate," *Journal of Composite Materials*, v 28, n 13, pp.1250-1260.

Morinaka, H., Fujii, T., and Amijima, S., [1991], "Effect of Loading and Unloading Duration on Fatigue Damage Process of Plain Woven GFRP," *Journal of the Society of Materials Science*, Japan, v 40, n 454, pp. 908-913.

Nakada, M., et al. , [1991], "Time and Temperature Dependences of Fatigue Behavior of C/A Hybrid Unidirectional FRP Laminates," *Journal of the Society of Materials Science*, Japan, v 40, n 449, pp. 199-204.

Nakai, Y. and Yamashita, M., [1994], "Effects of Frequency and Temperature on Delamination Fatigue Crack Growth of Unidirectional CFRP under Constant Delta K Conditions,"*Journal of the Society of Materials Science*, Japan, v 43, n 493, pp.1258-1263.

Neubert, H., Schulte, K., and Harig, H., [1990], "Evaluation of the Damage Development in Carbon Fiber Reinforced Plastics by Monitoring Load-Induced Temperature Changes," *Composite Materials : Testing and Design (Ninth Volume), ASTM STP 1059*, S.P. Garbo, ed., pp. 435-453.

Oberbach, K. and Heese, G., [1972], "Effect of Frequency and Type of Stress Application on the Fatigue Behavior of Plastics," *Materialpruefung*, v 14, n 6, pp.173-178.

Owen, M. J., and Howe, R. J., [1968], "Cumulative Damage of Chopped Strand Mat Polyester Resin Laminates," *Plastics and Polymers*, 33-44.

Palmgren, A., [1924], "Die Lebanstaver von Kugellagern, *ZVDI*, Volume 68.

Read, R. J. C. L., and Shenoi, R. A., [1995], "A Review of Fatigue Damage Modeling in the Context of Marine FRP Laminates," *Marine Structures*, 8, 257-278.

Reifsnider, K. L., and Talug, A., [1980], "Analysis of Fatigue Damage in Composite Laminates," *International Journal of Fatigue*, 3-11.

Reifsnider, K. L., [1990], "Damage and Damage Mechanics," in K. L. Reifsnider (Ed.), *Fatigue of Composite Materials*. Oxford: Elsevier.

Reifsnider, K.L., [1991], *Fatigue in Composite Materials*, Elsevier Science Publishers.

Smith, C. S., [1990], *Design of Marine Structures of Composite Materials*, Elsevier Science Publisher LTD.

Sun, C.T. and Chan, W.S., [1979], "Frequency Effect on the Fatigue Life of a Laminated Composites," *Composite Materials : Testing and Design (Fifth Conference), ASTM STP 674*, S.W. Tsai, ed., pp.418-430.

Talreya, R., [1987], *Fatigue of Composite Materials*, Technologic Publishing Company, Pennsylvania.

Tanimoto, T, and Amijima, S., [1975], "Progressive Nature of Fatigue Damage of Glass Fiber Reinforced Plastics," *Journal of Composite Materials*, 9, 380-390.

Tsai, G.C., Doyle, J.F., and Sun, C.T., [1987], "Frequency Effects on the Fatigue Life and Damage of Graphite/Epoxy Composites," *Journal of Composite Materials*, v 21, n 1, pp.2-13.

Yang, J.N. and L.J. Johnson, [1980], "The Effect of Load Sequence on Statistical Fatigue of Composites," *AIAA J.*, (18), pp. 1525-1531.

Yang, J.N. and Jones, D.L., [1981], "Load Sequence effects on the Fatigue of Unnotched Composite Materials," *Fatigue of Fibrous Composite Materials, ASTM STP 723*, pp. 213-231.

Yang, J.N. and L.J. Johnson, [1983], "Load Sequence Effects on Graphite/Epoxy Laminates," *Long-Term Behavior of Composites, ASTM STP 813*, pp. 246-262.

Yang, J.N., Yang, S.H., and Jones, D.L., [1989], "A Stiffness-based Statistical Model for Predicting the Fatigue Life of Graphite/Epoxy Laminates," *J. Comp. Technol. Res.*, 11, pp. 129-134.

Yang, J. N., Jones, D. L., Yang, S. H., and Meskini, A., [1990], "A Stiffness Degradation Model for Graphite Epoxy Laminates," *Journal of Composite Materials*, 24, 753-769.